AN ABSTRACT FOR THE THESIS OF

Jeffrey A. Cook for the degree of Master of Science

in Geophysics presented on 5 December 1980

Title: SONOBUOY REFRACTION STUDY OF THE CRUST IN THE GORDA BASIN

Abstract approved: Redacted for Privacy

L. Dale Bibee

The Gorda Basin is a young oceanic plate which comes in direct contact with the convergent margin of western North America. Two long sonobuoy refraction profiles crossing the basin provide nearly continuous data for computing the velocity structure of the crust and adjacent continental slope. Time-term analysis utilizing multiple receivers and overlapping profiles revealed a thick transition layer which averages 2.3 km but displays considerable lateral variation. The seismic compressional velocity of this layer is 5.3 km/sec. The average thickness of Layer 3 is 3.4 km with a velocity of 6.9 km/sec. The base of the crust is marked by the seismic Moho, the velocity below which is 8.1 km/sec. Refraction and reflection studies of sediment cover indicate a thickening of turbidite deposits to the southeast from less than 100 meters to over 2.5 km along the continental margin.

Ophiolite studies indicate that the top of Layer 3 marks the upper extent of amphibolite facies metamorphism of basaltic sheeted dikes. Lateral depth variations of this seismic boundary in the Gorda Basin may suggest the occurrence of isograd relief along the spreading center. The Moho marks the boundary between mafic and ultramafic rocks near the ridge but may represent the maximum depth of serpentinization in the crust after it moves away from the spreading axis.

Thin crust (4-5 km) and deep bathymetry in the central portion of the basin have resulted from crustal formation processes occurring at ridge crest offsets and are coincident with recent seismicity in the area. The Gorda ridge offsets and asymmetrical fan spreading of magnetic anomalies are features observed in response to a regional change in spreading directions and encroachment of the Pacific and North American plates. The Gorda plate as a whole does not respond rigidly to the resulting north-south compression.

Complex structures of the continental slope, revealed by seismic reflection, limited the reduction of refraction data using plane layer methods. A simplified seismic section was computed consisting of three probable sediment layers with velocities of 1.8, 2.5 and 4.0 km/sec overlying oceanic crust. The crust is observed to dip about two degrees towards the continent at the base of the slope.

A model of subduction unique to the northern California margin is one whereby young crust is subducted slowly and quickly reheated so that no brittle portion remains at normal Benioff depths. Rapid sedimentation rates balance the subduction of the crust at the margin, preventing the formation of a deep trench.

Sonobuoy Refraction Study of the Crust in the Gorda Basin

by

Jeffrey A. Cook

A THESIS

submitted to

Oregon State University

in partial fulfillment of
the requirements for the
degree of

Master of Science

Completed December 5, 1980

Commencement June 1981

APPROVED:

Redacted for Privacy

Assistant Professor of Geophysics
in charge of major

Redacted for Privacy

Dean of School of Oceanography

Redacted for Privacy

Dean of Graduate School

Date thesis presented on 5 December 1980

Typed by Margi Wolski for Jeffrey A. Cook

ACKNOWLEDGEMENTS

I had the privilege of conducting this research under two marine seismologists, my major professor, Dr. L. Dale Bibee, and also Dr. Stephen H. Johnson. I am grateful to them for the time and knowledge they gave in helping complete this thesis, and for the opportunities I received at sea.

Dr. Richard W. Couch has been generous with both time and advice throughout this study, and provided me experience in land seismology early in my graduate studies.

Discussions with fellow students Gudni Axelsson, Darrell Ibach and Gordon Ness were invaluable sources of information for both my research and education. Bart Brown, Gerry Connard and William Standing provided excellent technical support along the way. I also wish to thank Bill Gilbert for his efficient drafting, Dave Reinert, who did the photographic work, and Margi Wolski for typing the manuscript.

I am especially grateful to my wife, Tess, for her patience, love and understanding during my graduate studies and for the knowledge and interest she has in the Earth Sciences. She is also the most skillful and unselfish fishing partner I've ever had.

This research was supported by NSF grants OCE 75-20156 and OCE 79-19481. During my stay at Oregon State University I recieved financial assistance from a Texaco Fellowship.

TABLE OF CONTENTS

Table of Contents, continued

LIST OF FIGURES

List of Figures, continued.

List of Figures, continued.

List of Figures, continued.

LIST OF TABLES

SONOBUOY REFRACTION STUDY OF THE CRUST IN THE GORDA BASIN

The development of Plate Tectonic theory during the past two decades has drastically changed the thinking of geoscientists and their approach to studying the Earth's crust. According to this theory, oceanic crustal material is formed at oceanic ridges, and by the process of sea-floor spreading, moves laterally as a rigid plate away from the ridge until it reaches a convergent boundary, usually an oceanic trench. Besides the occurrence of divergent boundaries at ridges and convergent boundaries at trenches, a third type of plate boundary may form when two plates move past one another along transform faults, where material is neither created nor destroyed.

Although this theory is applicable to most oceanic crust, some plates are recognizably complex and may not adhere to the basic concepts. Such deviations as changes in speading rate or direction, ridge jumps and intraplate deformation have been observed through careful interpretation of marine geophysical data. These complications in the basic theory may be the norm rather than the exception. By determining the crustal structure of the more complex plates in detail, it may be possible to explain and predict why these exceptions to the general theory occur.

The Gorda Basin is situated off the coasts of southern Oregon and northern California and lies along the continental margin. It is bounded by the Blanco Fracture Zone to the north and the Mendocino Fracture Zone to the south (Figure 1). The basin is underlain by a roughly triangular oceanic plate believed to have formed at the Gorda

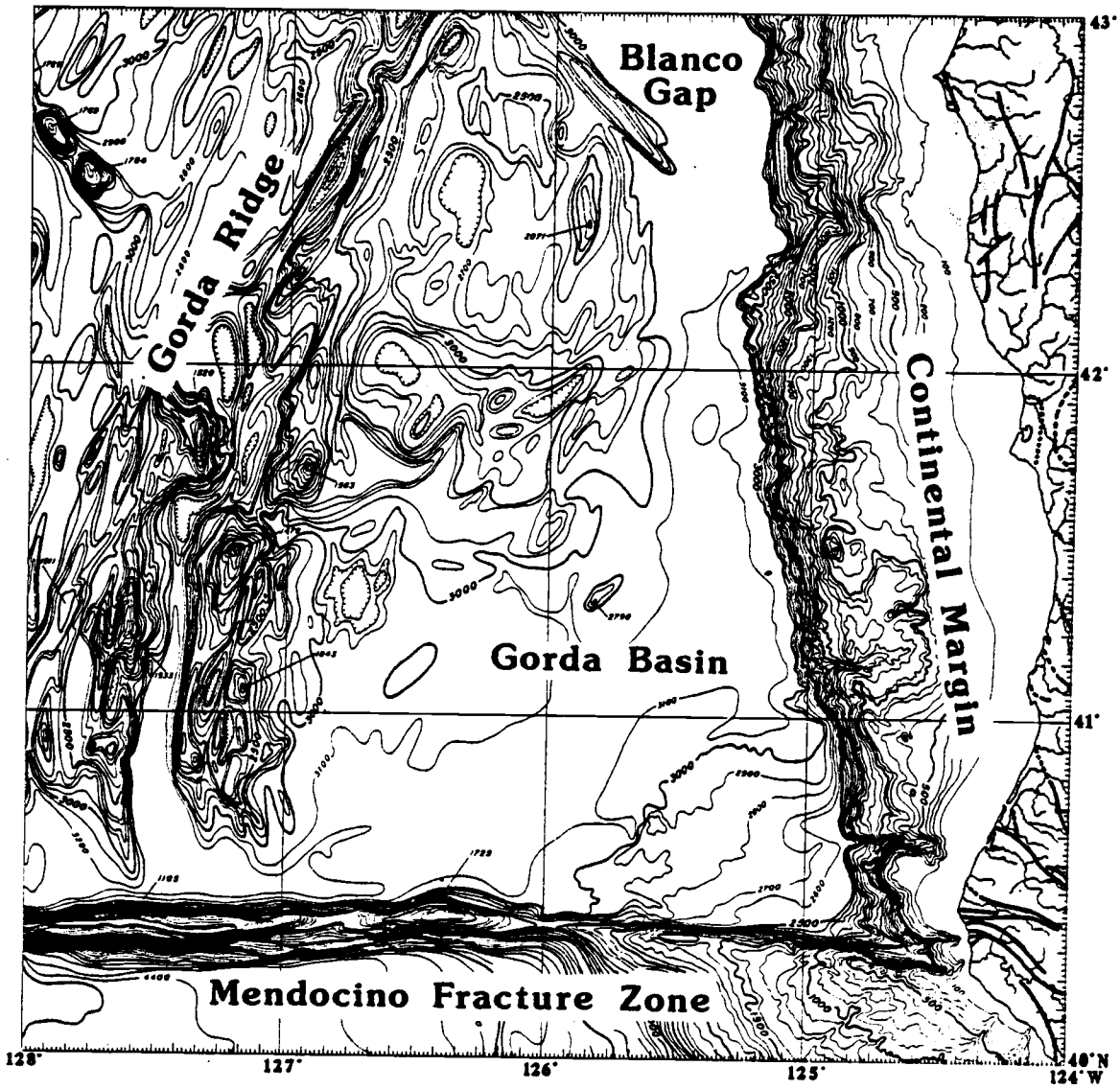

Figure 1. Bathymetry of the Gorda Basin, Gorda Ridge, Mendocino Fracture Zone, Blanco Gap and continental margin of northern California and southern Oregon. Contour interval = 100 m. (After Wilde et al., 1978)

Ridge spreading center to the west. Although it displays many of the characteristics of a typical crustal plate, the Gorda spreading system is quite complex and offers the marine geophysicist a unique region to study because of its compact areal extent. It contains both slow and fast spreading ridges and two bordering fracture zones, all of which are seismically active. Geophysical evidence suggests there have been changes in spreading rate and direction and possibly a propogation of spreading center jumps. Other evidence points to the existence of an aseismic convergent boundary between the Gorda and North American plates with the notable absence of an oceanic trench. In the southeast corner of the plate, active faulting and seismicity is an indication of intra-plate deformation, suggesting a non-rigid oceanic crustal model.

Because of the proximity and scientific problems of the Northeast Pacific region, the School of Oceanography at Oregon State University conducts an active research program in this area. During August and September of 1977 (cruise W7708C), the Geophysics Group of Oregon State conducted two ship-to-sonobuoy explosion refraction experiments within the Gorda Basin. This thesis describes the acquisition, reduction and analysis of the seismic data and an interpretation of the results. The purpose of the research is to determine a crustal structure model for the Gorda plate and a portion of the continental rise to further improve the knowledge and understanding of this tectonically diverse region.

PREVIOUS STUDIES

Geology and Physiography

The Gorda Basin is the prominent feature of the larger Gorda plate (Dehlinger et al., 1967; Shor et al., 1968), expressed as a triangular shaped region with low topographic relief and an average depth of 3 km (Figure 1). To the north and west, the basin province grades into a hilly region on the flanks of the Gorda Rise. The eastern edge of the basin is an elongate depression filled with a sedimentary wedge (Kulm and Fowler, 1974a; Silver, 1969b, 1971a) which terminates against the toe of the continental slope. Sea floor sediments in the region are mostly Cenozoic deposits of terrigenous turbidites overlying basement rocks that were created at the Gorda spreading center. The rate of sedimentation has increased in time due to continental glaciation, Cascade volcanism, and uplifting of the Coast Range (von Huene and Kulm, 1973; Kulm and Fowler, 1974a,b). At the continental margin, some of the sediments may have subducted along with oceanic crust while some may have been accreted to the margin, perhaps by means of an imbricate thrust mechanism (von Huene and Kulm, 1973; Karig and Sharman, 1975; Kulm and Fowler, 1974b; Couch, 1980).

The southern extent of the Gorda Basin is marked by the Mendocino and Gorda Escarpments, which are bathymetric expressions of the Mendocino Fracture Zone (Figure 1). This fracture zone is an east-west trending right-lateral transform fault offsetting the Gorda Ridge from its previously subducted counterpart to the south. The eastward extension of the Mendocino Fracture Zone now terminates at the San

Andreas fault of northern California near Cape Mendocino.

The northern boundary of the Gorda plate consists of two features, the Blanco Fracture Zone and Blanco Gap. The fracture zone is a northwest trending right-lateral transform fault which offsets the Gorda and Juan de Fuca Ridges (Figure 6) in the form of small, subparallel, elongate ridges and valleys. The Blanco Gap lies between the fracture zone and the continental margin and provides a natural passageway for transport of depositional material between the Cascadia and Gorda Basin (Duncan and Kulm, 1970; Kulm and Fowler, 1974a).

The oceanic crust of the Gorda plate is formed at the active spreading center along the Gorda Ridge (Atwater and Mudie, 1973). The ridge is located about 200 km west of the continental margin of south-central Oregon and northern California. The trend of the ridge axis changes at 41.6°N latitude from N-S to NNE-SSW for reasons undetermined (Dehlinger et al., 1968; McManus, 1967; Shor et al., 1968). Scheidegger (1973) used dredged volcanic rock samples to classify the magmas erupted at the Gorda Ridge as olivine tholeiites (basalt).

Geophysical Studies

I. Magnetics

The mapping of magnetic anomaly patterns on the seafloor provided the primary geophysical evidence for sea floor spreading and eventually lead to the development of modern Plate Tectonic theory. Raff and Mason (1961) mapped the magnetic anomalies in the Gorda-Juan de Fuca region and Vine (1966) constructed the much used map of Figure 2 from their data.

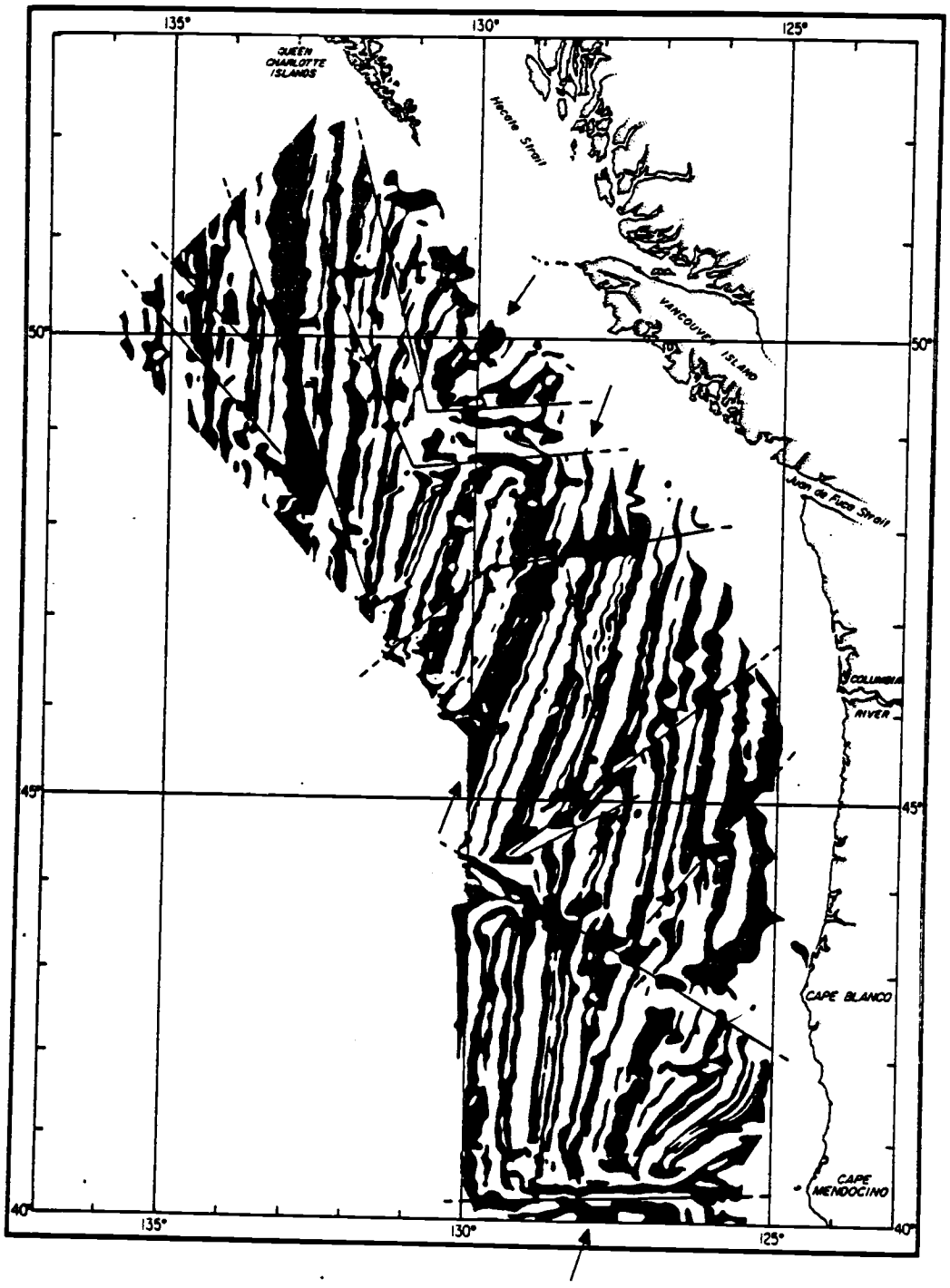

Figure 2. Summary diagram of total magnetic field anomalies southwest of Vancouver Island. Areas of positive anomaly are shown in black. Straight lines indicate anomaly pattern offsets: arrows, the axes (from north to south) of the Explorer, Juan de Fuca, and Gorda Ridges. (After Vine,1966)

Several workers (Wilson, 1965; Vine and Wilson, 1965; Tobin and Sykes, 1968; Atwater, 1970) established that the entire Juan de Fuca Rise is a spreading ridge and that the area between it and North America is a separate oceanic plate subducting along the continental margin. The subduction of the crust beneath the continental plate was suggested by the truncation of magnetic anomalies near the base of the slope (Atwater, 1970; Silver, 1969a,b; 1971a,b). In the Gorda Basin (Figures 2 and 7) magnetic anomalies are truncated at a maximum age of about 6-8 M.Y. (anomaly 4). Fracture zones in the area are seen to be right-lateral in sense and shift ridges on the north side to the left. The Mendocino and Blanco Fracture Zones bounding the Gorda plate are about 70 M.Y. and 15 M.Y. old, respectively. The rate of motion across these transforms is on the order of 5 cm/yr.

Age equivalent magnetic anomalies form an asymmetrical pattern about the Gorda Rise (Silver, 1969a, 1971a). In the past 30 M.Y. there have been various episodes of this asymmetric spreading with the faster limb on the east side of the ridge (Elvers et al., 1973; Riddihough, 1977). Silver (1971a,b) interpreted anomalies (1-3.5 M.Y.) to be bent about an eastward trending fracture at 42°N latitude with a similar bend occurring in anomaly 4 near 41.5°N. Atwater and Mudie (1973) assumed spreading to be symmetrical about and perpendicular to the ridge crest to arrive at a half rate of 3.7 cm/yr along the entire length of the Gorda Ridge until 2.1 M.Y. ago. The spreading rate and direction then changed with the section north of 41.6°N rotating to its present position and slowing to 3.0 cm/year while the southern section slowed to 1.2 cm/yr. There has been a general decrease in the whole

spreading rate along the system over the last 10 M.Y.: Explorer Ridge, from 7 to 4 cm/yr; Juan de Fuca Ridge, 8 to 6 cm/yr; Gorda Ridge North, 8 to 6 cm/yr; Gorda Ridge South, 8 to 3 cm/yr (Atwater and Mudie, 1973; Klitgord et al., 1975; Riddihough, 1977). Variable spreading rates have also been involved in progressive clockwise rotation of the axes of all Juan de Fuca Ridge segments. The major period of rotation occurred between 3 and 5 M.Y. ago and the amount of rotation was about 10-15 degrees (Atwater and Mudie, 1973).

The oblique orientation of the anomalies with respect to the trend of the Mendocino Fracture Zone has suggested to several investigators (Couch, 1980; Silver, 1971b) that the Gorda plate is underthrusting it. Silver (1971b) estimates that 45 km of ocean material has been underthrust along the Mendocino Escarpment in the last 2.5 M.Y. and Couch (1980) concludes this underthrusting to occur as far west as 126°W longitude (see Figure 7).

II. Gravity

A free-air gravity map for the Gorda plate was compiled by Dehlinger et al. (1967, 1971) and is shown in Figure 3. Much of the interpretation described below is from Couch (1980).

The long linear northeast trending negative anomaly is associated with the Gorda Ridge and is caused partly by the topographic rift in the ridge and low density mantle rock beneath it. Positive anomalies flanking the ridge are associated with topographic highs. Areas in the basin averaging near zero anomaly suggest that isostatic adjustment is at least as rapid as tectonic displacement. Dehlinger (1969) noted

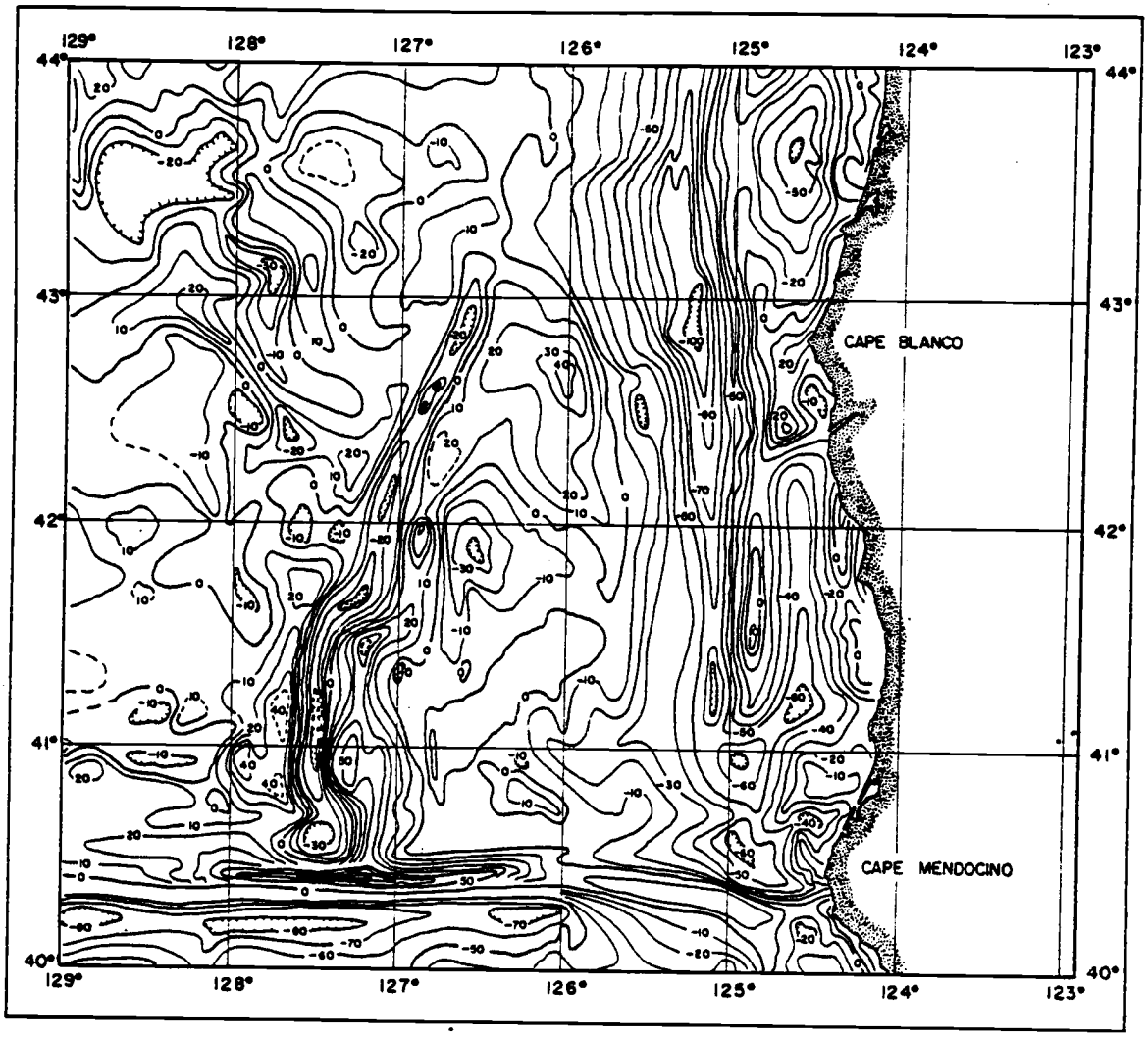

Figure 3. Free-air gravity anomaly map of the Gorda Ridge and Basin, Mendocino and Gorda escarpments and continental margin of northern California and southern Oregon. Contour interval= 10 mgls. (After Dehlinger et al., 1971)

that the average anomaly over the Gorda Ridge is approximately zero and concluded that the ridge must also be in near isostatic equilibrium. Lateral variations in the negative anomalies north of the Gorda Escarpment and along the base of the slope south of Cape Blanco have been attributed to deformation or segmentation of the downwarped lithospheric plate. A high negative regional anomaly (-70 to -100 mgal) marks the base of the southern Oregon continental slope and is probably due to the dip of the Mohorovicic Discontinuity beneath the continent (Dehlinger et al., 1971; Spigai, 1971). Finally, there is a narrow positive anomaly which extends westward from Cape Mendocino associated with the Gorda and Mendocino Escarpments.

III. Seismicity

Earthquake activity in the Gorda Plate region is represented in Figure 4 by epicentral locations of events occurring between 1853 and 1973 (Couch et al., 1974). Epicenters are offset on the order of a half degree to the northeast of the major physiographic features, perhaps due to inacurrate earth models and biased distribution of seismograph stations (Bolt et al., 1968; Tobin and Sykes, 1968; Northrup, 1970; Seeber et al., 1970). Among these features are the Gorda Ridge, Mendocino and Blanco Fracture Zones, and continental margin. There is considerably higher activity near the proposed triple junction of the Mendocino Fracture Zone, San Andreas Fault, and subducting margin than along the fracture zones and ridges. Also, an unusual amount of seismic activity occurs within the Gorda plate interior which is not observed further to the north on the Juan de Fuca plate.

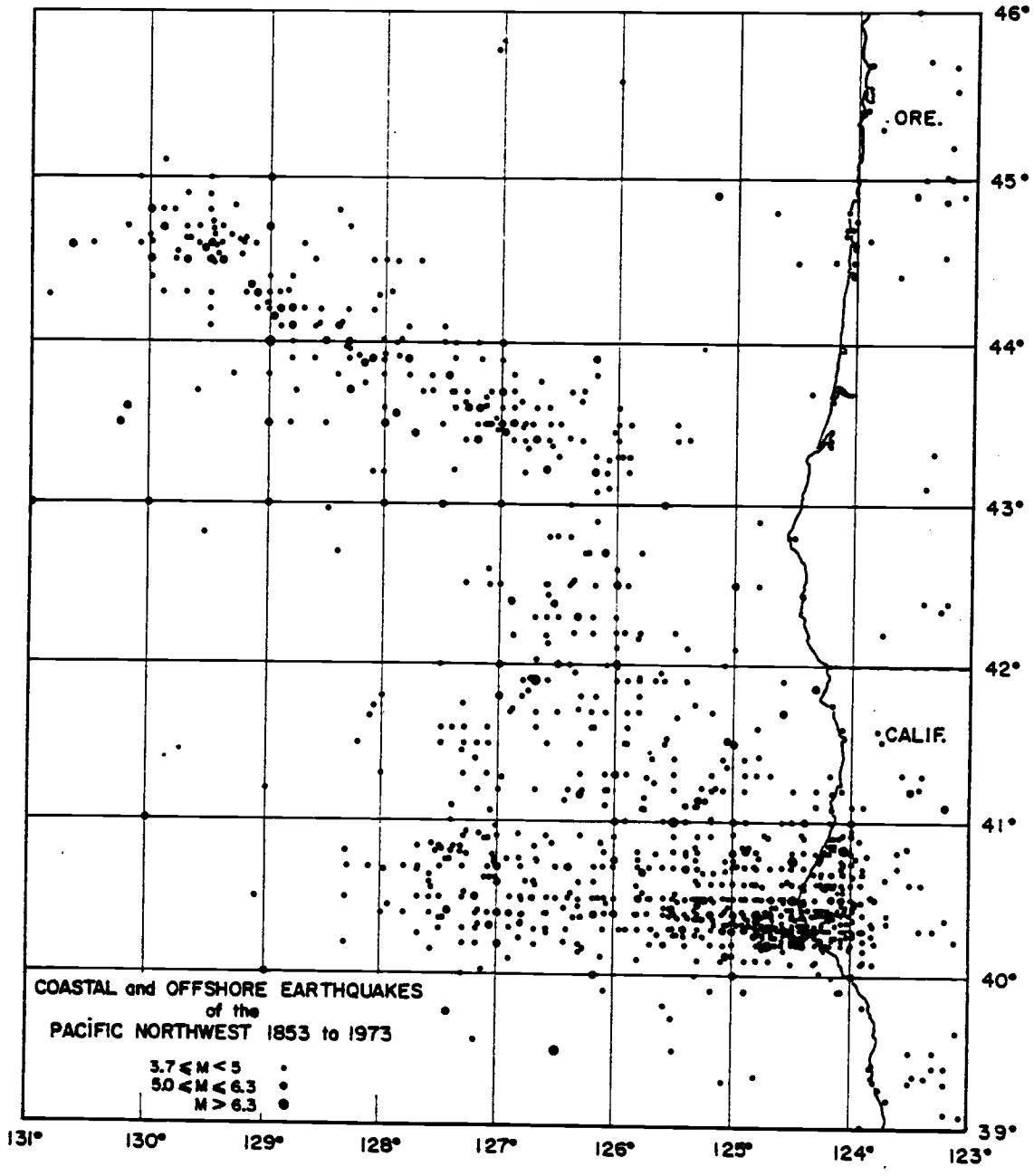

Figure 4. Coastal and offshore earthquakes of northern California, Oregon and Washington. (After Couch et al., 1974)

Fault plane solutions of coastal and offshore earthquakes of northern California and southern Oregon are plotted in Figure 5 (Byerly, 1938; Rinehart, 1964; Tobin and Sykes, 1968; Bolt et al., 1968; Seeber et al., 1970; Chandra, 1974). First motion studies of teleseismic data from the Gorda Ridge have yielded focal mechanisms typical of normal faulting (Chandra, 1974; Tobin and Sykes, 1968). Jones (1975) and Johnson and Jones (1978) on the other hand, observed high-angle reverse faulting using sonobuoy arrays. Atwater and Mudie (1968) deduced from topography that the walls of the Gorda Rise central rift valley are composed of fault blocks, and that normal faulting was associated with the uplift and displacement of these blocks away from the valley center to form the walls. The observed high-angle reverse faulting may be a result of subsidence of these same blocks on the flanks of the rise as they migrate away from the crest (Harrison, 1974). Seismicity trends on the ridge were used by Northrup et al. (1970) to suggest that the change in trend of the Gorda Ridge at 41.6^{o}N latitude represented the location of a new fracture zone.

Seismicity studies in the Gorda Basin by Seeber et al. (1970) revealed that earthquakes occurred north of the Mendocino Fracture Zone but not to the south of it. They demonstrated that right-lateral strike-slip faults radiate northwest from the Cape Mendocino area into the Gorda Basin. Tobin and Sykes (1968), Bolt et al. (1968), and Chandra (1974) interpreted focal mechanisms to indicate right-lateral movement on NW-SE trending faults in the southern Gorda Basin. Silver (1971a,b) concludes that the Gorda Basin is seismically active and that the motion

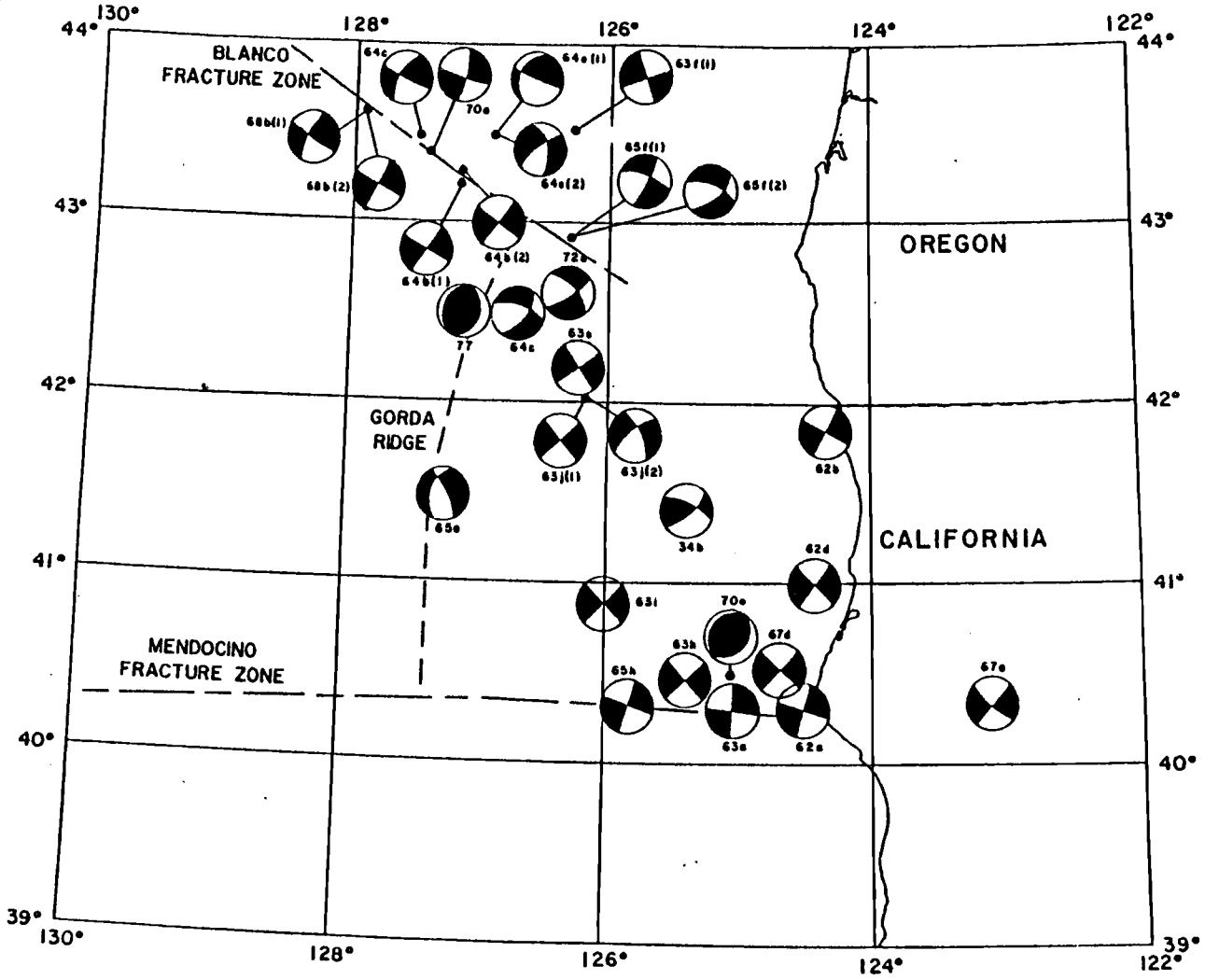

Figure 5. Fault plane solutions of coastal and offshore earthquakes of northern California and southern Oregon. Dark regions show compression. (After Couch et al., 1980).

could either be right-lateral on NW-SE faults or left-lateral on NE-SW faults. In any case, if the region of the Gorda Basin between the Blanco and Mendocino Fracture Zones is considered to be a single lithosphere plate, then the tectonic assumption of rigid plates is being violated (Seeber et al., 1970; Bolt et al., 1968; Nowroozi, 1973; Couch, 1980).

Along the continental margin of northern California and Oregon, seismic activity decreases north of the Cape Mendocino region. Seismicity trends here are unlike those for subduction zones elsewhere in the Pacific. Smith and Knapp (1977) examined hypocenters in the Cape Mendocino area and found that there was considerable activity down to depths of 30 km with a notable absence of earthquakes at typical Benioff zone depths of 300 km.

IV. Seismic Investigations

The first marine refraction experiments conducted in the Gorda Basin used the two-ship method, in which one ship provided the source and the other acted as a receiver. Shor et al. (1968) and Raitt (1963) employed this technique here and found relatively shallow mantle depths (depths between 6 and 8 km below sea level) and low mantle velocity (<8.0 km/sec). Shor et al. (1968) concluded the Gorda Ridge appears to have the same structure as the East Pacific Rise.

The airgun-to-sonobuoy wide-angle reflection technique was used by Wrolstad and Johnson (1976) to determine the velocity structure of the upper sea floor in the Gorda Basin and on the adjacent continental slope. At 41.7°N 125°W on the slope they found five kilometers of

sediment overlying basement with velocity of 5.6 km/sec. At the base of the slope the sediments (V_p = 1.72 to 2.1 km/sec) are 1.3 km thick and the mantle is about 7.5 km below the sea floor. Oceanic layer 2 velocities were observed to vary between 3.9 and 6.2 km/sec within the basin. On the eastern flank of the Gorda Ridge (1.1 M.Y. old crust) layer 2 was seen (6.2 km/sec) at a depth of 1 km below the sea floor.

Several investigators (Silver, 1971b; Keser, 1978; Kulm and Fowler, 1974b) have used single-channel air-gun reflection data to examine sediments of the Gorda Basin and continental slope. Silver (1971b) found sediment thicknesses to vary from an average of about 100 meters on the Gorda rise flanks to greater than a kilometer along the base of the continental slope. He also found a considerable number of northeast trending faults in the Gorda Basin which parallel the magnetic anomalies and appear to cut turbidites that were deposited away from the rise crest. He concluded that the faulting was a later deformation along lines of original mechanical weakness in the oceanic crust. The continental slope was seen to be highly deformed with considerable folding and faulting of the basal reflectors (Kulm and Fowler, 1974b; Keser, 1978; Silver, 1971b). Small basinal features formed on the irregular slope terrain contain lesser deformed sediments, which tend to smooth out the observed topography (Kulm and Fowler, 1974b).

Lithosphere Plate Interactions

The previous sections were designed to review the major results of marine research in the Gorda Basin region over the last twenty years. In this section, we will summarize many of these results as they relate

to the tectonics of interacting lithosphere plates.

The three major lithosphere plates in the region are the Pacific, Juan de Fuca, and North American and are shown in Figure 6. The first two are oceanic plates (crustal thickness $\leq$ 10 km) while the latter is continental (30-70 km crustal thickness). The proposed Gorda plate is the southern quarter of the Juan de Fuca plate, separated by the eastern extension of the Blanco Fracture Zone. To the north and south of this region, the Pacific plate is in direct contact with the North American plate along the Queen Charlotte and San Andreas faults, respectively. The relative motion between these plates is around 5.8 cm/yr (Atwater, 1970). The instantaneous relative motion of any two rigid plates on the surface of a sphere can be represented by a rotation about an axis (McKenzie and Morgan, 1969), the surface intersection of which is called the pole of rotation. The Pacific-North American pole is at about 49°N 74°W (Minster and Jordan, 1978).

Another requirement of rigid plate motion is that the fracture zones lie on small circles about the pole of rotation. Because small circles are non-intersecting, the orientations of the Sovanco, Blanco, and Mendocino Fracture Zones in Figure 6 suggest that the region between the Pacific and North American plates cannot be a single plate. If we just consider the Juan de Fuca plate (that portion normal to the Juan de Fuca Ridge), insufficient data are available for computing a pole for its motion relative to the Pacific. The Blanco Fracture Zone might be a good indicator for this pole position because of its length and age, but its straight trace would prevent the calculation of a convergence point.

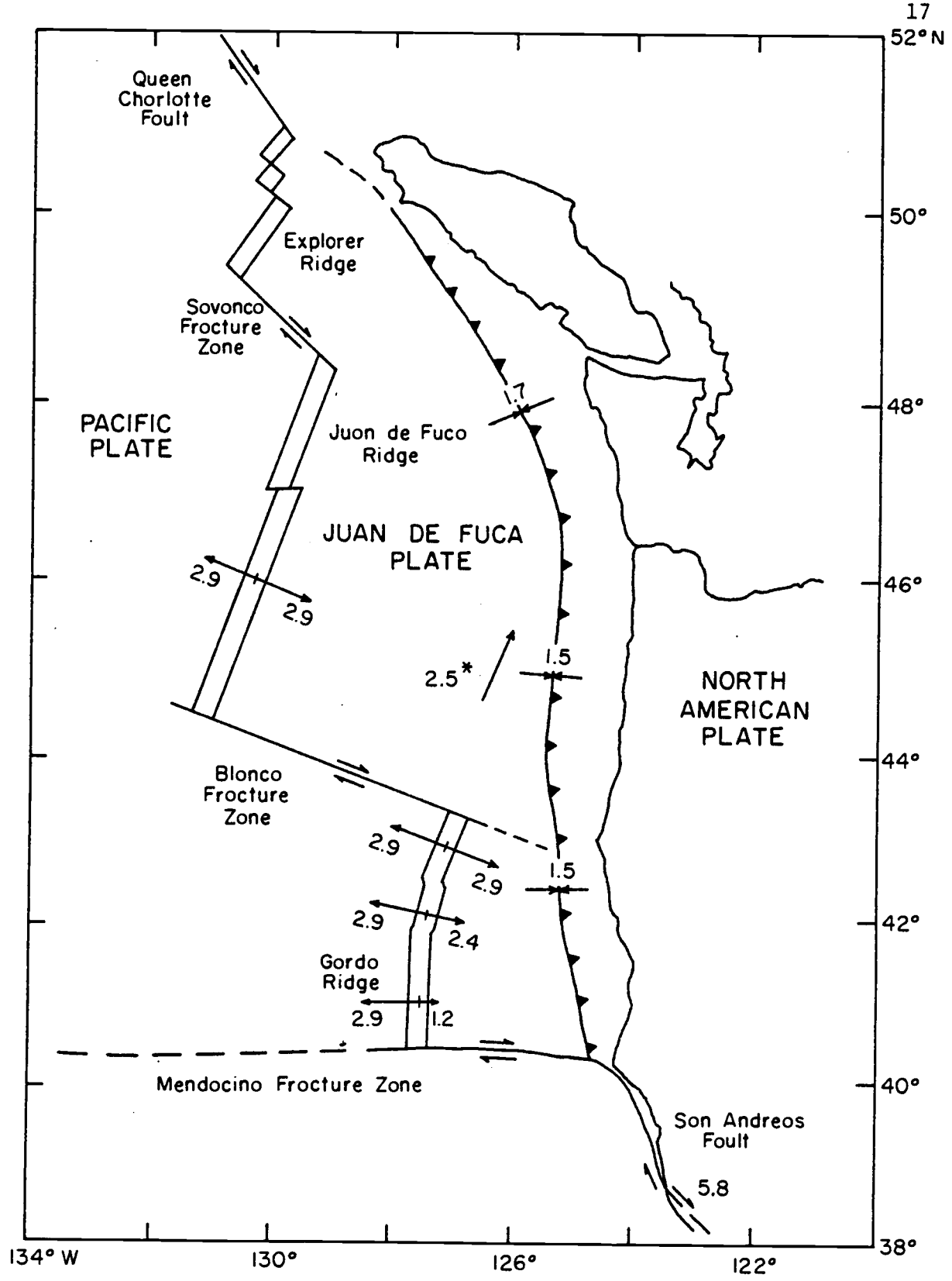

Figure 6. Plate tectonics southwest of Vancouver Island. Spreading rates based on magnetic anomalies for the past 2 M.Y. Convergent rates are components normal to the convergent margin and assume a stationary Pacific plate. * Juan de Fuca plate motion relative to N. America with Pacific plate stationary.

The Gorda plate is further complicated by the fact that the east side spreads asymmetrically with respect to the Pacific side. Thus, we cannot define a pole for the relative motion between the Gorda and Pacific plates. Again, the Mendocino and Blanco Fracture Zones bounding the Gorda plate do not lie on non-intersecting small circles as required by rigid plate theory.

Relative motions between the Juan de Fuca - Gorda plates and the North American plate are also shown in Figure 6. They reflect only the convergence rates in a direction normal to the plate boundary and assume the Pacific plate to be stationary. The total vector for the Juan de Fuca and northern Gorda motion is 2.5 cm/yr in a northeast direction. This amounts to about 1.5 cm/yr of east-west convergence along the continental margin. In the southern Gorda region there is no component of east-west convergence, and the total vector indicates motion parallel to the margin (Gorda moving north relative to North America). This motion may account for some of the strike-slip focal mechanisms of Figure 5 along the continental margin. Finally, we see that the triple junction off Cape Mendocino should be migrating to the northwest if the relative motions are correct.

SEISMIC MODELS

Seismic Refraction Profiles

The two refraction lines used in this study to examine upper lithospheric velocities in the Gorda Basin are shown in Figure 7. Each thirteen-station seismic refraction profile was configured for shooting overlapping refraction lines with more than 300 explosive charges overall. Line I was oriented approximately E-W at 41°15'N and went from the continental shelf break to the eastern crestal hills of the Gorda Ridge, a distance of 240 km. Line II was oriented N-S at 126°12'W and went from the northern portion of the Gorda Basin to the Mendocino Fracture Zone. A description of the method and instruments used on the cruise follows.

Method and Instrumentation

The marine seismic refraction method for this experiment used stationary receivers and moving shot points. Standard military sonobuoys of the type AN/SSQ-41A were seismic detectors for both lines. Sonic information detected by four hydrophones deployed 18 meters below the surface was transmitted from the sonobuoy to the ship by a frequency modulated transmitter in the frequency band of 162 to 174 MHz. The sonic response of these sonobuoys increases 5 db/octave in the 1-1000 Hz range. The transmitted signals were received on a modified police band receiver, amplified, band pass filtered and recorded at 50 mm/sec on an oscillograph camera and on an 8-channel reel-to-reel tape recorder. The camera traces included high frequency, low frequency and

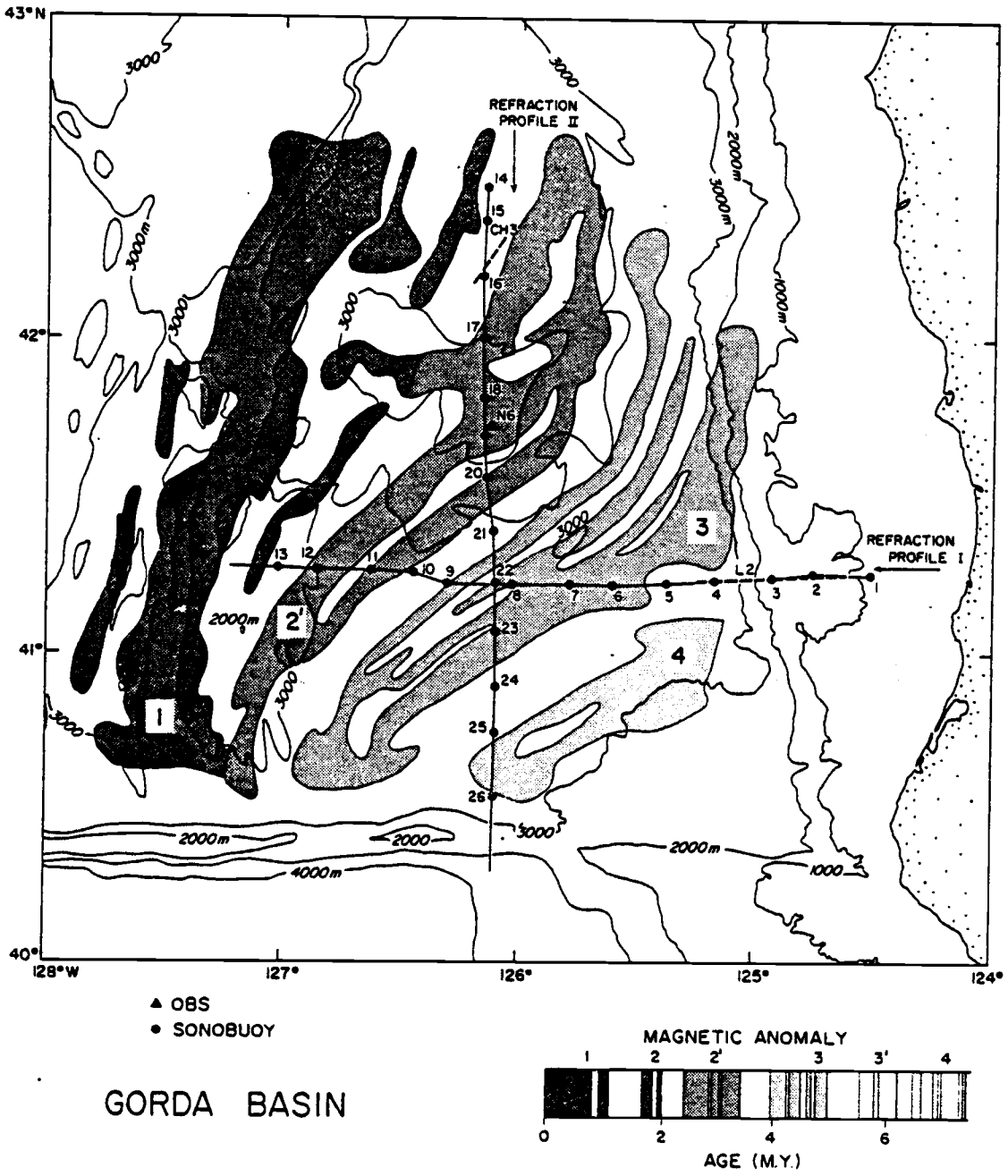

Figure 7. Bathymetry and magnetic anomalies of the Gorda Ridge and Basin and location of seismic lines and instruments. Circles are sonobuoy sites, the triangle is an ocean bottom seismometer position, and dashed lines mark reflection profiles. Bathymetry contour interval = 1000m.

unfiltered sonobuoy signals, clock channel and a signal from the streamer hydrophone which was used to detect the shot break. All traces except the streamer signal were simultaneously recorded analog as well.

For both refraction lines, a continuous line of shots at 5-minute intervals was fired to sonobuoys deployed during the shooting at 1 hour intervals. The size of the shots was varied on a regular time schedule to obtain even coverage at longer distances (Table I). Tovex was used as the chemical explosive with shot sizes varying from .9 to 27.3 kilograms. Overlapping profiles were obtained by deploying sonobuoys at an 18.5 km spacing and recording their transmissions up to a maximum sonobuoy-to-shot distance of over 50 km. For much of the two refraction profiles then, three sonobuoys were detecting and transmitting each shot.

TABLE I. Profile Shooting Schedule.

00 min.	27.3 kg	30 min.	13.6 kg
05	.9	35	.9
10	1.8	40	1.8
15	6.8	45	6.8
20	.9	50	.9
25	1.8	55	1.8

Repeated each hour.

Bathymetry and Navigation

Continuous 3.5 KHz bathymetry was obtained with EPC recorders on all tracklines. Although quite good bathymetric maps already exist for the Gorda Basin, bathymetry was recorded for use in analyzing the explosion data.

The position accuracy of marine seismic refraction profiles depends upon the errors in navigation of the shooting ship and the location of the sonobuoys (Sheriff, 1967). Because sonobuoys are free to drift, they require special techniques for accurate location. The R/V Wecoma navigational aids included satellite navigation, Loran A and C, and Omega. Satellite navigation points, speed and heading readings were used to compute navigation for all tracklines with O.S.U. computer programs. Loran A and Loran C provided accurate supplementary positioning for instrument drop points and shots between satellite fixes.

Navigation, bathymetry, and shot break times were merged using a computer program which computes shot times, shot locations and depths. These data were used for digitizing the analog records and also for plotting the shot locations.

Digitization

Analog to digital conversion of the sonobuoy refraction data was done to optimize data reduction and processing time. Computer programs allowed for automated filtering and plotting of seismic data in digital form. Four channels from the analog tape were digitized simultaneously including the GMT time code and from one to three different sonobuoy channels. After analog to digital conversion of an event, the

multiplexed 4-channel data was then demultiplexed, redigitized, and finally stored on magnetic tape. This procedure was repeated until all events were digitized and stored on tape. Prior to using the filtering and plotting programs, the digitized data was reformatted to match the "ROSE" format for marine seismic refraction data.

Initial Data Reduction

Range Determinations

The first step in analyzing the marine refraction data was to check the ranges between sources and receivers as computed from the navigational data. Because of sonobuoy drift and variations in the shooting ship's speed, navigational determinations for source and receiver positions could induce errors in the plotting of record sections. This may result in the deviation of refracted arrivals from the assumed straight-line fit, or perhaps influence the values of apparent velocities.

Observations of the direct water wave arrivals for all sonobuoys revealed that the navigational method for computing ranges was inadequate for this study, and that another technique should be used. For the second method, sonobuoys were assumed fixed at their satellite determined positions. Direct water wave travel times for each shot were then read from the oscillograph analog records where observed, otherwise first or second bottom bounces were used. A compressional velocity water model was determined by combining a computed shallow water structure with published[1] data for deep velocity structure. A

[1] Handbook of Oceanographic Tables, U.S. Naval Oceanographic Office, SP-68, 1966.

computer program was used to calculate the water velocity model from temperature-salinity data utilizing Wilson's equation (Wilson, 1960). Finally, a ray tracing program computed corrected ranges from the analog data and water velocity model.

The application of this technique to correct shot ranges proved to be extremely valuable in producing record sections free of drift errors in the "X"-direction. However, profile azimuthal orientations could not be uniquely determined. Because the drift is a function of time, subsequent shot-receiver pairs may have sampled different crust in the "y" direction. If the drift is small relative to the X direction sample spacing, however, a two-dimensional model suffices.

Unreversed Solutions

All 26 sonobuoys in this study were unreversed and when treated individually, could yield only apparent layer velocities and thicknesses. For this reason, it was assumed that seismic arrivals were head waves refracted from discrete planar layers that are homogenous and non-dipping throughout the sampling interval for each sonobuoy. This approximation does not allow for lateral variations in velocity or thickness over the range of refracted energy recorded by each instrument. However, longer wavelength variations are acceptable between those sonobuoy sites which do not have overlapping ray-path segments.

Prior to plotting the record sections, corrections were made for the depth of the charge at the time of detonation and for the variation in bottom topography. All the information needed for these corrections is contained in the plot files constructed during assembly of the "ROSE"

tapes. In order to keep the crustal models laterally coherent, all sonobuoy record sections except buoys SB1 and SB2 were corrected to a horizontal datum of 2.786 km (1500 fm). The first two buoys were over the shallower continental slope region and were corrected to a datum of 1.208 km (650 fm). The bathymetry for the Gorda Basin below each refraction line is shown in Figure 7.

Topographic variations of the sea floor were assumed to parallel variations in all interfaces down to and including the mantle boundary. Correcting for the topography was then reduced to computing water delays between the bottom and the datum, and then adding or subtracting these to the observed travel times according to the following equation:

$$\text{Water Delay} = H/V_1 \cos(\sin^{-1} V_1/V_2),$$

where H is the depth difference between the datum and seafloor and V_1 is the seismic velocity of water. The uppermost crustal phase velocity (V_2) was assumed constant for the entire section (5.0 km/sec). This value was chosen prior to analyzing the data and reflects the commonly observed first refractor from previous marine refraction studies of oceanic crust.

Record sections were constructed such that each seismogram is plotted versus reduced travel time for a reducing velocity of 5.0 km/s. The reduced plots (T_R vs. X) are related to normal T vs X plots by a rotation of the time (T) axis given by

$$T_R = T - X/V_R,$$

where X is the shot-receiver distance and V_R is the reducing velocity. This type of plot allows for seismograms to be displayed in less area

and with less distortion in the higher velocities. A refractor with a velocity of 5.0 km/sec would plot as a straight horizontal line.

Record Section Descriptions

The record section plot of sonobuoy SB20 and a simple non-dipping layer solution is shown in Figure 8. At the top of each seismogram is the corresponding shot number and shot size in pounds. Across the extreme top of the figure is a plot of the topographic correction in seconds used for each shot. Arrival times were chosen on the basis of changes in amplitude, period and wave shape. Digital bandpass filtering was achieved using an 8th order Chebyshev bandpass filter set at 5-20 Hz. This particular filter has sharp rolloff characteristics which are needed to eliminate any unwanted noise at frequencies close to the range of refracted seismic energy. In first motion studies, a strong first impulse is desired for obtaining accurate velocity determinations. Because the Chebyshev filter is causal (i.e. impulse response = 0 for time < 0), the first motion recorded for the refracted signal remains undistorted.

Refracted arrivals are fairly well defined for layers with apparent velocities of 5.23, 6.87, and 7.89 km/sec. These layer velocities are nearly identical to Pacific Ocean averages for Layer 2 (transition layer), Layer 3 (oceanic layer), and mantle, respectively (Shor et al., 1970). A further treatment of this designation will appear in a later section. The direct water wave (1.49 km/sec) and first bottom bounce arrivals (R_1) are also indicated on the record. As usual with the explosion-to-sonobuoy technique, the refracted

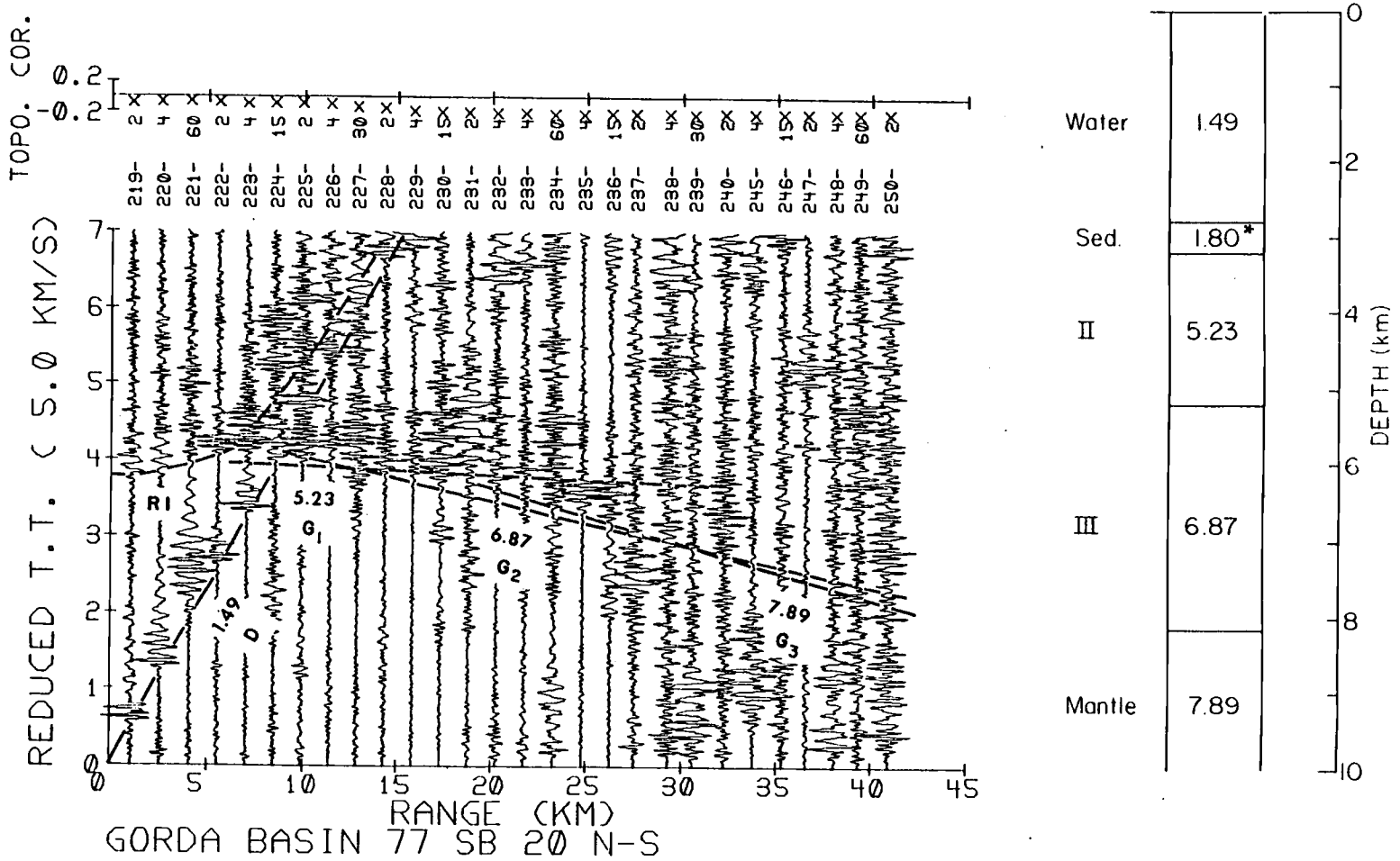

Figure 8. Sonobuoy SB20 reduced record section and velocity-depth model interpretation. Apparent seismic velocities shown in km/sec. Above each seismogram is listed the shot number and charge weight in pounds, and a plot of topographic corrections in seconds. * Assumed interval velocity.

arrivals from the sediment layer are not observed because of the water depth (~3.0 km) and relatively large shot spacing. Couch et al. (1978) used refraction and DSDP data from the Cascadia Abyssal Plain to construct an average velocity versus depth function for sediments. This relationship was applied to sediments in the Gorda Basin, using a thickness range of .1 - .5 km (Silver, 1971b) for the regions underlying sonobuoys SB6-SB26 to obtain an interval velocity of 1.8 km/sec.

The simple non-dipping layer solution for this sonobuoy was obtained by inputing layer velocities, refraction travel time intercepts ($x = 0$), hydrophone depth, and depth of the topographic datum into a computer program ("LAYER"). The program makes corrections for the hydrophone depth and uses a formula modified after Adachi (1954) for computing layer thicknesses from velocities and intercepts.

The layer velocities and thicknesses obtained for this sonobuoy are not unlike those for buoys SB3-SB26. It should be noted however, that the 7.89 km/sec (mantle) refractor was determined from both first and second arrivals, and was not seen clearly on all the records. Because of background noise, reflected refractions, variable time delays, small shot sizes and short ranges, choosing those arrivals from some of the records caused considerable ambiguity in the velocity and intercept values obtained. To reduce this problem, only those records showing higher signal/noise ratios and containing shot returns out to a range of about 40 km or more were considered for picking of mantle arrivals.

While most of the sonobuoy sites were located in the Gorda Basin or on the flanks of the Gorda Rise, buoys one and two were dropped over

the continental slope and required slightly different analysis. The record section plot for sonobuoy SB2 and a simple, non-dipping layer solution is shown in Figure 9. The final plot is reduced to 5.0 km/sec although a reduction at 3.0 km/sec was used to pick the low velocity refracted arrivals (layer b = 2.38 km/sec). As with sonobuoy SB20, seismic arrivals were observed having velocities typical of Layer 2 (5.29 km/sec) and Layer 3 (6.98 km/sec). In addition to the three layers mentioned above, a fourth layer was also indicated on buoys SB1 and SB2 with a seismic velocity of 3.9-4.0 km/sec (Layer c). No mantle refractions were discernible on either of these records.

The poor quality of the record sections from the continental rise was not entirely unexpected and may be attributed to several factors. First, the irregular topography and high relief of the region may cause false delays of refracted waves when correcting the depth to a single datum. Second, the structure of continental rises around the Circum-Pacific belt is generally quite complex (Kulm and Fowler, 1974b; Seely et al., 1974), and seismic arrivals from this region may contain many refractions, reflections and diffractions as a result. In this study, only the strongest refracted arrivals were considered even though intermediate layers probably exist. A third cause for the noisy records may be attributed to data acquisition problems. At the beginning of a marine sonobuoy refraction profile, radios must be tuned, filter amps adjusted, and adjustments made on the analog recording system. Until these refinements are made, unwanted noise may appear on the analog records and eventually get transferred to the record sections.

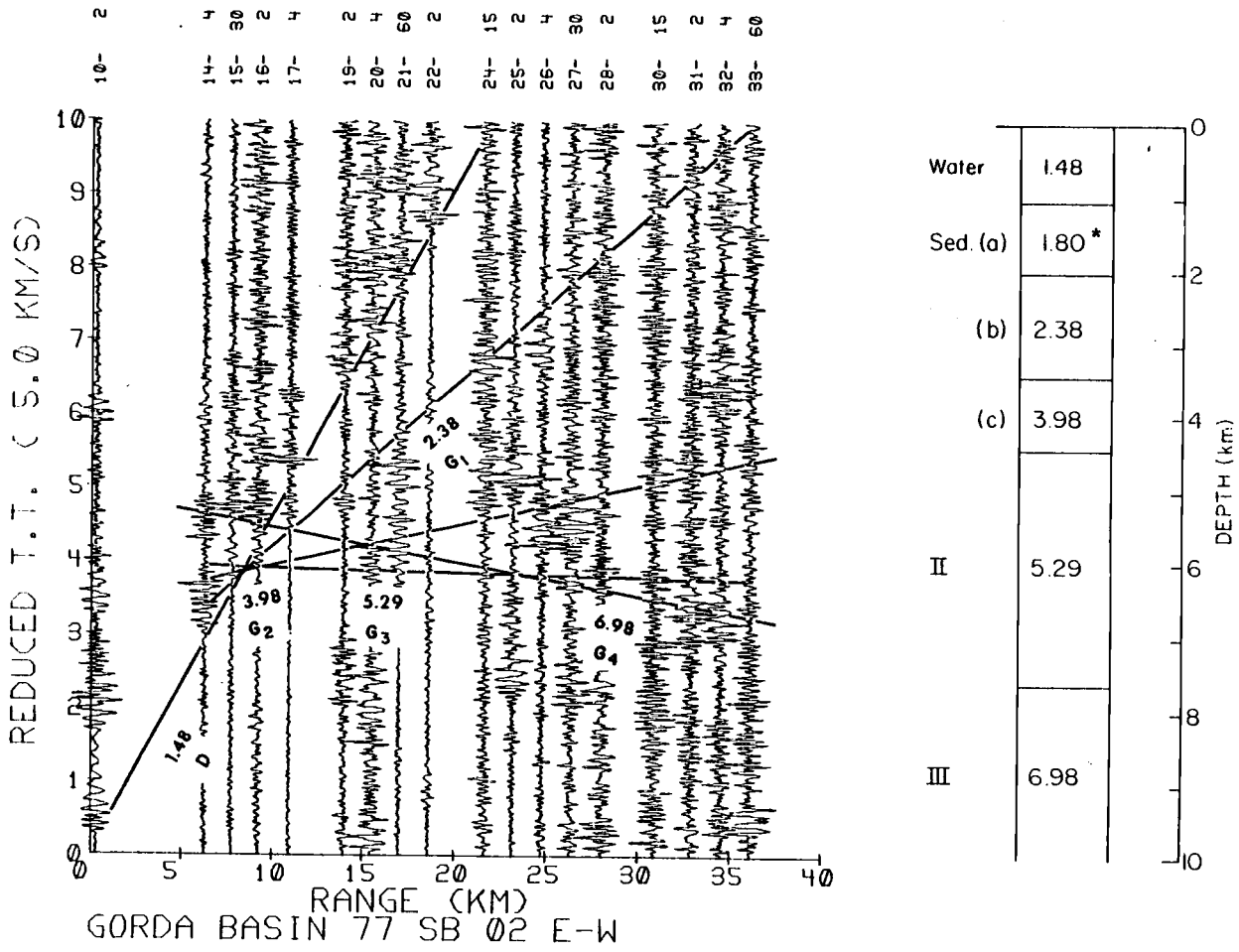

Figure 9. Sonobuoy SB2 reduced record section and velocity-depth interpretation. Apparent seismic velocities in km/sec. * Assumed interval velocity.

Summary of Unreversed Refraction Profiles

The record section plots of all 25 sonobuoy refraction profiles are shown in Appendix II with major refractor returns and velocities marked on each. Sonobuoy SB5 is not shown because of an absence of shot returns beyond a range of 15 km, thereby yielding no information on the oceanic crust. The plots are reduced at 5.0 km/sec and are corrected to a topographic datum of 2.786 km (buoys SB1 and SB2 are corrected to 1.208 km). Summaries of the unreversed plane layer solutions are listed in Tables II, III, and IV. Because these solutions assumed horizontallity of the refracting horizons, thickness determinations were plotted directly beneath the receivers to produce the two-dimensional cross-sections shown in Figures 10 and 11.

East-West Profile I

Results from the continental rise portion of profile I are given in Table II. Seismic returns from Layers 2 and 3 were observed in this region but were delayed due to the presence of at least two horizons not seen in the basin. These horizons, marked b and c, have average thicknesses of 1.6 and 1.0 km, respectively. Figure 10 shows a pinch-out of both layers towards the base of the slope as a simplified interpretation although a more complex geometry probably exists. A similar problem occurred in representing the uppermost sediment layer (assumed velocity of 1.8 km/sec). The one-kilometer thicknesses obtained along flat lying portions of the continental rise may be a fair approximation in contrast to the over-simplified geometry across the steep portion of the slope. The transition zone marked on the cross-section signifies

TABLE II. Receiving positions, seismic velocities, and layer thicknesses for the Northern California Continental Rise from sonobuoy refraction.

	SB01	SB02
Position (Lat., Long.)	41.257°N,124.503°W	41.262°N,124.741°W
Azimuth (Deg.)	271	267
Layer Velocities (km/sec)		
water	1.48	1.48
a	1.80*	1.80*
b	2.53	2.38
c	3.89	3.98
II	5.11	5.29
III	6.85	6.98
Layer Thicknesses (km)		
water	.714	1.17
a	.980	.973
b	1.77	1.42
c	1.02	1.02
II	3.57	3.19

* Assumed Interval velocities
All other velocities are apparent.

Table III. Receiving positions, seismic velocities, and layer thicknesses for the Gorda Basin and rise flanks from sonobuoy refraction. * Assumed interval velocities. All other seismic velocities are apparent.

STA	POSITION (lat,long)	AZM (deg)	VELOCITY (km/sec)					THICKNESS (km)			
			WATER	a*	II	III	MANTLE	WATER	a	II	III
SB03	41.249°N,124.955°W	267	1.48	2.15	5.22	7.18	8.53	1.544	2.66	3.19	3.63
SB04	41.237°N,125.160°W	268	1.48	2.15	5.31	7.23	-	3.092	1.41	2.65	-
SB06	41.220°N,125.600°W	269	1.48	1.80	5.15	7.06	8.19	3.092	0.68	2.15	4.13
SB07	41.217°N,125.772°W	270	1.48	1.80	5.22	7.05	-	3.063	0.56	2.36	-
SB08	41.218°N,126.000°W	272	1.48	1.80	5.17	6.76	-	3.076	0.51	2.64	-
SB09	41.228°N,126.318°W	284	1.48	1.80	5.30	6.88	8.09	3.039	0.21	2.82	3.19
SB10	41.257°N,126.435°W	271	1.48	1.80	5.27	6.77	-	3.042	0.43	1.88	-
SB11	41.262°N,126.643°W	271	1.48	1.80	5.14	6.92	-	3.070	0.38	1.79	-
SB12	41.266°N,126.857°W	272	1.48	1.80	5.22	6.77	7.94	3.117	0.10	1.98	3.27
SB13	41.271°N,127.035°W	272	1.48	1.80	5.24	6.73	-	2.707	0.27	1.76	-
SB14	42.485°N,126.154°W	184	1.49	1.80	5.59	6.70	8.00	2.779	0.36	1.53	3.52
SB15	42.371°N,126.162°W	183	1.49	1.80	5.54	6.76	7.87	2.686	0.27	1.59	3.78
SB16	42.203°N,126.172°W	178	1.49	1.80	5.24	6.67	-	2.655	0.18	1.76	-
SB17	42.007°N,126.164°W	178	1.49	1.80	5.18	7.16	-	3.065	0.24	3.08	-
SB18	41.828°N,126.159°W	179	1.49	1.80	5.11	6.83	-	2.922	0.38	1.87	-
SB19	41.709°N,126.156°W	177	1.49	1.80	5.36	7.01	-	3.144	0.39	2.49	-
SB20	41.563°N,126.149°W	171	1.49	1.80	5.23	6.87	7.89	2.810	0.40	2.00	2.96
SB21	41.399°N,126.122°W	174	1.49	1.80	5.35	6.88	-	3.030	0.44	1.83	-
SB22	41.232°N,126.104°W	180	1.49	1.80	5.16	6.78	-	3.055	0.31	2.17	-
SB23	41.069°N,126.103°W	180	1.49	1.80	5.16	7.08	-	3.067	0.53	2.69	-
SB24	40.893°N,126.102°W	180	1.49	1.80	5.20	6.83	-	3.116	0.67	2.51	-
SB25	40.744°N,126.102°W	181	1.49	1.80	5.24	6.67	8.04	3.112	0.61	3.06	2.98
SB26	40.539°N,126.104°W	182	1.49	1.80	5.38	7.06	-	3.102	0.87	2.87	-

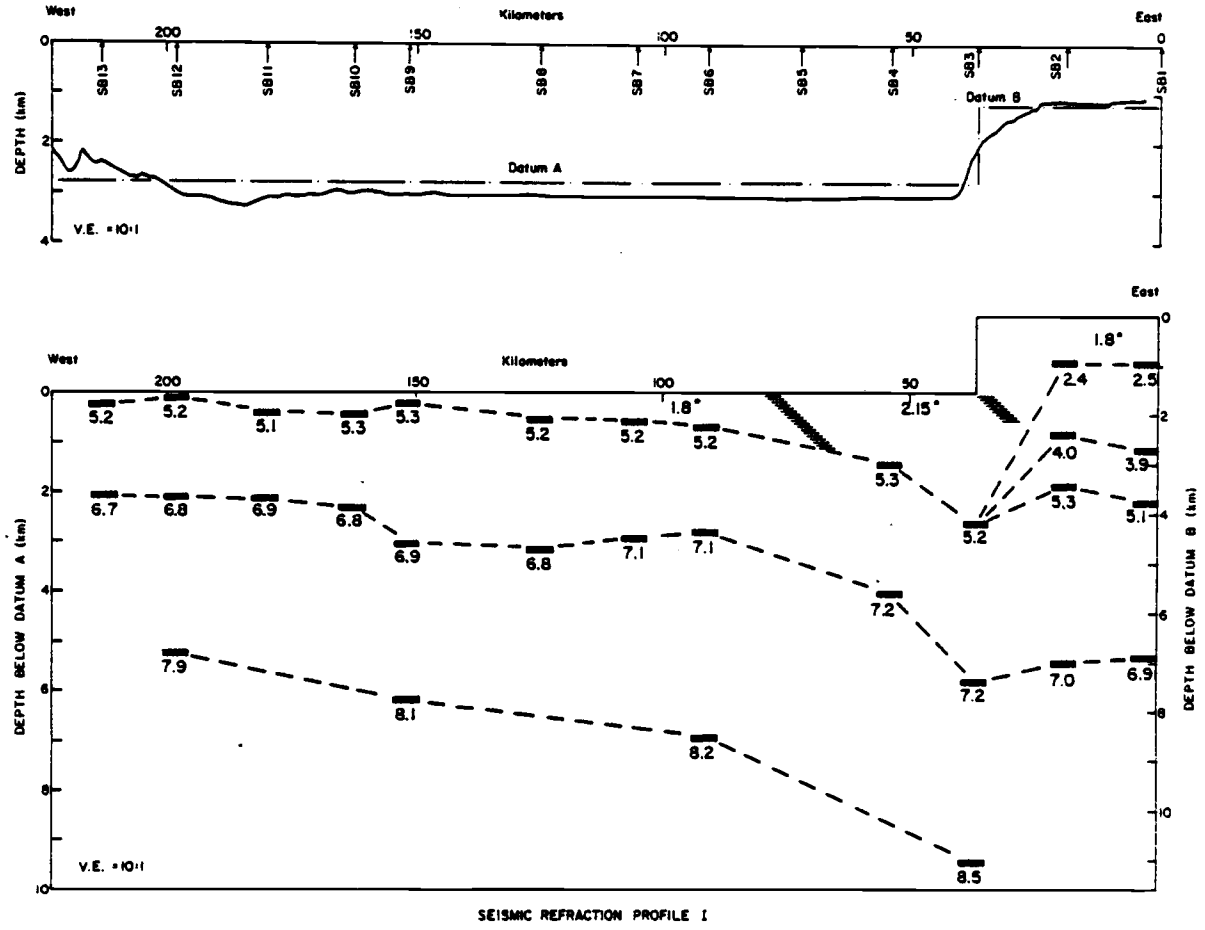

Figure 10. East-west seismic structure section summarizing the subdatum velocity and depth information computed from unreversed refraction data. The upper profile shows bathymetry and instrument positions along this line. * Assumed interval velocities (km/sec), all other velocities are apparent.

a change in assumed interval velocities for these sediments.

The tops of Layers 2 and 3 display a general upward dip from the base of the slope eastward to the continent. This may be only an apparent effect caused by the inability to resolve all the refractors. Even though the thickness determinations for Layer 2 may be correct (~3.4 km), depth calculations to the top of this horizon are dependent upon the accuracy in defining the overlying structure.

The absence of mantle returns is most likely an operational effect related to short profile lengths and low S/N data. Based on results west of the slope, the top of the mantle dips from 1.0-1.5 degrees towards the continent and probably extends under the slope region.

Progressing westward across the Gorda Basin from the base of the slope to the rise flanks, the oceanic crust is seen to follow a relatively constant geometry. The tops of Layers 2, 3 and mantle all have gentle (1.0 degree) landward dips which increase to greater than 1.5 degrees at the eastern edge of the basin. There is an increase in apparent velocities for Layer 3 and mantle associated with this dip (7.2 and 8.5 km/sec, respectively). As expected, higher apparent velocities are obtained when profiles extend in the up-dip direction. Excluding the sediment layer, the crust thickens slightly from greater than 5 km near the ridge to about 6 km at the slope with notable depth variations occurring at the Layer 2/3 interface in the central portion of the basin. The sediment cover parallels this structure and also thickens considerably from less than 100 m on the rise flanks to about 2.7 km near the base of the continental slope. The transition zone between the two assumed interval velocities was positioned based on results of Silver (1971b) and Couch et al. (1978).

North-South Profile II

The north-south cross section (Figure 11) is very similar to the basin portion of profile I in that there is also a slight crustal thickening from greater than 5 km in the north to about 6 km near the Mendocino Fracture Zone to the south. Sediments thicken southward from a few hundred meters up to around one kilometer. Again, there is a down-dip associated with this thickening but of magnitude less than a degree in profile II. The major feature of this profile is the large depth perturbation of the Layer 2/3 interface near sonobuoy SB18 and an associated crustal thinning to about 4 km. Data plotted on the cross section includes results from an ocean bottom seismometer which will be described later.

In summarizing Tables II and III, averages and standard deviations were computed for the sonobuoy results and are listed in Table IV. A comparison of the average Gorda Basin crust from unreversed sonobuoys with a composite Pacific Ocean crustal section (Shor et al., 1970) is shown in Figure 12. It is seen that when averaged, the single ended refraction lines yield layer velocities and a total crustal thickness consistent with the ocean-wide averages.

Ocean Bottom Seismometer Results

Prior to shooting the two refraction profile lines, several ocean bottom seismometers (OBS) were deployed for the primary purpose of monitoring microseismic activity throughout the Gorda Basin. One of these instruments, OBSN 6, was located near sonobuoy SB19 (see Figure 7) and recorded seismic returns from shots in two different directions. The

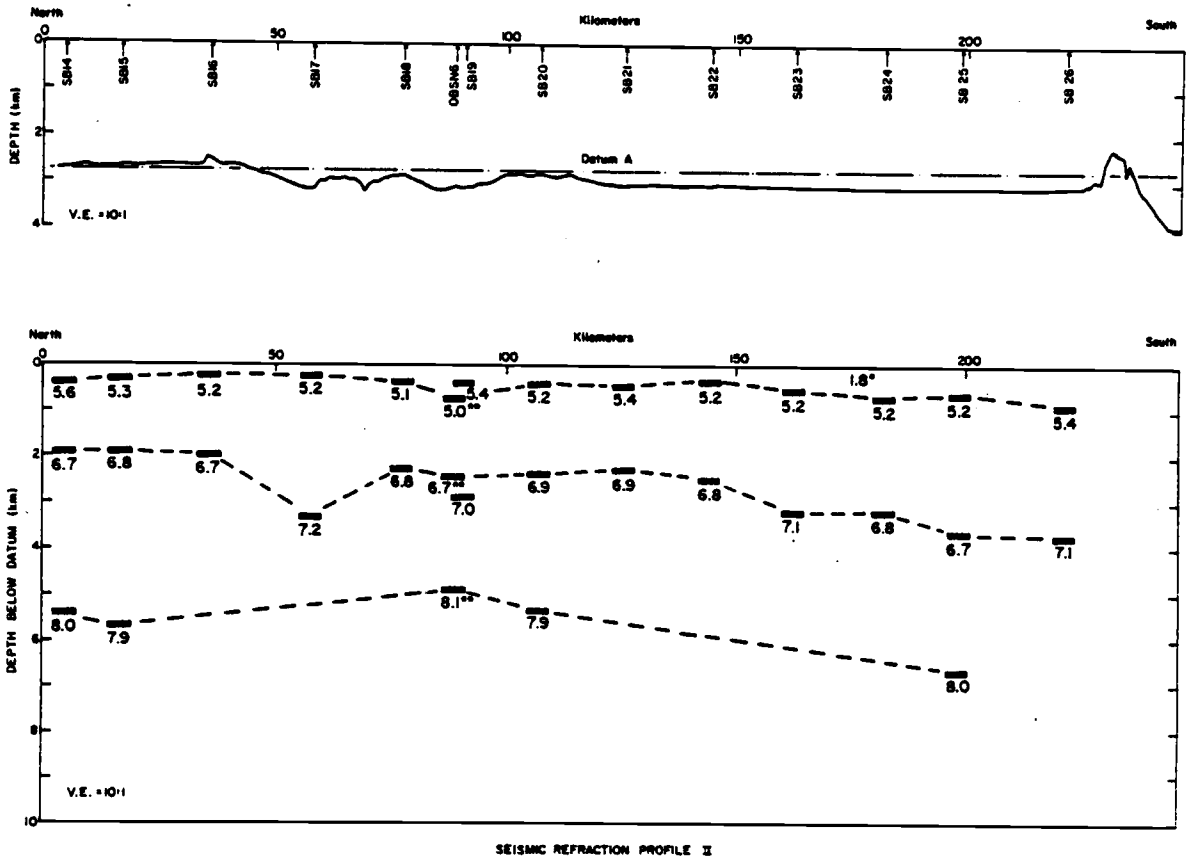

SEISMIC REFRACTION PROFILE II

Figure 11. North-south seismic strucure section including split-spread results from OBS N6 and the bathymetry profile. * Assumed interval velocities(km/sec), ** true layer velocities, all other velocities are apparent.

TABLE IV. Statistical summary of Gorda Basin seismic structure from single-ended sonobuoy refraction data.

Layer	Velocity (km/sec)				Thickness (km)			
	No. of Stations	Average	St.Dev.	Range	Stations	Average	St.Dev.	Range
Sediment	23	(1.8-2.15)*	--	--	23	.56	.53	.1-2.66
Layer 2	25	5.26	.12	5.11-5.59	23	2.29	.51	1.53-3.19
Layer 3	25	6.90	.17	6.67-7.18	8	3.43	.41	2.96-4.13
Mantle	8	8.07	.21	7.87-8.53	--	--	--	--

*Assumed interval velocities

All other velocities used were apparent.

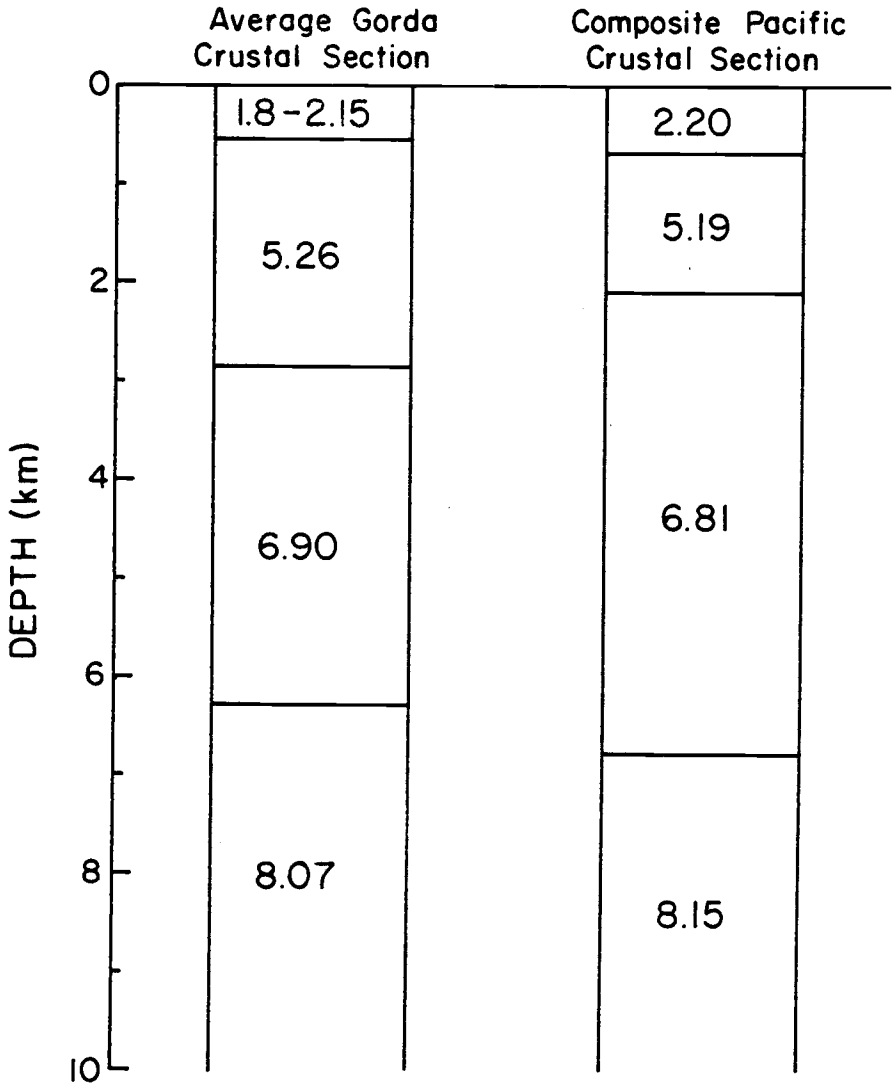

Figure 12. Comparison of the average seismic structure from the Gorda Basin with a composite Pacific Ocean crustal section (after Shor et al., 1970).

geometry for this refraction profile is called a "split-spread" line and it permits the calculation of true layer velocities and thicknesses. Because the OBS is anchored directly to the sea floor, seismograms recorded from the geophones commonly have higher S/N ratios than those from sonobuoys and contain only one water column ray path. For these reasons, OBSN6 was used as a base reference for correlation with the sonobuoy results.

The OBS is a free-fall direct recording type developed at Oregon State University (Johnson et al., 1977). Recording is continuous analog using low-frequency amplitude modulation and designed for a bandpass of approximately 2-40 Hz. After recovery of the instrument, the analog tape was processed in much the same manner as the sonobuoy data. Events were digitized, put into ROSE format and stored on magnetic tape. The sonobuoy plotting programs are compatible with OBS data, and filtered record sections were routinely made for refraction interpretation.

Figures 13 and 14 are the north and south halves of the OBS refraction line, respectively. Refracted arrivals from Layers 2, 3 and mantle were observed on both ends. The analysis of the data follows the method of Johnson (1976) who described the interpretation of split-spread refraction lines using the formula of Adachi (1954). Assumptions of the method are that the profiles be linear, that refractions are from homogeneous plane dipping layers, and that layer velocities increase with depth.

Results from OBS N6 are listed in Table V and illustrated in Figure 15, which compares the computed depth section with those of adjacent sonobuoys SB18, SB19 and SB20. As with the sonobuoy data,

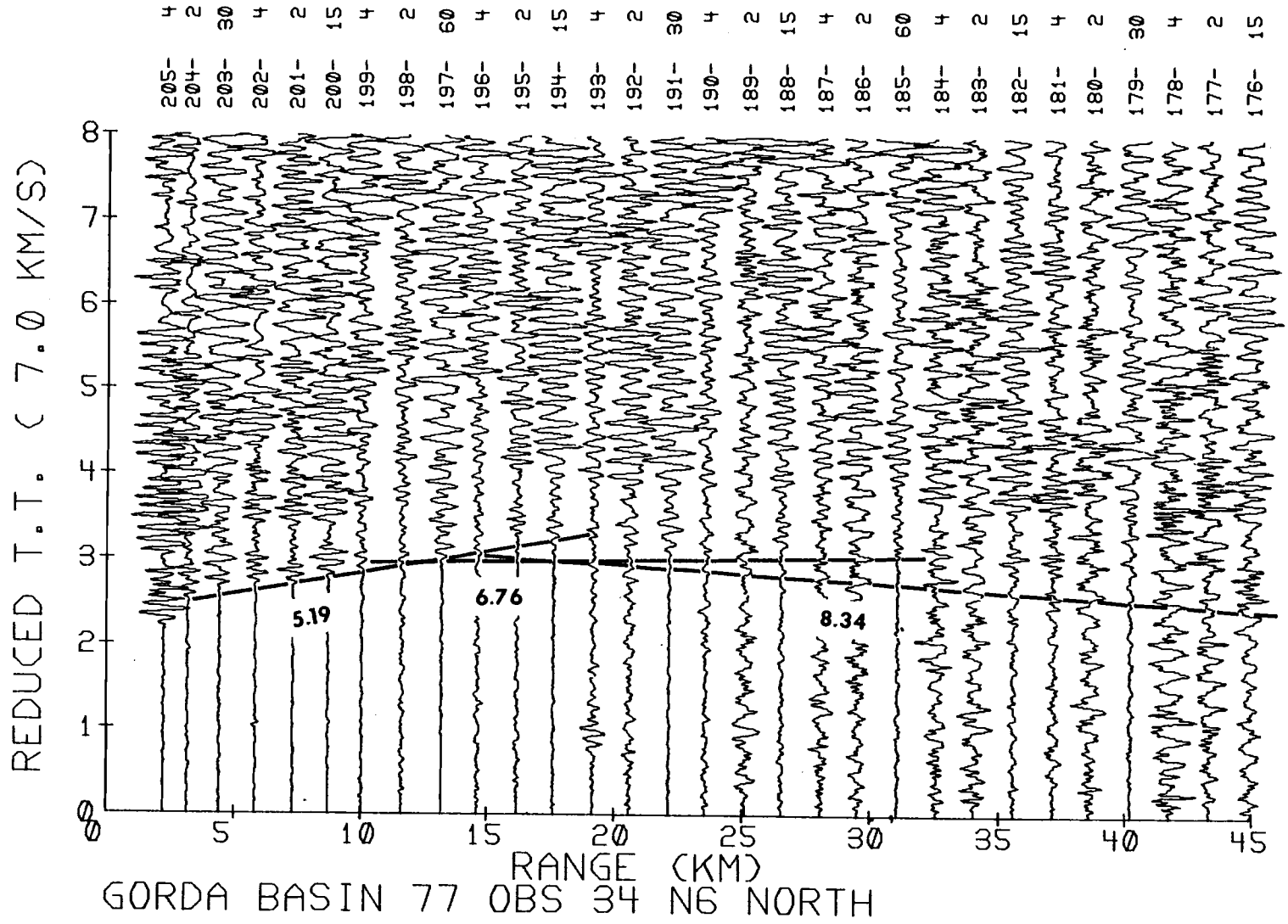

Figure 13. Ocean bottom seismometer N6 (north end) reduced record section. Apparent velocities,km/s.

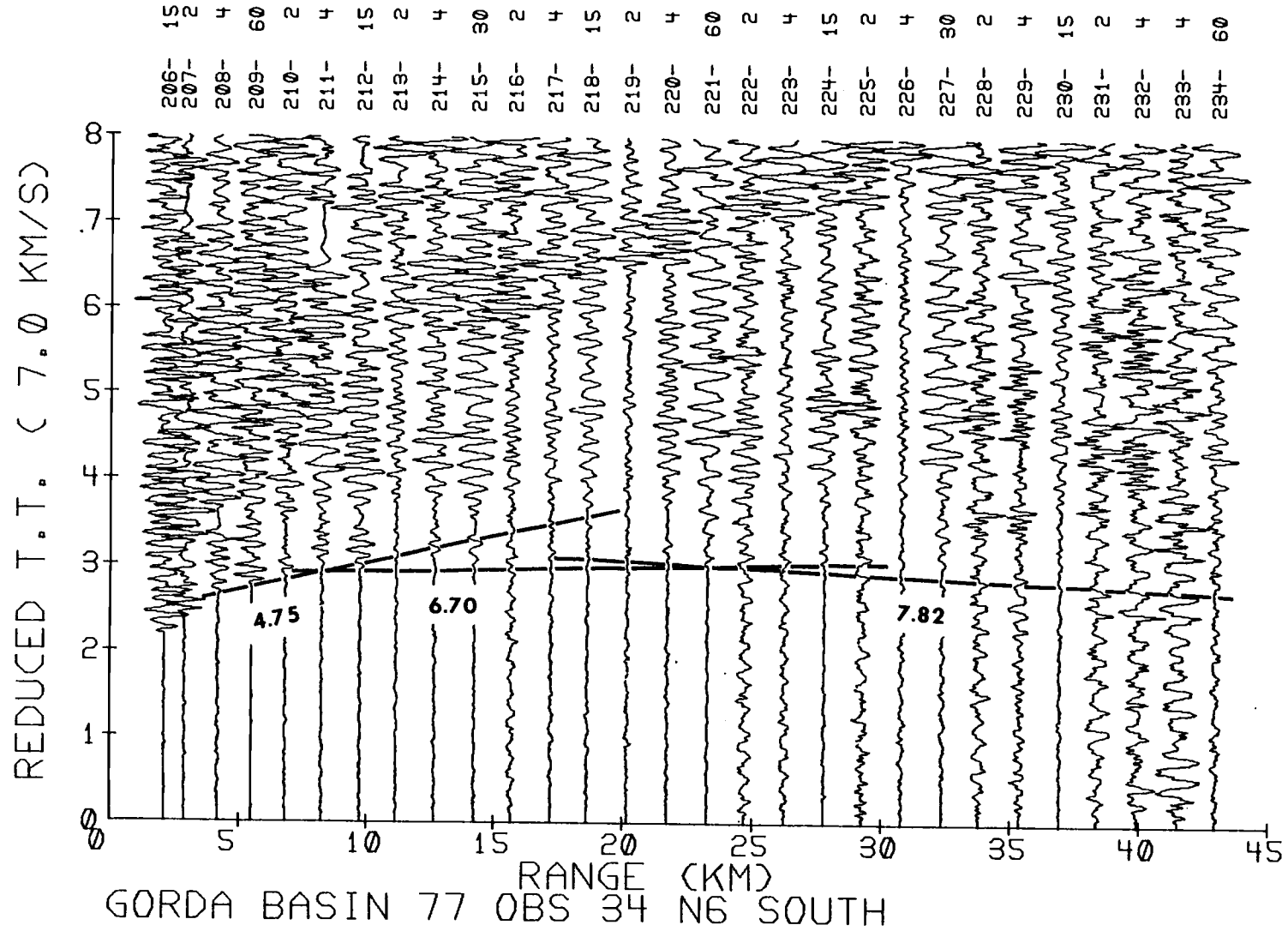

Figure 14. OBS N6 (south end) reduced record section. Apparent seismic velocities in km/sec.

TABLE V. Receiving position, seismic velocities, and layer thicknesses for ocean bottom seismometer OBS N6.

Location, OBS N6 41.742°N, 126.156°W

Water Depth 3.140 km

Layer	Apparent Velocity (km/sec) North	Apparent Velocity (km/sec) South	True Velocity	Layer Thickness	DIP (Deg, N-S)
Sediment	1.8*	1.8*	1.8*	.31	-.99
Layer 2	5.19	4.75	4.96	1.71	2.62
Layer 3	6.76	6.70	6.72	2.38	-.63
Mantle	8.34	7.82	8.06	--	--

* Assumed interval velocities.

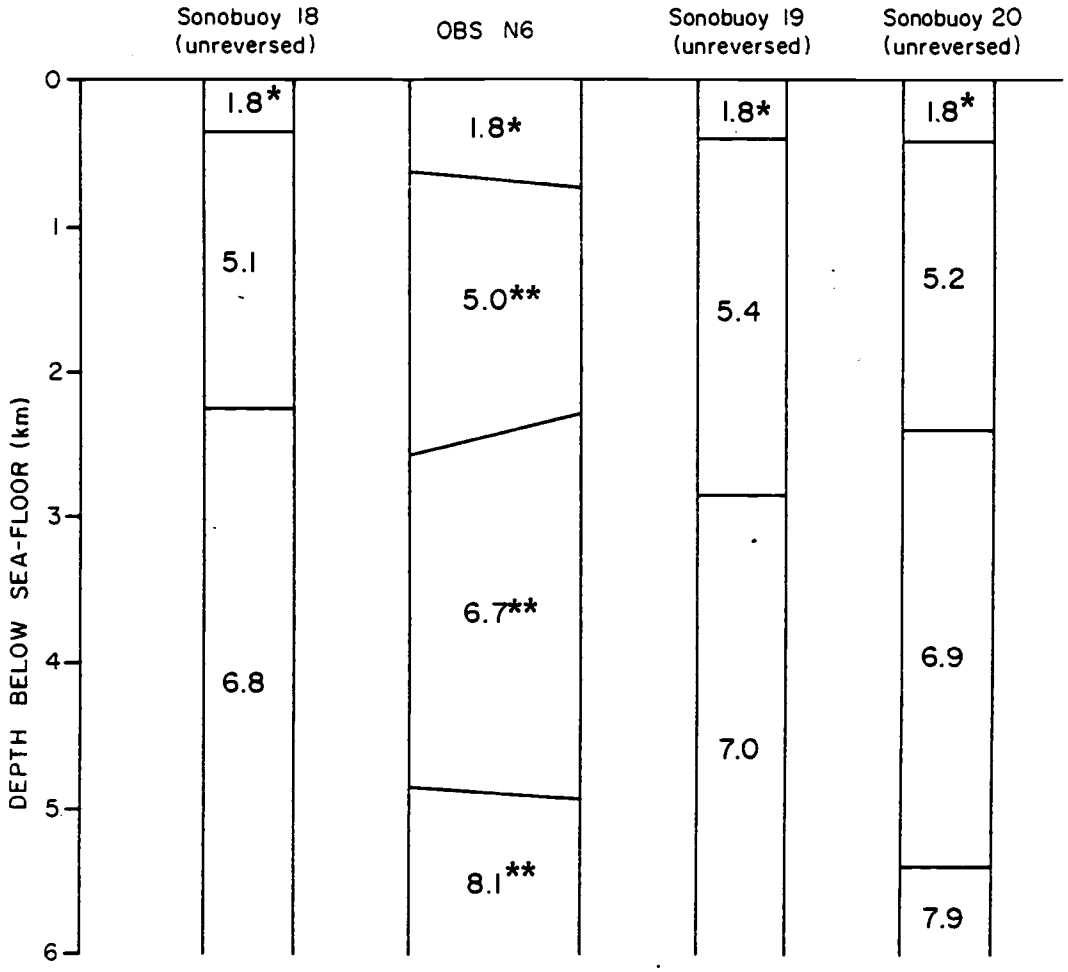

Figure 15. Split-spread refraction interpretation for OBS N6 and results from adjacent sonobuoy sites SB18, SB19 and SB20. * Assumed interval velocities, ** true layer velocities, all other velocities apparent (km/sec).

refracted arrivals from the upper sediment layer were not resolvable and an assumed velocity of 1.8 km/sec was used. The true layer velocities calculated for the OBS (5.0, 6.7 and 8.1 km/sec) are in fairly close agreement with the Gorda Basin sonobuoy averages (5.25, 6.90 and 8.08 km/sec) although the computed mantle depth (4.4 km below the sea floor) is slightly less than seen elsewhere. This difference could be caused by using incorrect apparent velocities for sonobuoy structure sections or by the actual existence of a locally thin crust. Trends observed in the cross section of Figure 11 suggest that the crust does thin near the region of OBS N6 to less than 5 km.

Delay-Time-Function Method

The initial method used in processing the marine seismic refraction profiles was useful in that it parameterized the data, reducing a large number of travel times to a few layer velocities and thicknesses. However, the unreversed lines yield apparent layer velocities and thicknesses which may not represent the actual earth structure sufficiently for detailed analysis. Another method was therefore employed which utilized the overlapping design of the profiles to determine true layer velocities and allow for undulations in the previously assumed horizontal and planar interfaces. This is the delay-time-function method used by Rosendahl et al. (1976) and discussed by Morris (1972). The method is a linear multilayer generalization of the delay time function method originally developed by Morris et al. (1969) and Raitt et al. (1969) for investigating mantle anisotropy. It is related to the delay-time method of Gardner (1939) and the time-term method of

Scheidegger and Willmore (1957) and Willmore and Bancroft (1960). The major difference of this newer version is that a delay surface is represented by some simple mathematical function of position instead of calculating delay times for each shot and receiver position. A summary of the theory and techniques of the method is discussed in the following sections.

Theory

A delay time is defined as the ray path time between a datum and the refractor minus the time necessary to travel the normal projection of the ray path on the refractor (Barry, 1967). For the single layer case shown in Figure 16a, the delay time τ_i for the shot is given by

$$\tau_i = t_{OB} - \overline{AB}/V_2 \qquad (1)$$

where t_{OB} is the travel time of the downgoing ray along path $\overline{OB}$ ($t_{OB} = \overline{OB}/V_1$), $\overline{AB}$ is the horizontal component of $\overline{OB}$, and V_2 is the velocity of the lower horizon. Making a trigonometric substitution for $\overline{AB}$ using the angle of incidence (α) of the downgoing ray, (1) becomes

$$\tau_i = \overline{OB}/V_1 - (\overline{OB}\ \sin\alpha)/V_2 \qquad (2)$$

For the critically refracted wave,

$$\sin\alpha = V_1/V_2,\ \overline{OB} = Zi/\cos\alpha \qquad (3)$$

where Zi is the thickness of the first layer. Equation (1) is then reduced to the following:

$$\tau_i = Zi/V_1\ (1 - V_1^2/V_2^2)^{\frac{1}{2}} \qquad (4)$$

A similar expression is obtained for the receiver delay.

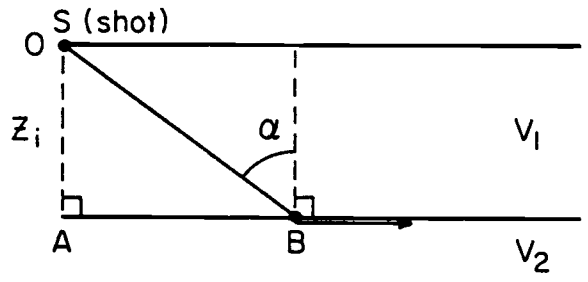

Figure 16a. Critically refracted ray path.

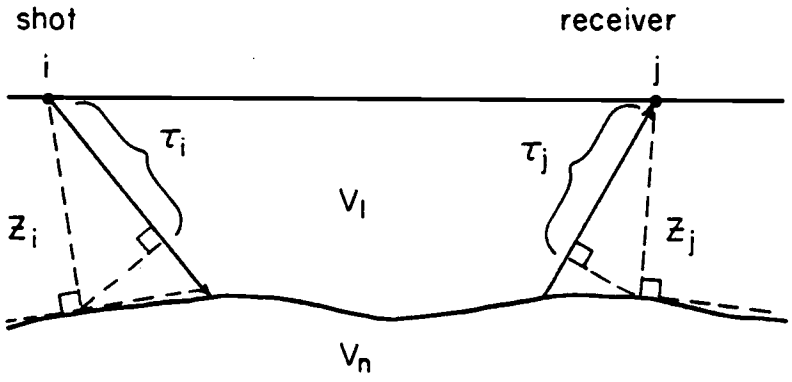

Figure 16b. Ray path diagram for a critically refracted wave travelling from shot i to receiver j.

For the delay-time-function method, several assumptions which should be noted are listed below.

1. The velocity in the upper layer varies only with depth within the critically refracted ray cone under the shot or receiver station. This means that lateral inhomogeneities are not allowed for the down or up going rays. More specifically for this work, all layers are assumed to be homogeneous and isotropic, and successively deeper layers must have increasingly higher velocities.

2. All seismic arrivals are head waves refracted from the tops of the vertically and laterally homogeneous layers.

3. Layer boundaries are represented by low-order polynomial functions of position or by linear combinations of polynomials and Fourier series terms.

4. The slope and curvature of the refracting surface is small, especially in the region of the critically refracted ray cone under the shot and receiver stations. This is important in that the delay time is assumed to indicate the refractor depth immediately beneath the shot or receiver position.

5. The travel time T_{ij} of a critically refracted wave between surface points i and j (see Figure 16b) is given by

$$T_{ij} = \Delta_{ij}/V_n + \tau_i + \tau_j \qquad (5)$$

where Δ_{ij} = surface distance between i and j

V_n = velocity of basal refractor

τ_i, τ_j = delay times or time terms of i and j, respectively as given by equation (4) for the case shown in Figure 16b.

For several layers overlying the refracting half space, equation (4) can be extended to give the following:

$$\tau_i = \sum_{\ell=1}^{n-1} Zi\ell/V_\ell \, (1 - V_\ell^2/V_n^2)^{\frac{1}{2}} \qquad (6)$$

where V_ℓ = velocity of layer ℓ.

$Z_{i\ell}$ = the thickness of layer ℓ at point i.

To express the delay times as a function of position along a gently undulating refracting interface, a low order polynomial function is commonly used as a first approximation. Equation (5) is then modified to the form

$$T(x_i,x_j) \simeq G\Delta_{ij} + 2a_o + a_1 (x_i+x_j) + a_2(x_i^2 + x_j^2) + \ldots + a_n (x_i^n + x_j^n) \qquad (7)$$

where x_i and x_j represent the surface positions of i and j, respectively.

$G = 1/V$, or slowness of the basal refractor.

$a_o, a_1, \ldots, a_n$ are the unknown coefficients of the polynomial terms.

Since G is assumed to be a constant, equation (7) is a linear function of the unknown constants $G, a_o, a_1, \ldots, a_n$.

Final solutions of the delay time surface are often obtained using a linear combination of Fourier series terms with a first degree polynomial. For this case, equation (5) takes the form

$$T(x_i,x_j) \simeq G\Delta_{ij} + 2a_o + a_1(x_i + x_j) + \sum_{m=1}^{(M-3)/2} [\, bm(\sin mUx_i + \sin mUx_j) +$$

$$+ cm(\cos mUx_i + \cos mUx_j)] \qquad (8)$$

where bm,cm are unknown coefficients of the Fourier series terms.

U = 2π divided by the fundamental wavelength of the Fourier terms.

Both equations (7) and (8) represent linear functions of the unknown constants and can therefore be solved using the standard method of least squares (Bloomfield, 1976) if the following conditions are met.

1. Sufficient number of observed travel times, N, are needed. If there exist M unknown parameters in equations (7) and (8), then N must be much larger than M.
2. Adequate areal coverage is required to provide a representative sampling of the refractors.
3. Pseudoreverse control for the velocity determination is necessary and requires that there is not a high correlation between shot-receiver distance and position. This relaxes the condition of having an exact reversal of shot-receiver positions as required in the dipping plane-layer solution of Officer (1958).

Following computation of the velocity and delay time function, some indication of the overall fit of the solution is desired. The time differences R_i between observed travel times and solution-predicted travel times can be used to calculate the standard error about the regression σ from

$$\sigma = \sum_{i=1}^{N} [R_i^2/(N-M)]^{\frac{1}{2}} \qquad (9)$$

where N is the number of observed travel times and M is the total number

of coefficients in the least squares solutions (Morris, 1972). The quantity σ is an indicator of the overall fit of the solution and can be used to judge whether higher order polynomials significantly improve the solution.

Procedure

In order to use the delay-time-function method, crustal models must be simplified to accommodate the conditions of linearity. As previously stated, the Gorda Basin model consists of a number of homogeneous layers, whereby successively deeper layers have higher compressional wave velocities. These are the assumptions of the plane layer method, which is actually a special case of the more general delay time method. The former uses one receiver and fits a zero th order polynomial to the data, whereas the latter employs multiple receivers and fits higher order functions of position to the data. To satisfy these conditions when extracting data from the travel-time plots, refracted arrivals for each shot were assigned to a specific refracting horizon. With the exception of the continental rise (SB1 and SB2), the three major refractors determined from the conventional plane layer analysis were Layer 2, Layer 3 and mantle.

Record sections were replotted at the same reducing velocity of 5.0 km/sec, but without the topographic and water surface corrections. Travel times were input as recorded from the reduced sections and corrections were made by the delay time programs for shot and receiver depths so that water delays could be removed. Unlike the previous plane layer method, the phase velocity used for the upper crust is a

least-squares velocity computed from the uncorrected data. A simplified flowchart for this procedure and the programs used are illustrated in Appendix I.

Because the method fits gently undulating surfaces to the delay times, sharp discontinuities or marked lateral structural variation may result in large errors between computed and observed travel times. To avoid these errors and relax the condition of continuity, the two overlapping profiles were split into four major subdivisions based on results from the unreversed plane-layer solutions.

The north-south profile was divided into sub-plates 1N and 2S, the boundary lying between sonobuoys SB18 and SB19. Initial interpretations of buoy SB18 revealed a discontinuity in refracted arrivals from Layer 2, suggesting the presence of a fault in the basement rock. This offset in arrivals was smoothed over when finding a plane layer solution but could not be avoided when computing a delay-time surface. This same division coincides with a localized thinning of the crust which lies approximately midway between the faster and slower spreading portions of the Gorda plate (see Figures 7 and 11).

Sub-plates 3E and 4W meet at the base of the continental slope (Figure 10) and are distinguished by the large change in bathymetry and number of crustal layers. Sub-plate 3E (PL3E) consists of sonobuoys SB1 and SB2 while PL4W initially included buoys SB3 to SB13. Due to the poor quality and small number of clear returns seen on the records for PL3E, it was decided that the delay-time-function method could not be applied in this region. A low-order polynomial fit was attempted but revealed the complexity of the continental slope would not yield adequate

solutions. A similar problem resulted for PL4W in the region near the base of the continental slope. The layer interfaces have a relatively high dip here and cause the delay-function computed velocities to be only apparent. In general, high dips do not conform adquately to the assumption of gently undulating surfaces and cannot be well constrained. For this reason, data from sonobuoys SB3 and SB4 were removed and only buoys SB6 to SB13 were used (sub-plate PL4Y).

Surface Fitting

Delay-time functions were found for the tops of oceanic Layer 2 and Layer 3, but not for the mantle. Insufficient data were recorded for the mantle refractions and could not be adequately represented by delay-time functions. As a result, this boundary is represented only by the previous plane layer solutions.

Figure 17 is an illustrative example of how solutions were obtained for the delay-time data. The surface shown is the top of Layer 2 for section PL2S. Each solution contains at least a first order polynomial and most have additional Fourier series terms. The number of parameters (M) is increased until the root-mean-square error is minimized. In the example of Figure 17, the solution did not improve beyond M=9 and gave a velocity of 5.302 km/sec with an RMS error of 0.058 sec. Shown are the delay-time surface plots and RMS residuals between observed and computed delay times.

Summary of Results

Final solutions for each of the three subplates are plotted in

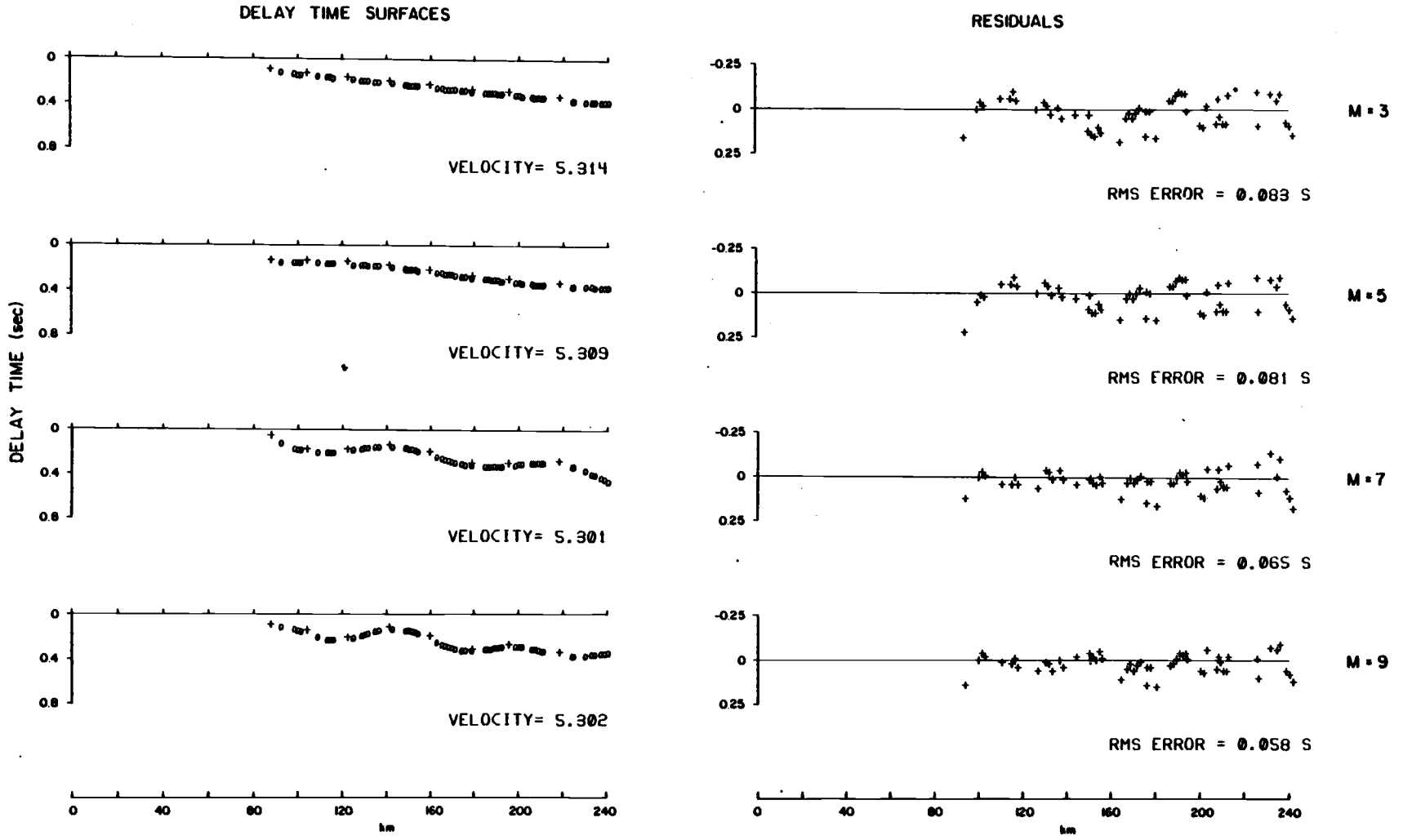

Figure 17. Delay-time surfaces and residuals calculated for 55 arrivals from oceanic basement observed at sonobuoys SB19-SB26 in the Gorda Basin. Receiver locations are indicated by + signs and shot locations by circles. M is the number of coefficients used in the least-squares solution for each delay-time surface. The calculated Layer 2 velocities and RMS difference between observed and computed travel times are shown for each surface.

Figures 18 and 20. Solid lines are the computed depth representations of the delay-time functions, while dashed lines represent supportive data from the plane layer models. Mantle depth solutions are included to provide a more complete crustal model.

East-West Profile I

Delay-time-function solutions for the western portion of the Gorda plate were found for the tops of Layers 2 and 3 using a combination of first order polynomial and third degree Fourier terms. Root-mean-square velocities for the two layers were 5.3 and 6.8 km/sec with corresponding RMS errors of .086 and .117 sec, respectively (see Figure 19). The RMS residual plots of Figure 19 suggest a slight correlation between large residuals and topographic relief, especially for the Layer 3 delay-time functions.

Because the delay-time method assumes that calculated depths to horizons are located vertically beneath shot and receiver sites, a mismatch of bathymetry may have been used in finding the theoretical water delays. This may especially be a problem when there is a high lateral variation in bathymetry, resulting in large residuals between observed and computed travel times. There may also be some geological significance to the observed high residuals in that the flanks of the Gorda Rise crest are proposed to contain numerous high-angle faults (Atwater and Mudie, 1968). The lateral discontinuities produced by these faults may distort the true ray path geometries from the theoretical ones used for computing residuals.

The depth section for the East-West profile of Figure 18 is very

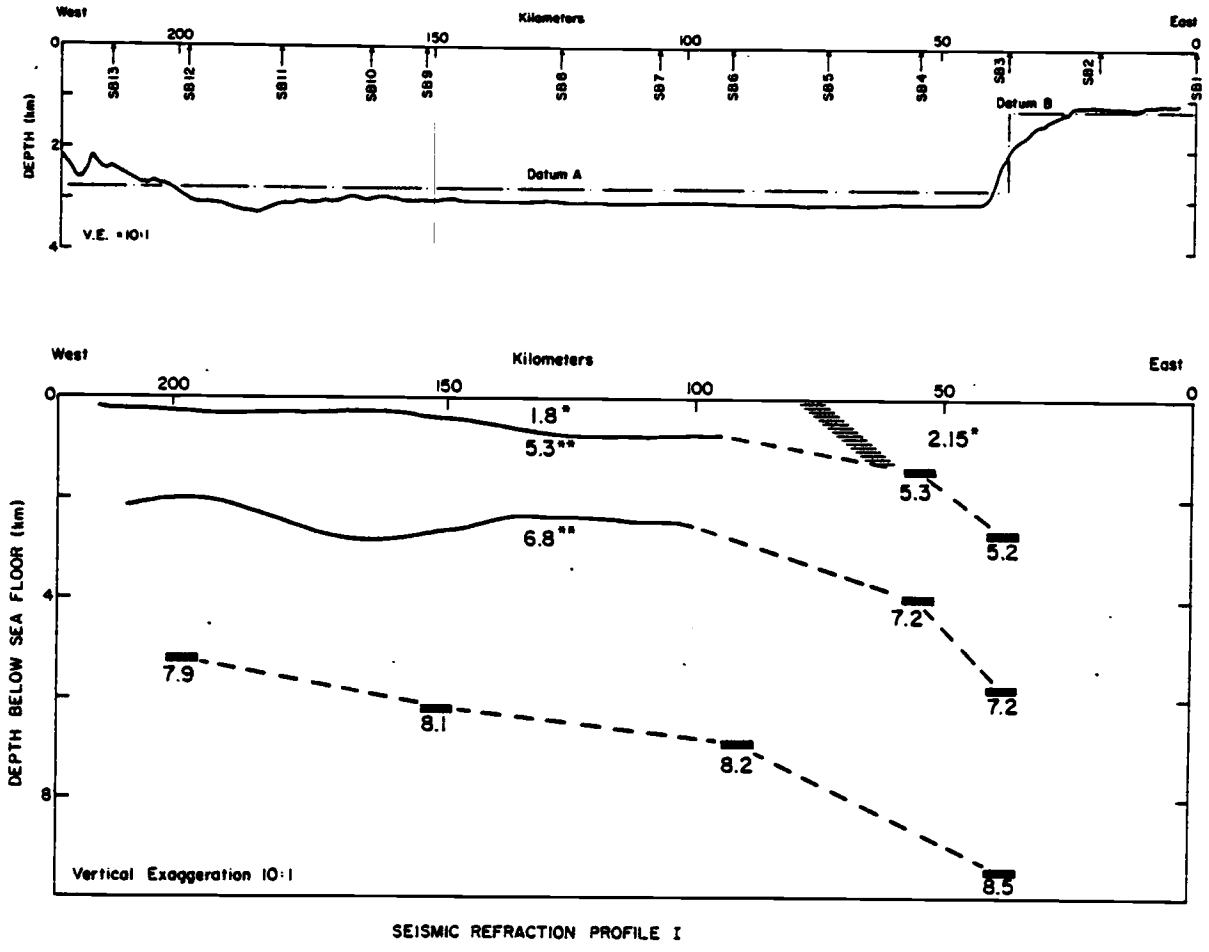

SEISMIC REFRACTION PROFILE I

Figure 18. Summary of the crustal structure from delay-time analysis along east-west profile I in the Gorda Basin. Solid lines represent final delay-time-function solutions for the tops of Layers 2 and 3. Dashed lines are interpreted solutions from the unreversed sonobuoy data, also shown in Fig. 9.

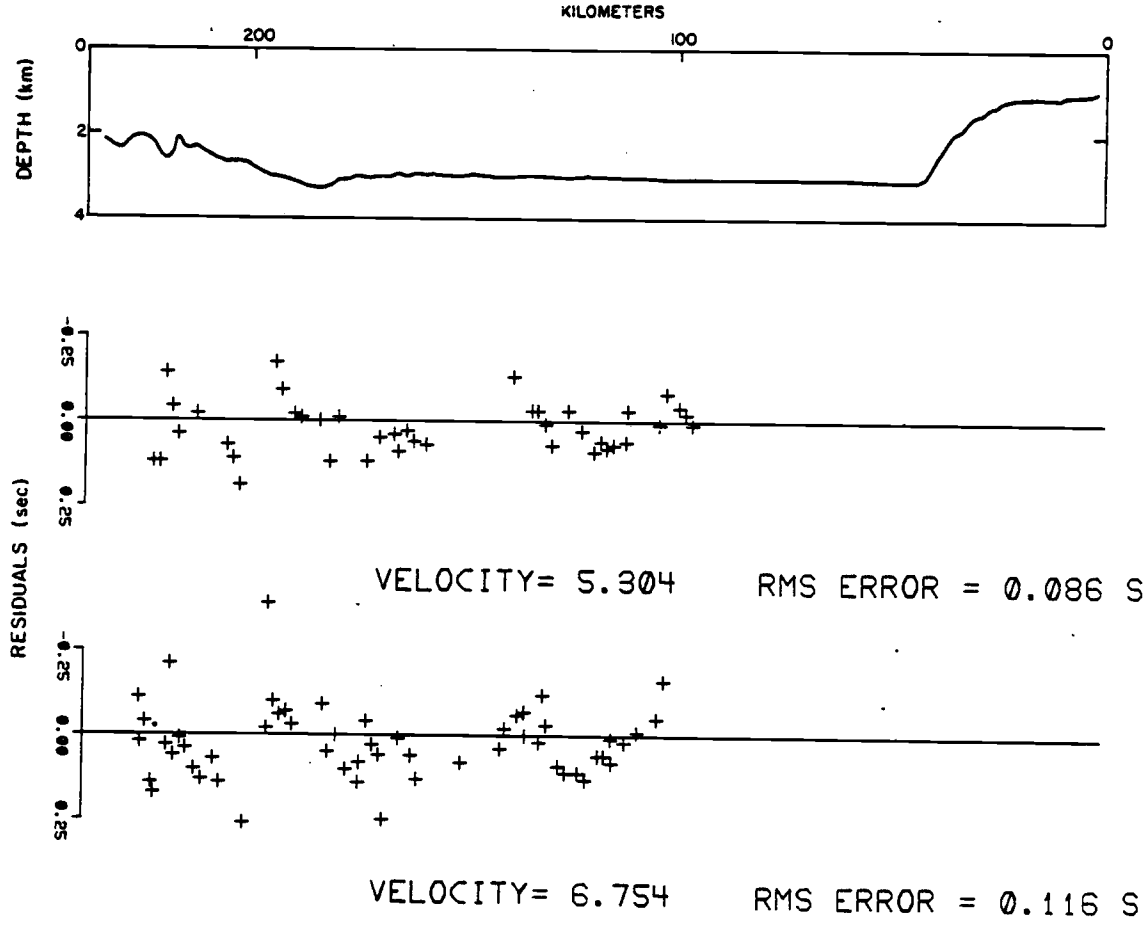

Figure 19. Bathymetry profile and travel-time residual plots of arrivals from Layers 2 and 3 for the east-west profile I (sonobuoys SB6-SB13). Solutions reflect best RMS fits.

similar to the plane-layer model with respect to the depth variation of the Layer 2/3 interface. The thickness of Layer 2 varies from about 1.8 km to nearly 2.5 km. The sediment layer thickens towards the continental slope as in the earlier model. Delay-time surface depths were computed at 2 km intervals for each surface and are listed in Table VI under the PL4Y heading.

North-South Profile II

PL1N. The northern portion of the profile (0-90 km range in Figure 20) yielded delay-time functions which did not improve beyond the M=7 solution (first-order polynomial plus second-degree Fourier terms). Root-mean-square solutions included seismic velocities of 5.3 and 7.0 km/sec for Layers 2 and 3 with delay surface errors of .053 and .069 sec, respectively. Residual plots for the data are given in Figure 21. The depth section of Figure 20 indicates a marked thinning of the crust, especially Layer 2, near the juncture between the two subplates (70-90 km range). Again, there is a fair similarity between the geometry of the delay-time-function surfaces and those inferred from the plane-layer solutions. We also note the large variation in Layer 2 thickness (1.5 - 3.0 km).

PL2S. The southern end of profile II resulted in solutions very close in value to the north end (5.3 and 7.1 km/sec). Both delay-time-functions are third degree Fourier terms combined with a first-order polynomial. Residual plots (Figure 22) again demonstrate some correlation between high topographic relief and large residuals. Here, the large residuals occur near the Mendocino Escarpment and probably result

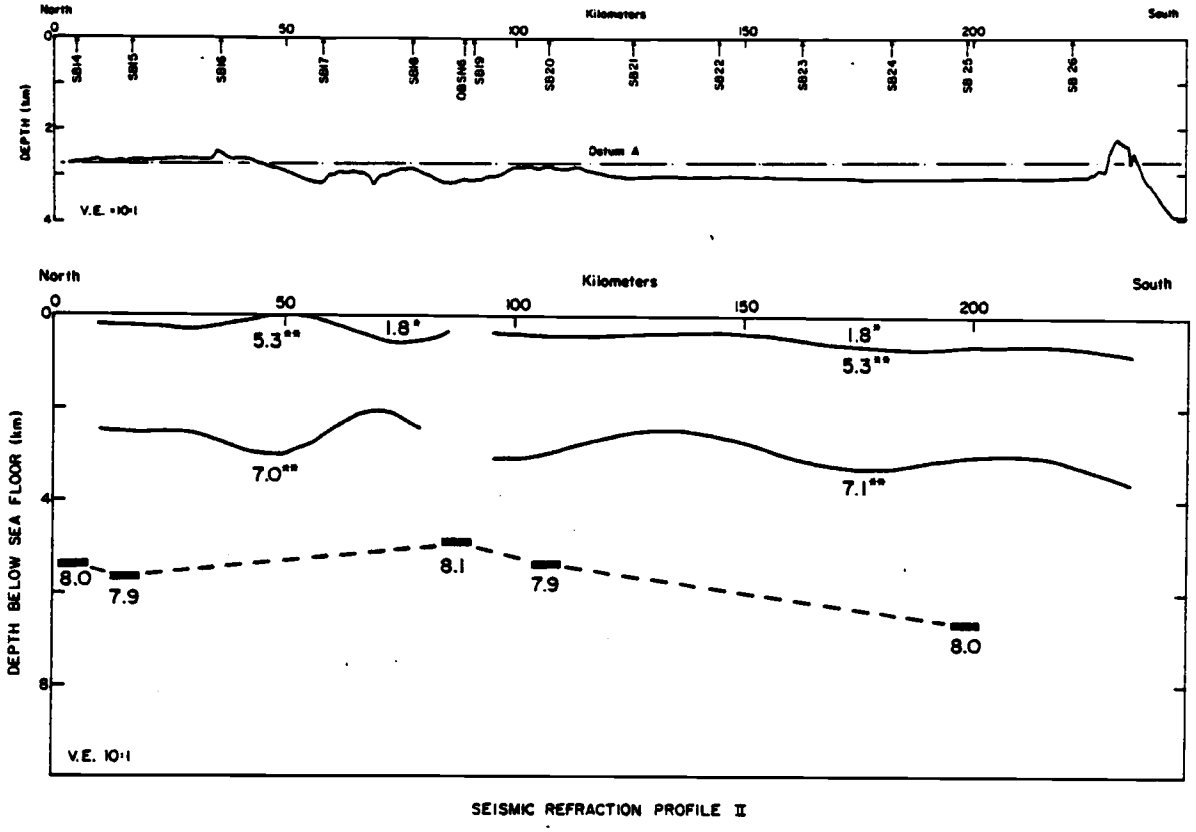

SEISMIC REFRACTION PROFILE II

Figure 20. Summary of the crustal structure from delay-time analysis along north-south profile II. Solid lines are final delay-time-function solutions for the tops of Layers 2 and 3. Dashed line information for the mantle is from the sonobuoy and OBS data of Figure 10.

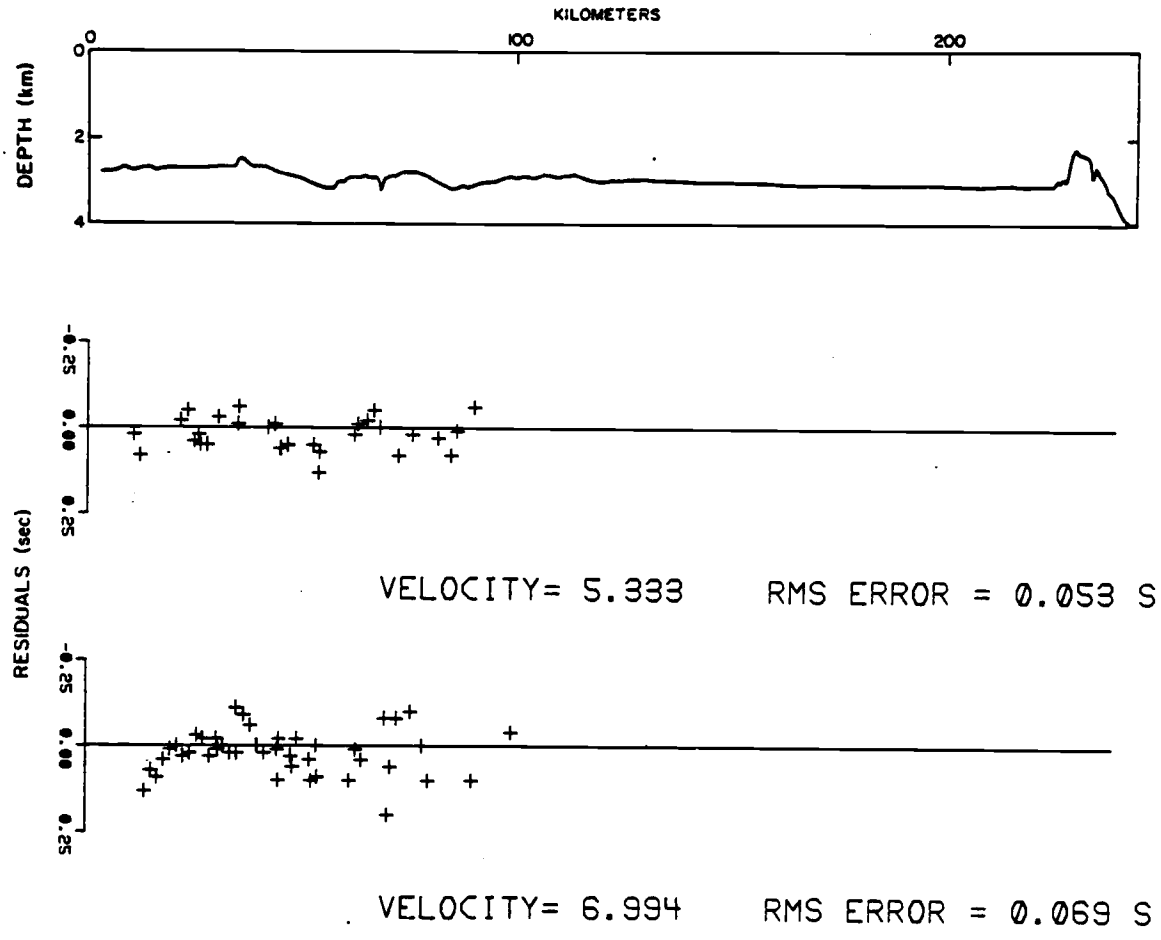

Figure 21. Bathymetry and travel-time residual plots of arrivals from Layers 2 and 3 for section PL1N of north-south profile II (sonobuoys SB14-SB18).

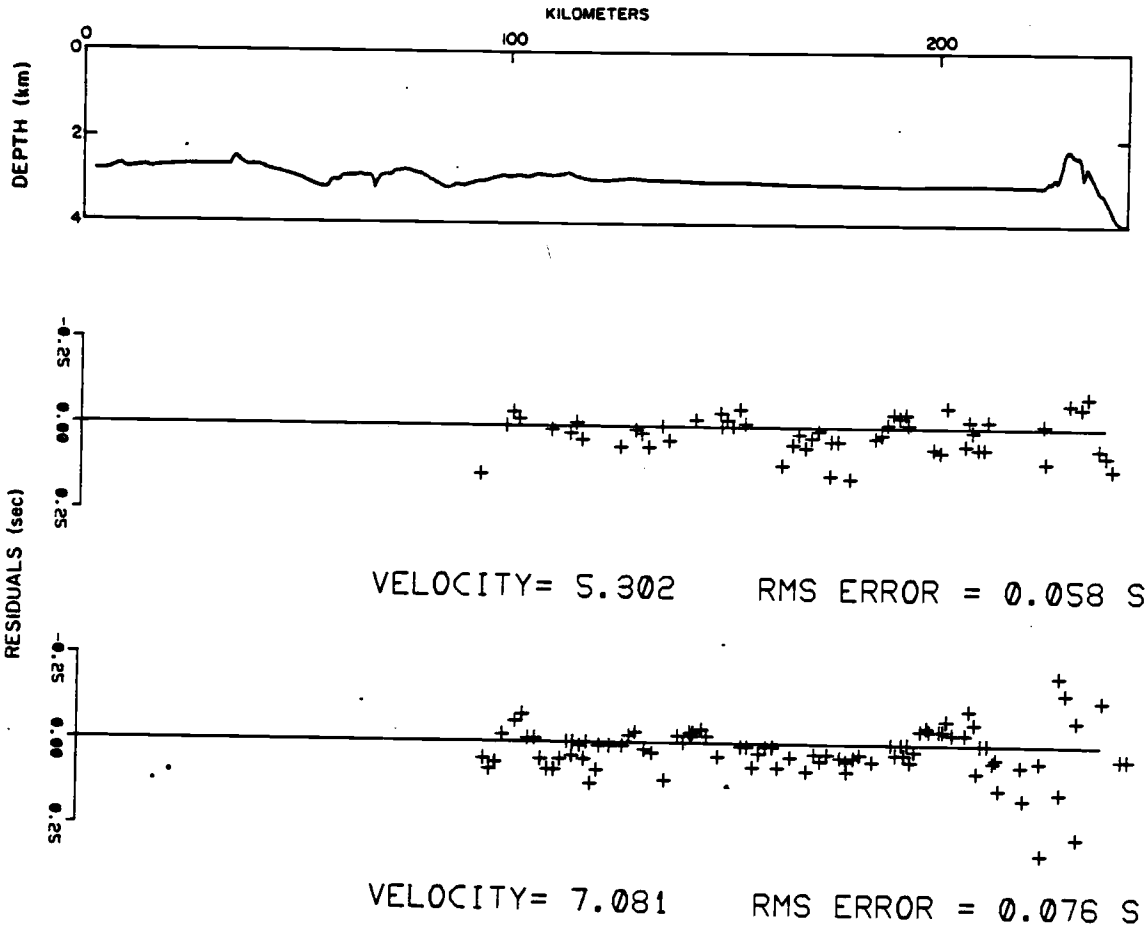

Figure 22. Bathymetry and travel-time residual plots of arrivals from Layers 2 and 3 for section PL2S of profile II (sonobuoys SB19-SB26).

from the same problem of ray path geometries described earlier.

Depth section plots are shown in Figure 20 and indicate considerably less variation in Layer 2 thickness. There appears to be a slight dip in the direction of the Mendocino Fracture Zone with an associated thickening of overlying sediments. The two subplates (PL1N and PL2S) contain independent sets of data but appear to yield consistent results at the juncture of the profiles (85-95 km range). Layer depth computations at 2 km intervals are listed in Table VI under the headings of PL1N and PL2S.

A comparison of delay-time-function and unreversed sonobuoy results at the intersection of the two profiles is shown in Figure 23. A strong correlation, especially for the delay function surfaces, indicate that the data are consistent and essentially unbiased by profile azimuths.

Seismic Reflection Profiles

Two single-channel seismic reflection lines were examined for determining the nature of the sediment cover in the Gorda Basin. Locations of both lines are shown in Figure 7 and are seen to provide a representative sampling of the three major sediment regimes in the area. Line CH3 comes from Leg 3 of the chaneel, 1968 cruise (Silver, personal communication) and crosses the O.S.U. refraction profile II on the flanks of the rise crest. Line L2 is from the 1977 sonobuoy refraction study and follows refraction profile I from sonobuoy SB1 out to sonobuoy SB4. It samples both the lower continental slope and the thick sediment wedge at the eastern margin of the basin.

Table VI. Delay-time-function results from Gorda Basin: depths below the sea floor to the bottoms of the sediment and transition layers. Ranges are measured along refraction profile I for PL4Y and along profile II for PL1N and PL2S.

W7708C GB 1N LAYER SOLUTION FOR DISTANCE KM	PL1N LAYER DEPTHS KM 1	V1 1.80 PARAMETERS 2	V2 5.33 7	V3 6.99 7
.00	.24	2.33		
5.00	.24	2.33		
10.00	.20	2.49		
15.00	.19	2.56		
20.00	.24	2.51		
25.00	.28	2.48		
30.00	.28	2.54		
35.00	.21	2.70		
40.00	.11	2.89		
45.00	.01	3.02		
50.00	.00	3.03		
55.00	.01	2.79		
60.00	.15	2.47		
65.00	.33	2.15		
70.00	.49	2.00		
75.00	.56	2.13		
80.00	.51	2.59		
85.00	.33	-		
90.00	.33	-		

W7708C GB 2S LAYER SOLUTION FOR DISTANCE KM	PL2S LAYER DEPTHS KM 1	V1 1.80 PARAMETERS 2	V2 5.30 8	V3 7.06 7
80.00	.30	-		
85.00	.30	-		
90.00	.30	3.10		
95.00	.34	3.11		
100.00	.40	3.08		
105.00	.44	3.00		
110.00	.45	2.89		
115.00	.44	2.75		
120.00	.42	2.62		
125.00	.39	2.52		
130.00	.36	2.46		
135.00	.34	2.46		
140.00	.34	2.51		
145.00	.35	2.61		
150.00	.38	2.74		
155.00	.43	2.89		
160.00	.48	3.04		
165.00	.54	3.17		
170.00	.59	3.26		
175.00	.64	3.30		
180.00	.67	3.29		
185.00	.68	3.25		
190.00	.67	3.17		
195.00	.65	3.09		
200.00	.63	3.02		
205.00	.61	2.99		
210.00	.60	2.99		
215.00	.61	3.05		
220.00	.64	3.16		
225.00	.69	3.30		

W7708C GB 4Y LAYER SOLUTION FOR DISTANCE KM	PL4Y LAYER DEPTHS KM 1	V1 1.80 PARAMETERS 2	V2 5.30 8	V3 6.75 8
85.00	.72	-		
90.00	.72	-		
95.00	.72	2.56		
100.00	.72	2.56		
105.00	.75	2.47		
110.00	.77	2.49		
115.00	.78	2.47		
120.00	.77	2.43		
125.00	.75	2.39		
130.00	.70	2.38		
135.00	.63	2.39		
140.00	.55	2.46		
145.00	.47	2.55		
150.00	.40	2.66		
155.00	.35	2.77		
160.00	.31	2.85		
165.00	.29	2.87		
170.00	.28	2.83		
175.00	.29	2.73		
180.00	.30	2.57		
185.00	.31	2.40		
190.00	.32	2.22		
195.00	.31	2.08		
200.00	.29	2.01		
205.00	.26	2.01		
210.00	.23	2.09		
215.00	.20	2.24		
220.00	.18	2.43		

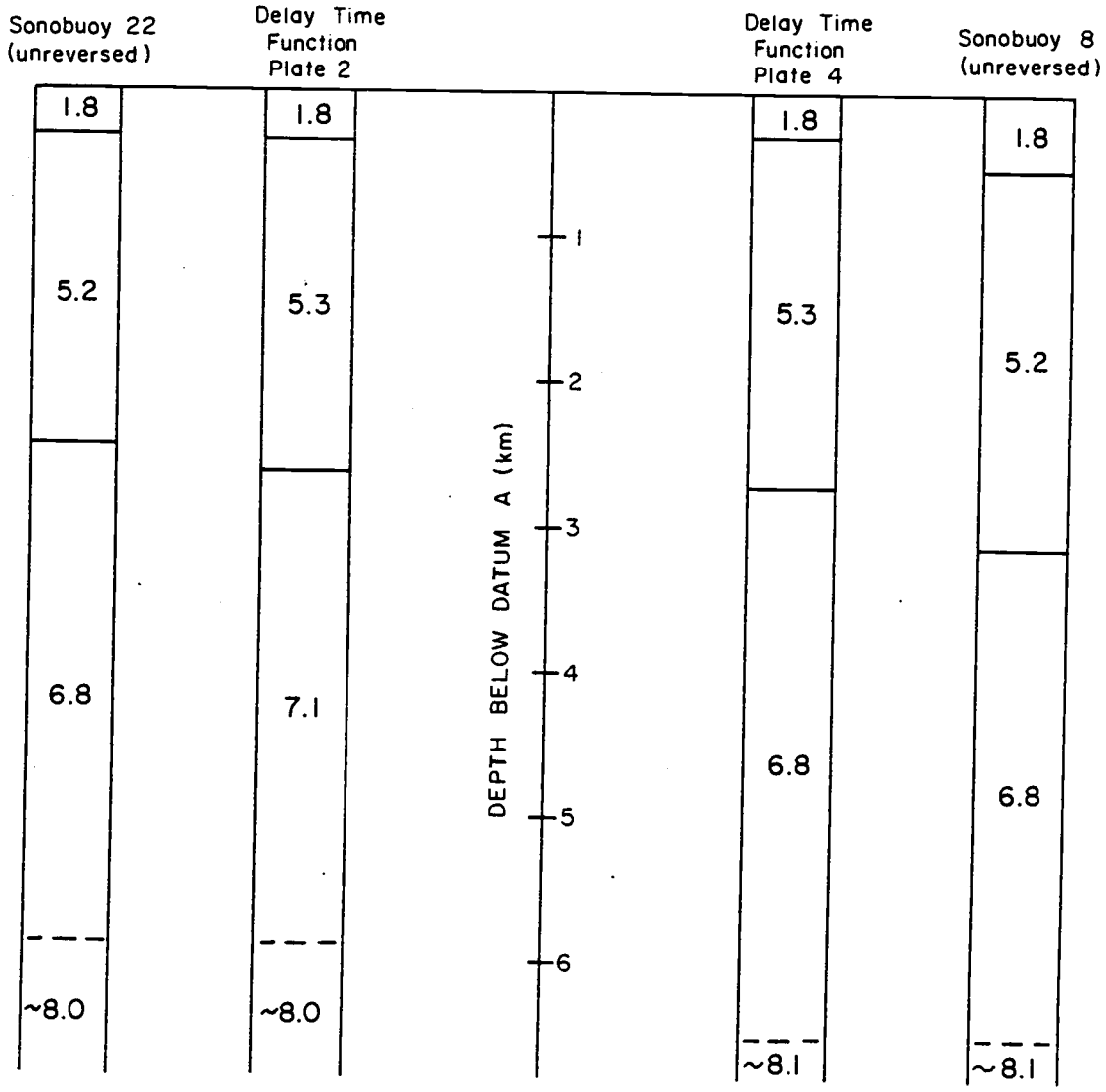

Figure 23. Comparison of delay-time-function and unreversed sonobuoy structure sections at the intersection of profiles I and II (41.23°N,126.10°W).

Line CH3

The line drawing interpretation of seismic reflection profile CH3 is shown in Figure 24 and extends from 42.17°N 126.22°W to 42.3°N 126.1°W, crossing the position of sonobuoy SB16 at the 1100Z time mark. The turbidite sediments (Silver, 1971b) are about 0.11 seconds thick (2-way travel-time) and overlie the rough surface of the oceanic basement. Using an assumed interval velocity of 1.8 km/sec, a corresponding thickness of about 105 meters is obtained. This is slightly less than the thickness obtained from the refraction data (about 180 meters), but of the same order. From the reflection record it can be seen that the sediment cover varies from about 45 to 90 meters thick within a small range of only 20 km, suggesting that local variations on the order of tens of meters may be quite common. In conclusion then, the sonobuoy determined sediment thicknesses on the rise flanks are correct to at least an order of magnitude, and perhaps to within a hundred meters. Also, the top of Layer 2 is observed to be quite bumpy and irregular at short wavelengths, but at long wavelengths may be similar to the smoother delay-time-function surfaces.

Line L2

Seismic Line L2 (Figure 25) extends from 41.25°N 124.57°W to 41.23°N 125.20°W across the northern California continental margin-slope region and is about 50 km in length. The line drawing interpretation has a range scale equivalent to the E-W sonobuoy refraction profile I. The irregular basement reflector seen on the upper portion of the slope may be a result of folded or faulted material (Silver, 1971b;

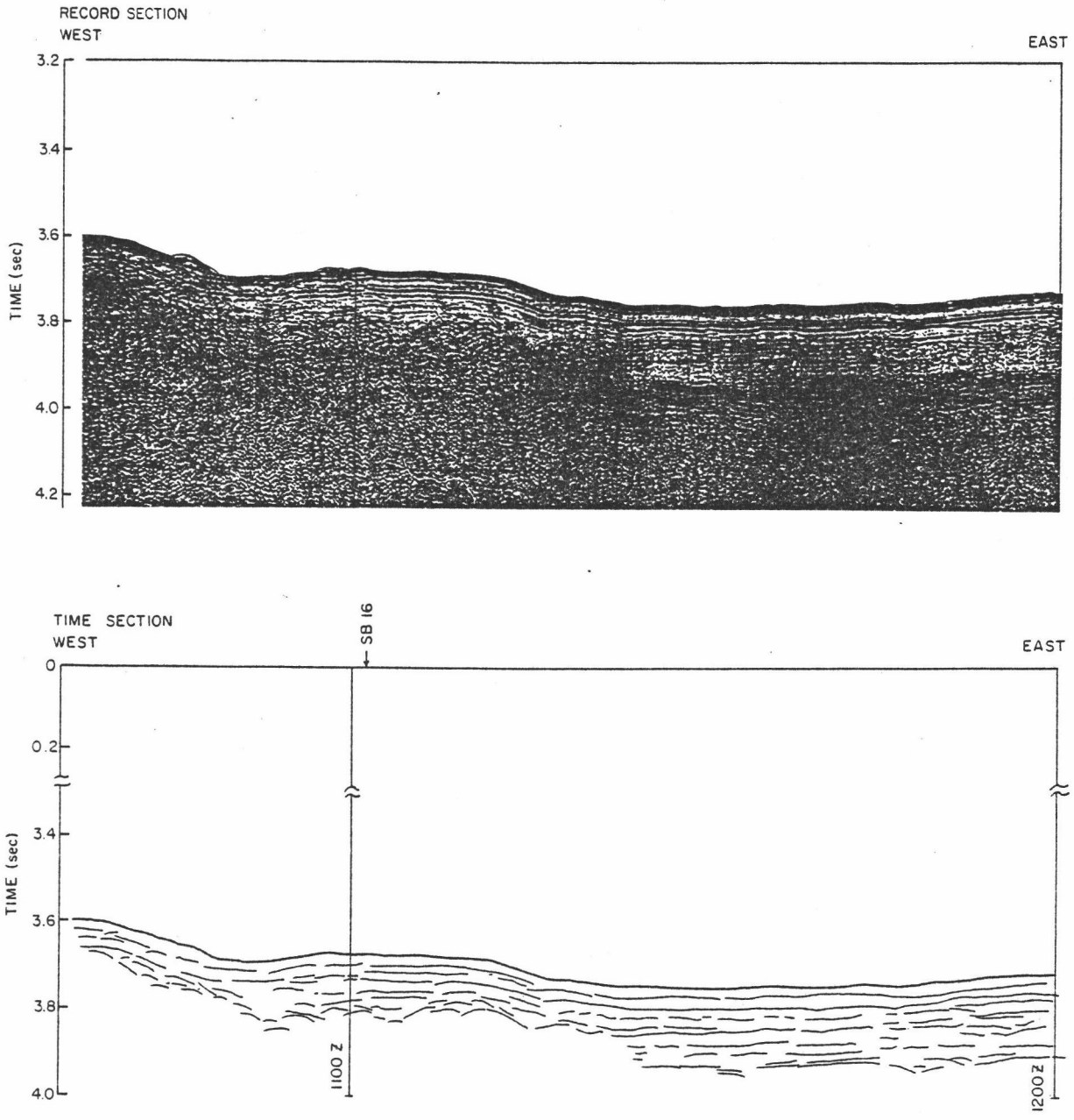

Figure 24. Record and time sections for seismic reflection line CH3 on the Gorda Rise flanks (Silver, E., personal communication).

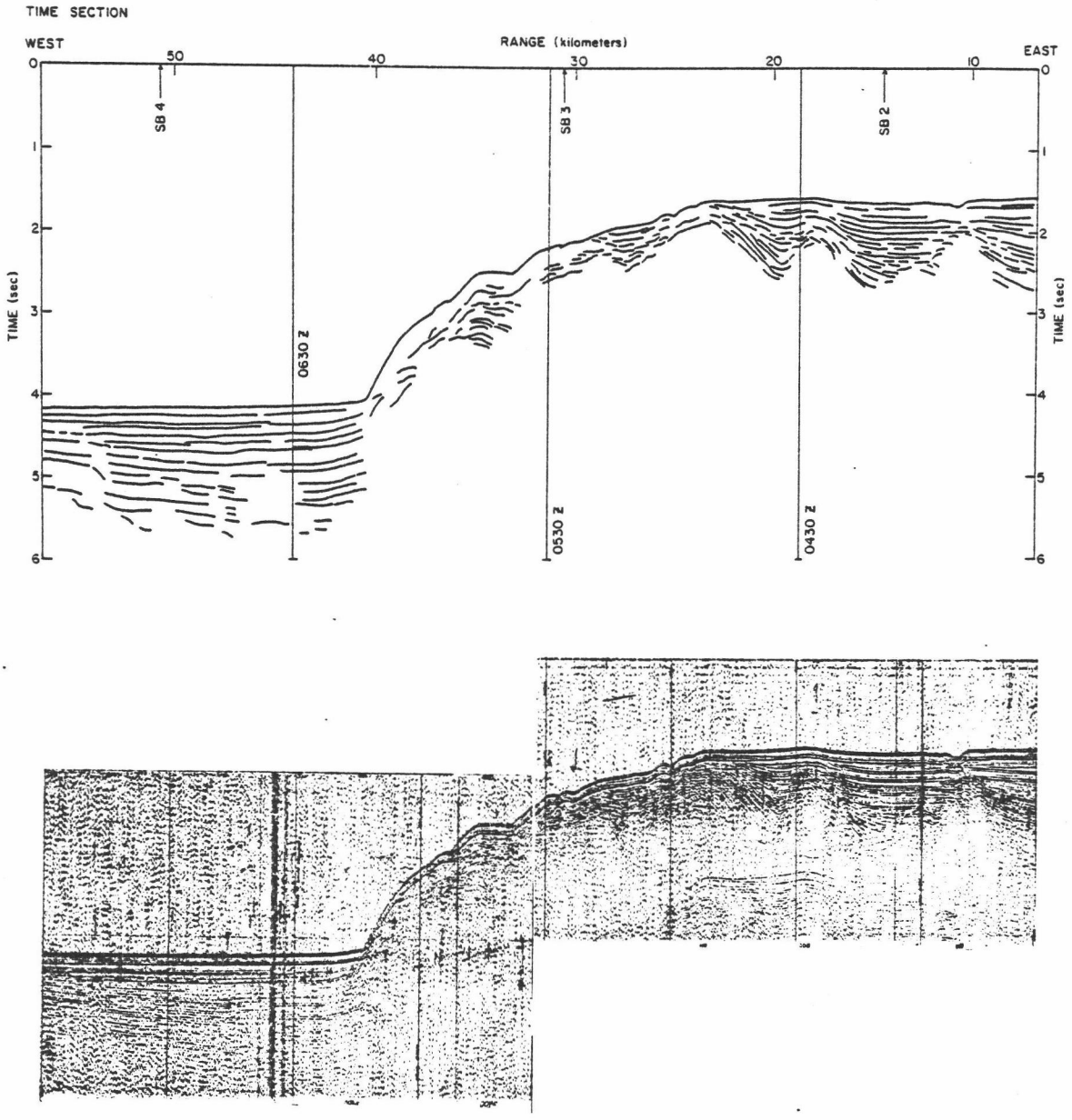

Figure 25. Record and time sections for seismic reflection line L2 on the northern California continental margin.

Keser, 1978) with a seismic velocity around 2.6-2.9 km/sec (Wrolstad, 1978). Using an interval velocity of 1.8 km/sec for the ponded sediments on the slope, a thickness variation of .5 to 1.0 km is obtained and is in close agreement with the 0.98 km value calculated from the sonobuoy data.

Basement reflections at the base of the continental slope were poorly defined, probably as a result of signal attenuation through the thick sedimentary wedge. Calculations of sediment thickness, using a 2.15 km/sec interval velocity and assuming the basement to be the latest seismic return, gave a maximum of 2.3 km at the east end of the wedge. Again, this is in close agreement with the 2.6 km thickness obtained from sonobuoy 3, situated directly over the area. There is a slight increase in the deformation and dip of these sediments with depth.

Results from the two seismic reflection lines give a clearer understanding of the nature of the sediment cover in the Gorda Basin and on the continental slope, and provide a check on the plane layer solutions from sonobuoys. The irregular surface of the oceanic basement is also revealed, thus reminding us that only long wavelength structures can be obtained from present sonobuoy refraction methods.

INTERPRETATION AND DISCUSSION OF RESULTS

Gorda Basin and Rise Flanks

Seismic Model

The seismic velocity structure of the Gorda plate has been determined in nearly continuous sections both parallel and normal to the ridge axis. The division of the crust into three layers (sediment, Layer 2, and Layer 3) overlying the mantle has provided consistency not only within the 1977 data, but also with results of earlier investigators. The computed sections of Shor et al. (1968) and Raitt (1963) are shown together with sonobuoy results of this study in Figure 26 to further illustrate this consistency. The poor correlation for line CU2 may be only apparent since they did not include a Layer 3 refractor (velocity 6.8 to >7.0 km/sec). The average Gorda seismic structure was shown previously in Figure 12.

Geologic Model

To formulate a model for the geologic structure in the Gorda Basin requires knowledge about the petrology of each seismic layer. Determining the petrologic content of the oceanic crust is difficult since present drilling techniques are unable to penetrate the depths required. One method of obtaining this information is to examine ophiolite assemblages and dredged oceanic samples and to compare them with the seismic structure. Although ophiolites are widely regarded as fragments of oceanic crust tectonically emplaced on land, direct correlation remains difficult since ophiolites are described by petrologic field

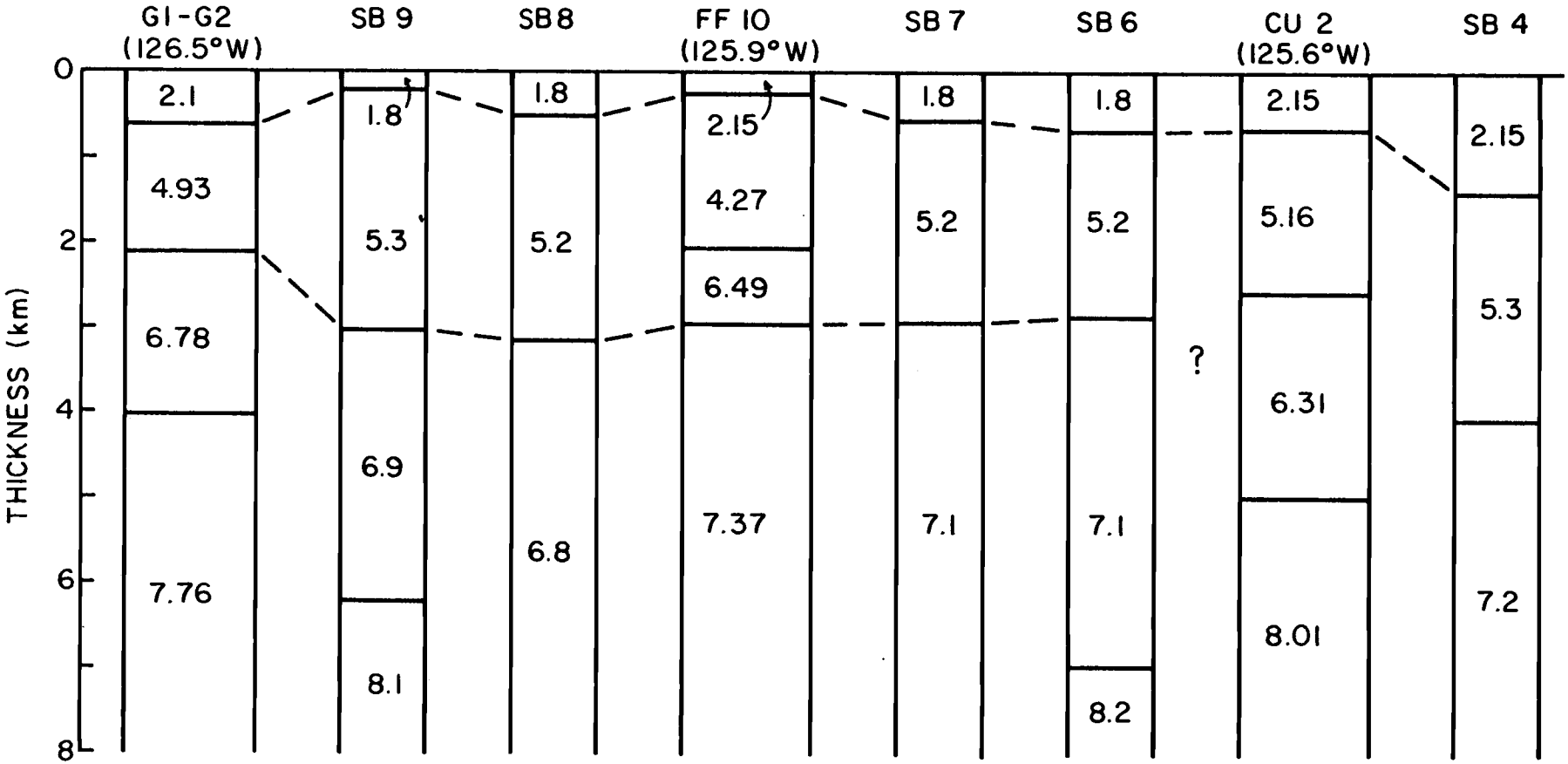

Figure 26. Comparison of seismic structure sections obtained in the Gorda Basin by refraction methods: from this study (SB4-SB9); Shor et al., 1968 (G1-G2); and Raitt, 1963 (CU2 and FF10). Seismic velocities in km/sec.

studies and the crust is defined seismically. Salisbury and Christensen (1978), however, have performed detailed velocity structure studies on ophiolites for direct comparison with oceanic crust. Their results from the Blow-Me-Down Massif of the Bay of Islands ophiolite complex are summarized in Figure 27 together with a composite section of the average Gorda Basin seismic structure. The velocity structure they determined from the ophiolite complex is very similar to normal oceanic crust and is summarized below.

--Layer 2: Consists of pillow basalts and brecciated dikes with two degrees of metamorphism. The lower degree is prehnite-pumpellyite facies and forms the upper .5 km with $V_p \leq 5.70$ km/sec. This overlies a .8 km thick greenschist facies with $V_p \leq 6.20$ km/sec.

--Layer 3: From 1.3 to 6.4 km depth and composed of metadolerite sheeted dikes underlain by coarse-grained metagabbro which grades downward to olivine gabbro. V_p increases from 6.75 km/sec near the top to 7.40 km/sec near the base in a gradational manner.

--Mantle: The top of the mantle or Mohorovicic discontinuity represents a sharp transition from gabbro to dunite and peridotite (mafic vs. ultramafic rocks) with $V_p = 8.4$ km/sec.

Salisbury and Christensen (1978) suggest that the layer 2-3 boundary separates two degrees of metamorphism, greenschist facies metabasalts and brecciated dikes at the base of Layer 2 from epidote-amphibolite facies sheeted dikes at the top of Layer 3. For the seismic Moho boundary they feel the contact is a petrologic change from mafic to ultramafic rocks. On the other hand, Moores and Jackson (1974) and

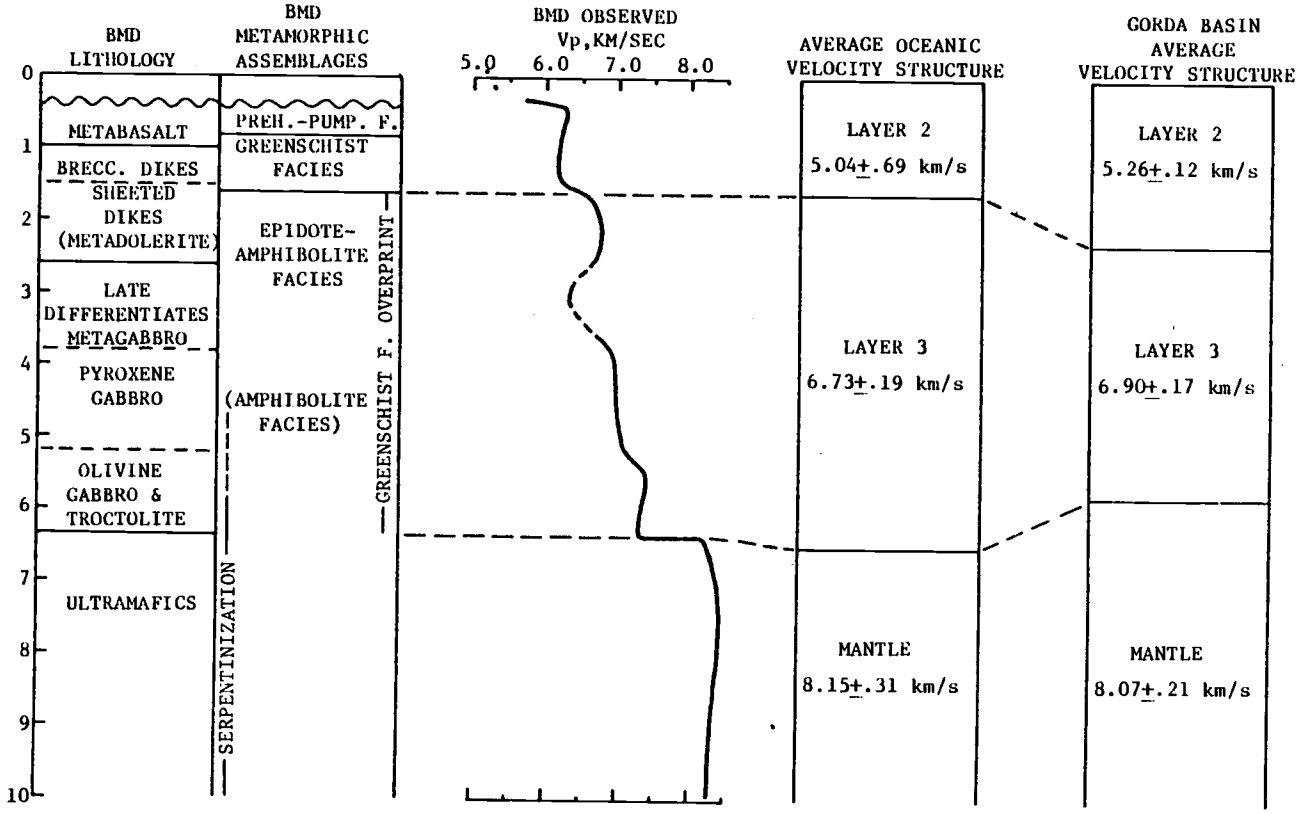

Figure 27. Results of an ophiolite study from the Blow-Me-Down massif in the Bay of Islands compared with the average seismic section from the Gorda Basin. The BMD observed seismic profile is a best fit curve to the data. The dashed line between 2.6 and 3.8 km indicates discontinuous velocity inversions. (Modified after Salisbury and Christensen, 1978).

Clague and Straley (1977) all favor a model which places the Moho at a metamorphic contact between serpentinized and fresh rocks within the ultramafic unit. Both interpretations may be correct if one considers the suggestion of Lewis and Snydsman (1977) that the observed thickening of the oceanic crust with age is due to serpentinization of mantle peridotite. This is envisioned by Lister's (1974, 1977) model whereby hydrothermal circulation penetrates deeper into the crust with age and the resulting metamorphism of the mafic and ultramafic rocks moves the seismic Moho downward into the ultramafic unit.

Tectonic Implications

The idea of metamorphic facies changes and their relation to isotherm depths may be used to explain some of the unique characteristics of the Gorda plate crust. Figure 12 shows a comparison of the average Gorda seismic section with a composite Pacific Ocean crustal section from Shor et al. (1970). It is apparent that the layer velocities and total crustal thickness are nearly indistinguishable for the two sections. One very notable difference, however, is the thickness of Layer 2, or position of the Layer 2-3 boundary in the crust. The Gorda section shows a thicker transition layer than the average Pacific crust and is probably related to different spreading mechanisms. The Gorda Ridge is anomalous in the Pacific because its spreading rate is of the slower Atlantic type, with a half-rate between 1.2 and 2.9 cm/yr. Menard (1967) concluded that the thickness of Layer 2 is roughly inversely proportional to the spreading rate at the ridge crest where it is produced. A plot of this relationship from Shor et al. (1970) is

shown in Figure 28 and includes the average results from the Gorda Basin.

If one accepts the Salisbury and Christensen (1978) suggestion that the Layer 2-3 boundary is a metamorphic facies contact, then we might infer the thick transition layer (Atlantic-Gorda type) results from a depressed isograd marking the upper extent of epidote-amphibolite facies metamorphism. By depressed isograd we mean an equivalent one on the faster spreading Pacific type ridges would occur shallower in the crust, yielding a thinner Layer 2 with respect to seismic velocity and metamorphic grade.

From the final cross sections of the refraction profiles (Figures 18 and 20) we concluded considerable variation in the transition layer thickness. The delay-time-function surfaces for the Layer 2-3 boundary suggest that this variation is slightly greater along the N-S profile if we neglect the regional dip in the E-W section. Considering this observation in conjunction with the earlier discussion on metamorphic facies, one might infer that epidote-amphibolite facies isograds occur at varying depths along the length of the Gorda Ridge spreading axis. This model is probably not unique but does permit variations in the transition layer thickness along a section of lithosphere with relatively constant total crustal thickness.

Intraplate Deformation

In order to understand the problem of intraplate deformation in the Gorda Basin, we will first consider the more regional tectonic view of the Juan de Fuca system. The San Andreas and Queen Charlotte Islands

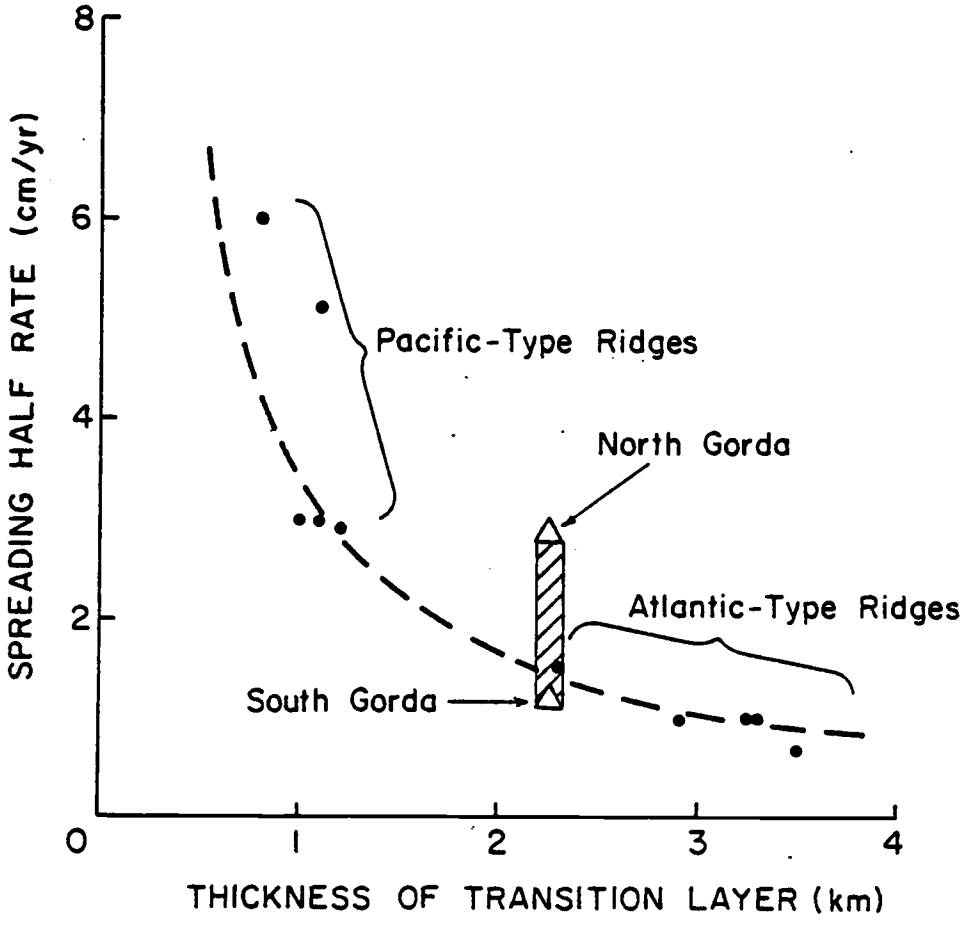

Figure 28. Spreading half-rate as a function of thickness of the transition layer from Shor et al. (1970). Includes results from the present Gorda Basin study (shaded region).

transform faults represent the direction of motion of the Pacific plate relative to the North American plate. The fracture zones of the Juan de Fuca plate are gradually becoming more aligned with the trends of these larger features, as evidenced by the noticeable clockwise rotation, from south to north, of the Mendocino, Blanco, Sovanco, and Revere-Delwood fractures (Figure 6). The shorter, younger transforms to the north are more closely aligned than the longer, older Blanco and Mendocino fracture zones to the south. There is a similar re-alignment trend of the spreading ridges as well. In the Gorda plate, the response to this change of plate motions is seemingly quite different from the rest of the Juan de Fuca system. The following is a list of observations from the Gorda Basin which may be related to the tectonic complexities of the region resulting from this shift in motion directions.

(1) At least two offsets occur in the Gorda Ridge axis between 41.6^{o}N and 42^{o}N; causing a change in its orientation from N-S to NE-SW.

(2) Faster spreading away from the northern ridge segment and slower spreading to the south (based on magnetic anomalies).

(3) Intraplate seismic activity within the transition zone between the two spreading rates.

(4) Thin Layer 2 and an overall thinning of the crust (~4 km) coincident with the transition zone mentioned in (3) above.

(5) Deeper bathymetry along the same zone of (3) and (4) above.

First, consider that the offsets in the ridge described above are analogous to fracture zones, in that they both cause abrupt discontinuities in the normal two-dimensional nature of oceanic ridges along the axis. Using marine refraction, Detrick and Purdy (1980) found

anomalously thin crust (2-3 km) in the Kane Fracture Zone and suggested that this type of crustal structure might be typical of many Atlantic fracture zones. They proposed that the thin crust is a primary feature caused by the accretion of a thinner volcanic and plutonic layer within the fracture zone. They point out that thinner crust could explain other geophysical observations such as the gravity anomalies across the Romanche and Vema fracture zones. A similar mechanism would explain the thin crust observed in the Gorda Basin. If we can assume spreading occurs in a direction normal to the ridge, then the thin crust originally formed at the present location of the 42^{o}N offset. The deep bathymetric trends may be an isostatic response to the elevated mantle boundary associated with the thin crust.

The offsets in the Gorda Ridge axis are only one type of response to the change in relative motions between the Pacific and North American plates. The asymmetrical spreading observed from magnetic anomalies may be another. The right-lateral shear couple across the Gorda plate has resulted in fan-shaped spreading, faster to the north and slower to the south with a fairly gradational change in rates. This fan spreading is in a clockwise sense, consistent with the realignment of other features in the Juan de Fuca system. In response to the general north-south compression of the Gorda plate is seen a concentration of crustal deformation towards the central region, coincident with the zone of thin crust. This is evidenced by the high amount of seismic activity with strike-slip focal mechanisms. It should be noted, however, that the estimated fault planes do not parallel the direction of spreading, and we should probably rule out any decoupling or segmentation of

the Gorda plate (such as a transform fault) associated with the thin crust.

Recent investigations of spreading ridge and magnetic anomaly offsets have led Hey (1977) to propose a model of propogating rifts to explain these features using rigid plate motions. Instead of calling upon intraplate faulting for the offsets in anomalies, the new model proposes the existence of pseudofaults consisting of en echelon sets of fracture zones frozen into progressively younger crust. This special set of fracture zones result from sequences of spreading center jumps propagating down the spreading center and begin with an initial offset in the ridge axis. Several sets of these V-shaped pseudofaults have been identified by Hey (1977) in the Juan de Fuca plate, most of which resulted from southward migration of spreading centers offset by slight changes in axis orientation.

As noted before, the Gorda Ridge may contain several small offsets. The result of a propagating rift with such small offsets would be the occurrence of a narrow zone of en echelon fractures radiating away from the ridge. Magnetic anomaly offsets would be small or even undetected, which is the case in the Gorda Basin. Therefore, although this model for ridge migration may apply to the Gorda plate in some form, its effects fail to explain the non-rigid characteristics observed away from the spreading axis.

The Gorda plate has been shown to resemble Atlantic type spreading systems in several respects. The morphology of the ridge, slow spreading rates, and thick transition layer are all features common to the Atlantic. A comparison of the Gorda plate topographic profile was made with

theoretical curves computed by Sclater and Francheteau (1970) for Atlantic and North Pacific type lithosphere. For both models they used a lithosphere thickness of 100 km, but a 4 cm/yr half spreading rate for the Pacific and 2 cm/yr for the Atlantic. Although the Gorda Basin is only about 200 km wide, its topographic profile clearly follows the theoretical North Pacific profile. The Atlantic topography lies about 700 meters deeper than the Gorda at a similar distance of 200 km. Theoretical profiles which used other lithosphere thicknesses did not have the same initial depth of 2000 m over the ridge crest as observed over the Gorda Rise. Regardless of sediment loading, the Gorda Basin topographic profile is a feature typical of Pacific Ocean morphology.

Eastern Gorda Basin and Continental Slope

Seismic Model for the Basin

Results from sonobuoys at the base of the continental margin revealed crust of approximately the same thickness and velocity structure as seen in the basin interior. The major difference is a landward dip of 1-2 degrees and the existence of a thick sedimentary wedge (2-3 km) with an assumed interval velocity of 2.15 km/sec. In Figure 29 is a comparison of a velocity section (Snavely et al., 1980) from the base of the slope off Siletz Bay, Oregon (44.8°N) with the section from sonobuoy SB3 of this study. The morphology of the outer slope from these two locations is similar and vertical reflection records both show about two seconds two-way travel time for the sediment wedge. The sediment section from the Oregon coast is comparable in thickness to the Gorda section but is resolved into three seismic layers (A, B, and

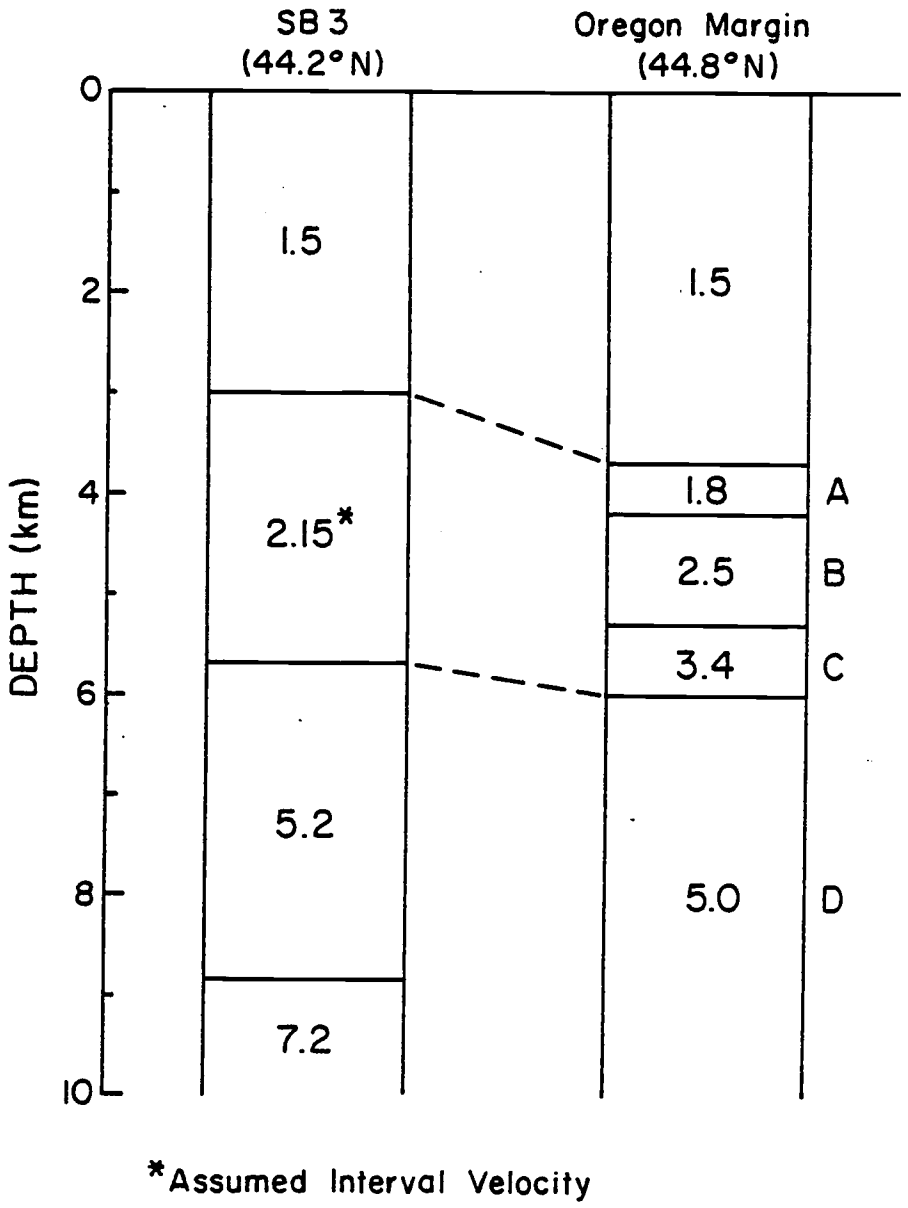

Figure 29. Comparison of the sediment wedge from profile I of this study with a section at the base of the slope off Siletz Bay, Oregon (44.8°N 125.5°W) after Snavely et al. (1980). Seismic velocities in km/sec.

C of Figure 29) with velocities of 1.8, 2.5, and 3.4 km/sec, respectively.

Geologic Model

Sediment information from DSDP site 174 (Kulm and Fowler, 1974b) has been correlated with the three sediment layers by Snavely et al. (1980).

Unit A, V_p = 1.8 km/sec: Holocene and upper Pleistocene (.5 MY - present) semiconsolidated silts and sands.

Unit B, V_p = 2.5 km/sec: Middle (1.2 - 0.6 MY) and lower (1.85 - 1.2 MY) Pleistocene fine to medium grained turbidite sands and interbedded muds.

Unit C, V_p = 3.4 km/sec: Pliocene (5.0 - 1.85 MY) siltstone, turbidites and interbedded mudstone; also, upper Miocene to early Pliocene (8 - 4 MY) pelagic calcareous ooze which grades upward into calcareous hemipelagic muds.

Unit D: Upper Miocene (10 - 8 MY) tholeiitic basalt, assumed to be Layer 2 of the oceanic crust.

The sand turbidites are typical of submarine fans which commonly form at the base of the slope, while the silt turbidites are more characteristic of abyssal plain deposits (Kulm and Fowler, 1974b). The loading effect of this thick sedimentary wedge may be partly responsible for the landward dip of the crust at the eastern edge of the Gorda plate.

Seismic Model for the Slope

Seismic record sections from the continental slope off northern California had considerable noise content, but were fairly consistent for the two sonobuoys. A comparison of the two sections from this study is shown along with sonobuoy results from Wrolstad and Johnson, 1976) and two-ship refraction studies by Shor et al. (1968) in Figure 30. Although the velocity structures are quite variable, basement overburden thicknesses are about the same (around 4 km overlying Layer 2). The seismic variability of this material may be a result of the complex folded and faulted structures of the continental slope (Kulm and Fowler, 1974b; Silver, 1971b).

Geology of the Slope

Sampling of the sediments on the slope was achieved by coring (DSDP Site 175) and dredging (Kulm and Fowler, 1974b). Again, both sites were situated near 44.8^{o}N off the Oregon coast, but because of the similarities in morphology and source regions (predominately the Klamath Mountains of northern California and southern Oregon, and the Columbia River drainage, Keser, 1978; Kulm and Fowler, 1974b), they may be useful in describing the slope east of the Gorda Basin. Dredgings from the continental slope yielded Pleistocene (<.3 MY) sandstones and mudstones which were fairly well consolidated. DSDP Site 175 produced middle Pleistocene (1.2 - 0.6 MY) silt turbidites and interbedded muds which became noticeably consolidated at subsurface depths of 125 - 180 meters. The seismic velocities of this unit increased rapidly from 1.6 to 1.9 km/sec within the 180 meter interval. Overlying this were upper

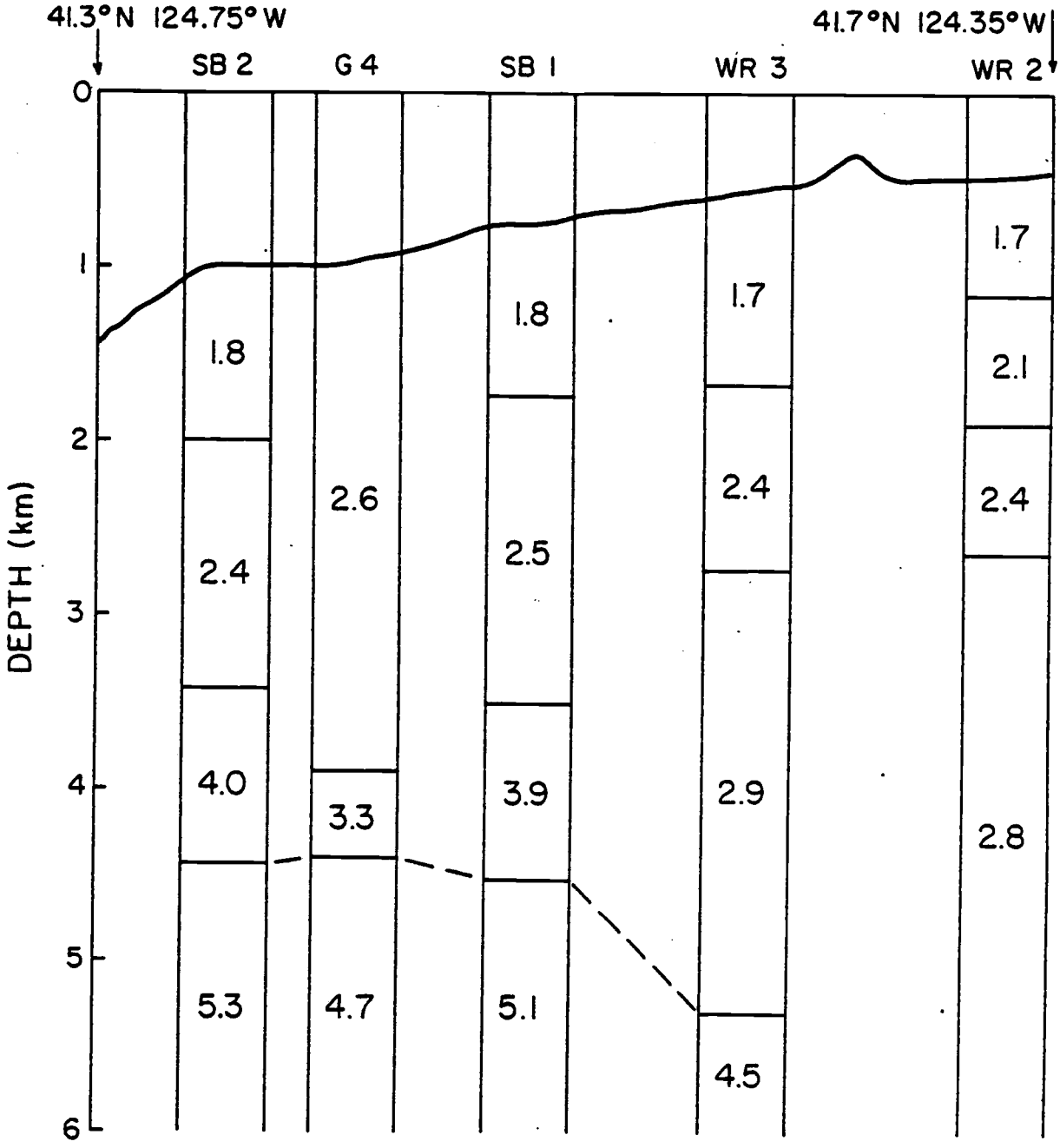

Figure 30. Seismic sections from sonobuoys on the northern California continental slope. Seismic velocities in km/sec. After Wrolstad and Johnson, 1976 (WR2,WR3) and Shor et al., 1968 (G4).

Pleistocene (0.6 MY - present) unconsolidated hemipelagic sediments with an interval velocity of 1.6 km/sec. As indicated, these samples do not penetrate the slope region sufficiently to provide geologic information about the material above Layer 2. Without petrologic control, it is difficult to explain the origin of these units with seismic velocities between 2.0 and 5.0 km/sec. Biologic studies of rock samples from the Oregon continental slope have indicated an uplift of as much as 1 km for many of these surface materials (Kulm and Fowler, 1974b). However, the refraction and reflection data presented here are insufficient for devising a model of continental slope formation.

Tectonic Implications

The composite east-west cross section for the Gorda Basin (Figure 10) revealed a distinct landward dip of the crust on the order of 1-2 degrees. Although a continuous deep trench does not exist, it may perhaps be masked by the infilling of sediments from the rapidly eroding Coast and Cascade ranges. Other features typical of subduction zones are seen, including the large negative gravity anomaly and angular termination of magnetic anomalies at the continental slope. Data from the slope are consistent but insufficient for revealing the accretionary processes generally accepted to occur on the lower slope region. Evidence for the uplift of material from the thick sedimentary wedge at the base of the slope, coupled with the highly deformed nature of the basal slope reflectors seen on vertical profiling records at least support the idea that compressive forces are affecting the lower slope. This is also consistent with the processes occurring along subduction

zones. However, the absence of earthquake foci at typical Benioff depths (300 km) requires a special mechanism for the Gorda plate subduction. Earthquakes are seen to depths of 30 km which is deep for California, but an order of magnitude less than Benioff zones. Because the crust is young(<10MY)and subducting slowly (1-2 cm/y, Silver, 1971a), the Gorda Plate may become plastic at a shallow depth, so that the brittle region disappears at depths near 30 km (Atwater, 1970).

SUMMARY AND CONCLUSIONS

Two long refraction lines in the Gorda Basin (including 23 sonobuoys and 1 OBS) revealed the presence of normal oceanic crust with an average thickness of 5.7 kilometers. Sediment cover thickens to the east and south on progressively older crust from less than 100 meters to more than 2.5 km. Time-term analysis utilizing multiple receivers shows a thick transition layer (Layer 2) which averages about 2.3 km but displays considerable lateral variation. Seismic compressional velocities averaged about 5.3 km/sec throughout the basin with little variation. The average thickness of Layer 3 is 3.4 km with a velocity of 6.9 km/sec. Again, this value was consistent along both lines. The average mantle velocity is near 8.1 km/sec.

Comparisons of seismic velocity structure were made with ophiolites from the Bay of Islands complex to provide a petrologic model for the Gorda crust. The transition layer probably consists of pillow basalts and brecciated dikes while Layer 3 is made up of metadolerite sheeted dikes overlying coarse metagabbros and olivine gabbro. The seismic boundary separating these two layers represents an isograd marking the contact between low-grade (greenschist facies) and medium-grade (amphibolite facies) metamorphism. Lateral variations in Layer 2 thickness parallel to the spreading ridge suggests the occurrence of isotherm relief along the ridge axis where the crust is formed. The seismic Moho marks the boundary between mafic gabbros of Layer 3 and ultramafic rocks of the mantle (dunite and peridotite) but may also be associated with the maximum depth of serpentinization in the crust as it moves away from the ridge crests. Seismic reflection studies reveal

that the Cenozoic turbidite sediments overlie an irregular and bumpy basement (Layer 2).

The thick transition layer and slow spreading rates are seen to be characteristic features of Atlantic-type crust. However, the bathymetry of the Gorda Ridge crest and adjacent basin are more typical of Pacific-type spreading. Thin crust (4-5 km) and deep bathymetry in the central portion of the basin have resulted from crustal formation processes occurring at ridge crest offsets and are coincident with recent seismicity in the area. The Gorda Ridge offsets and asymmetrical fan spreading of magnetic anomalies are features observed in response to a regional change in spreading directions and encroachment of the Pacific and North American plates. The Gorda plate as a whole, does not respond rigidly to the resulting north-south compression.

The eastern edge of the Gorda Plate is marked by the continental margins of northern California and southern Oregon. Both reflection and refraction experiments revealed a thick wedge of Cenozoic sediments (2-3 km) overlying crust with a landward dip of about two degrees. The velocity profile of this crust is similar to the average basin structure except that slightly higher apparent velocities were obtained in up-dip directions.

Complex structures of the continental slope limited the reduction of refraction data using plane layer methods, and only a simplified velocity section was produced. Both sonobuoys here revealed the presence of Layers 2 and 3 overlain by unconsolidated sediment ($V_p \approx 1.8$ km/sec), and two other units of unknown composition (seismic velocities of about 2.5 and 4.0 km/sec, respectively). Analysis of material from

a sedimentary wedge off the coast of Oregon indicated that seismic velocities between 2.5 and 3.4 km/sec were seen for semi-consolidated Pleistocene to Miocene silts and sands. Reflection studies revealed the complex folded and faulted structures of the continental slope at penetration depths of about one kilometer.

The question of whether or not subduction is presently occurring at the eastern margin of the Gorda plate still remains unanswered. However, considerable evidence for the subduction processes are observed in the area. Included are the presence of a trench (although presently filled with sediment), the landward dip of the crust, a deformed continental slope, and earthquake activity to at least 30 km depth. A model of subduction unique to the northern California margin is one whereby young crust is subducted slowly and quickly reheated so that no brittle portion remains at typical Benioff depths. High sedimentation rates balance the subduction of the crust at the margin, preventing the formation of a deep trench. Accretion and deformation of sediments on the continental slope are associated with the subduction, but the mechanism for these processes cannot be determined from present refraction methods.

BIBLIOGRAPHY

Adachi, R., Fundamental relations on the seismic prospecting, Kumamoto Journal of Science, Series A, 2, 18-23, 1954.

Atwater, T., Implications of plate tectonics for the Cenozoic tectonic evolution of western North America, Geol. Soc. Amer. Bull., 81, 3513-3536, 1970.

Atwater, T. M., and J. D. Mudie, Block faulting on the Gorda Rise, Science, 159, 729-731, 1968.

Atwater, T. M., and J. D. Mudie, Detailed near-bottom geophysical study of the Gorda Rise, J. Geophys. Res., 78, 8665-8686, 1973.

Barry, K. M., Delay time and its application to refraction profile interpretation, In: Seismic Refraction Prospecting (A. W. Musgrave, ed.), Tulsa, Soc. of Exploration Geophysicists, 348-362, 1967.

Bloomfield, P., Fourier Analysis of Time Series: An Introduction, John Wiley and Sons, Inc., New York, 1976.

Bolt, B. A., C. Lomnitz, and T. V. McEvilly, Seismological evidence on the tectonics of central and northern California and the Mendocino escarpment, Bull. Seism. Soc. Am., 58, 1725, 1968.

Byerly, P., The earthquake of July 6, 1934, amplitudes and first motion, Bull. Seism. Soc. Am., 28, 1-13, 1938.

Chandra, U., Seismicity, earthquake mechanisms, and tectonics along the western coast of North America, from 42°N to 61°N, Bull. Seism. Soc. Am., 64, 1529-1549, 1974.

Clague, D. A. and P. F. Straley, Petrologic nature of the oceanic Moho, Geology, 5, 133-136, 1977.

Couch, R., Seismicity and crustal structure near the north end of the San Andreas fault system, In: Studies of the San Andreas Fault in Northern California, California Division of Mines and Geology, Special Report 140, eds. R. Streitz and R. Sherburne, 1980.

Couch, R., C. Kienle, and G. Connard, The continental margin of the Pacific Northwest: a summary of the geological and geophysical data, A report prepared for the Department of State, U.S.A., 1978.

Couch, R., L. Victor, and K. Keeling, Coastal and offshore earthquakes of the Pacific Northwest between 39° and 49°10'N latitude and 123° and 131°W longitude, School of Oceanography, Oregon State University, Tech. Rep., 1974.

Dehlinger, P., Evidence regarding the development of Juan de Fuca and Gorda Ridges in the Northeast Pacific Ocean, New York Academy of Sciences Trans., 31, 379-403, 1969.

Dehlinger, P., R. W. Couch, and M. Gemperle, Gravity and structure of the east part of the Mendocino escarpment, J. Geophys. Res., 72, 1233-1247, 1967.

Dehlinger, P., R. W. Couch, and M. Gemperle, Continental and oceanic structure from the Oregon coast westward across the Juan de Fuca Ridge, Can. J. Earth Sci., 5, 1079-1090, 1968.

Dehlinger, P., R. W. Couch, D. A. McManus, and M. Gemperle, Northeast Pacific structure, In: The Sea, (A.E. Maxwell, ed.), New York, John Wiley and Sons, Inc., V. r, pt. 2, 133-189, 1971.

Detrick, R. S., and G. M. Purdy, The crustal structure of the Kane fracture zone from seismic refraction studies, J. Geophys. Res., 85, 3759-3777, 1980.

Duncan, J. R., and L. D. Kulm, Mineralogy, provenance, and dispersal history of late Quaternary deep-sea sands in Cascadia Basin and Blanco fracture zone off Oregon, Jour. Sed. Pet., 40, 874-887, 1970.

Elvers, D., S. P. Srivastava, K. Putter, J. Morley, and D. Seidel, Asymmetric spreading across the Juan de Fuca and Gorda Rises as obtained from a detailed magnetic survey, Earth and Planet. Sci. Lett., 20, 211-219, 1973.

Gardner, L. W., An areal plan of mapping subsurface structure by refraction shooting, Geophysics, 4, 247, 1939.

Handbook of Oceanographic Tables, U. S. Naval Oceanographic Office, SP-68, 1966.

Harrison, C. G. A., Tectonics of mid-ocean ridges, Tectonophysics, 22, 301, 1974.

Hey, R. N., A new class of pseudofaults and their bearing on plate tectonics: A propagating rift model, Earth Planet. Sci. Lett., 37, 321-325, 1977.

Johnson, S. H., Interpretation of split-spread refraction data in terms of plane dipping layers, Geophysics, 41, 418-424, 1976.

Johnson, S. H., M. D. Cranford, B. T. Brown, J. E. Bowers, and R. E. McAllister, A free-fall direct-recording ocean bottom seismograph, Marine Geophysical Researches, 3, 103-117, 1977.

Johnson, S. H., and P. R. Jones, Microearthquakes located on the Blanco fracture zone with sonobuoy arrays, J. Geophys. Res., 83, 255-261, 1978.

Jones, P. R. III, Microearthquakes studies of the Blanco fracture zone and Gorda Ridge using sonobuoy arrays, Master's thesis, Oregon State University, Corvallis, 1975.

Karig, D. E. and G. F. Sharman, Subduction and accretion in trenches, Geol. Soc. Amer. Bull., 86, 377-389, 1975.

Keser, J. C., Wide-angle seismic refraction and reflection studies of the northern California and southern Oregon continental margins, Master's thesis, Oregon State University, Corvallis, 1978.

Klitgord, K. D., S. P. Huestis, J. D. Mudie, and R. L. Parker, An analysis of near-bottom magnetic anomalies: sea-floor spreading and the magnitized layer, Geophys. J. Roy. Astron. Soc., 43, 387-424, 1975.

Kulm, L. D. and G. Fowler, Cenozoic sedimentary framework of the Gorda-Juan de Fuca Plate and adjacent continental margin - a review, In: Modern and Ancient Geosynclinal Sedimentation, Soc. Econ. Paleo. Min., Sp. Pub. 19, Dotland Shaw, eds., 1974a.

Kulm, L. D. and G. Fowler, Oregon continental margin structures and stratigraphy: A test of the imbricate thrust model. In: The Geology of Continental Margins, Burk and Drakes, eds., Springer-Verlag, New York, 261-283, 1974b.

Lewis, B. T. R., and W. E. Snydsman, Evidence for a low velocity layer at the base of the oceanic crust, Nature, 266, 340-344, 1977.

Lister, C. R. B., On the penetration of water into hot rock, Geophys. J. Roy. Astron. Soc., 39, 465-509, 1974.

Lister, C. R. B., Qualitative models of spreading-center processes, including hydrothermal penetration, Tectonophysics, 37, 203-218, 1977.

McKenzie, D. P., and W. J. Morgan, The evolution of triple junctions, Nature, 224, 125-133, 1969.

McManus, D. A., Physiography of Cobb and Gorda Rises, northeast Pacific Ocean, Geol. Soc. Amer. Bull., 78, 527-546, 1967.

Menard, H. W., Sea-floor spreading, topography, and the second layer, Science, 157, 923-924, 1967.

Minster, J. B. and T. H. Jordan, Present-day plate motions, J. Geophys. Res., 83, 5331-5354, 1978.

Moores, E. M., and E. D. Jackson, Ophiolites and oceanic crust, Nature, 250, 136-139, 1974.

Morris, G. B., Delay time function method and its application to the Lake Superior refraction data, J. Geophys. Res., 27, 297-314, 1972.

Morris, G. B., R. W. Raitt, and G. G. Shor, Jr., Velocity anisotropy and delay-time maps of the mantle near Hawaii, J. Geophys. Res., 74, 4300-4316, 1969.

Northrup, J., Accuracy of earthquake epicenters on the Gorda Ridge, Bull. Seism. Soc. Am., 60, 265-267, 1970.

Northrup, J. and M. F. Morrison, Seismic slip rate versus sea floor spreading rate on the Eastern Pacific Rise and Pacific Antarctic Ridge, J. Geophys. Res., 75, 1970.

Nowroozi, A. A., Seismicity of the Mendocino Escarpment and the aftershock sequence of June 26, 1968: ocean bottom seismic measurements, Bull. Seism. Soc. Amer., 63, 441-456, 1973.

Officer, C. B., Jr., Introduction to the Theory of Sound Transmission, New York, McGraw-Hill, 1958.

Raff, A. D. and R. G. Mason, Magnetic survey off the west coast of North America, 40°N latitude to 52°N latitude, Geol. Soc. Amer. Bull., 72, 1267-1270, 1961.

Raitt, R. W., Seismic refraction studies of the Mendocino fracture zone, Abstracts of Papers, International Association of Physical Oceanography, 13th General Assembly, 1963, Berkeley, 6, 71, 1963.

Raitt, R. W., G. G. Shor, Jr., T. J. G. Francis, and G. B. Morris, Anisotropy of the Pacific upper mantle, J. Geophys. Res., 74, 3095, 1969.

Riddihough, R. P., A model for recent plate interactions off Canada's west coast, Can. J. Earth Sci., 14, 384-396, 1977.

Rinehart, V. J., Investigations of 12 earthquakes off the Oregon and northern California coasts, M.S. thesis, Oregon State University, Corvallis, 42 p., 1964.

Rosendahl, B. R., R. W. Raitt, L. M. Dorman, L. D. Bibee, D. M. Hussong, and G. H. Sutton, Evolution of oceanic crust, 1. A physical model of the East Pacific Rise crest derived from seismic refraction data, J. Geophys. Res., 81, 5294-5304, 1976.

Salisbury, M. H. and N. I. Christensen, The seismic velocity structure of a traverse through the Bay of Islands ophiolite complex, Newfoundland, an exposure of oceanic crust and upper mantle, J. Geophys. Res., 83, 1978.

Scheidegger, A. E. and P. L. Willmore, The use of a least-squares method for the interpretation of data from seismic surveys, Geophysics, 22, 9, 1957.

Scheidegger, K. F., Volcanic ash layers in deep-sea sediments and their petrological significance, Earth Planet. Sci. Lett., 17, 397-407, 1973.

Sclater, J. G. and J. Francheteau, The implication of terrestrial heat flow observations on current tectonic and geochemical models of the crust and upper mantle of the earth, Geophys. J. Roy. Astron. Soc., 20, 509-537, 1970.

Seeber, L., M. Barazanzi, and A. A. Nowroozi, Microearthquakes, seismicity and tectonics of coastal northern California, Bull. Seism. Soc. Amer., 60, 1669-1699, 1970.

Seely, D. R., P. R. Vail, and G. G. Walton, Trench slope model, In: The Geology of Continental Margins, Springer-Verlag, New York, 1974.

Sheriff, R. E., Operational problems in marine refraction work, In: Seismic Refraction Prospecting (A. W. Musgrave, ed.), Tulsa, Soc. of Exploration Geophysicists, 482-490, 1967.

Shor, G. G., Jr., P. Dehlinger, H. K. Kirk, and W. S. French, Seismic refraction studies off Oregon and northern California, J. Geophys. Res., 73, 2175-2194, 1968.

Shor, G. G., Jr., H. W. Menard, and R. W. Raitt, Structure of the Pacific Basin, In: The Sea (A. E. Maxwell, ed.), New York, John Wiley and Sons, Inc., v. 4, pt. 2, 3-27, 1971.

Silver, E. A., Late Cenozoic underthrusting of the continental margin off northernmost California, Science, 166, 1265-1266, 1969a.

Silver, E. A., Structure of the continental margin off northern California, north of the Gorda Escarpment, Ph. dissert., California Univ., San Diego, California, 133 p., 1969b.

Silver, E. A., Tectonics of the Mendocino triple junction, Geol. Soc. Amer. Bull., 82, 2965-2978, 1971a.

Silver, E. A., Transitional tectonics and late Cenozoic structure of the continental margin off northernmost California, Geol. Soc. Amer. Bull., 82, 1-22, 1971b.

Smith, S. W., and J. S. Knapp, The northern termination of the San Andreas fault, Geophysics Program, University of Washington, Seattle, 1977.

Snavely, P. D., Jr., H. C. Wagner, and D. L. Lander, Geologic cross section of the central Oregon continental margin, G.S.A. Map and Chart Series MC-28J, 1980.

Spigai, J. J., Marine Geology of the continental margin off southern Oregon. Ph.D. Thesis, Oregon State University, Corvallis, 214 p., 1971.

Tobin, D. G., and L. R. Sykes, Seismicity and tectonics of the northeast Pacific Ocean, J. Geophys. Res., 73, 3821-3845, 1968.

Vine, F. J., Spreading of the ocean floor: new evidence, Science, 154, 1405-1415, 1966.

Vine, F. J. and J. T. Wilson, Magnetic anomalies over a young oceanic ridge off Vancouver Island, Science, 150, 485-489, 1965.

von Huene, R., and L. D. Kulm, Tectonic summary of Leg 18, In: Initial Reports of the DSDP, Vol. 18, Washington, D. C., U. S. Government Printing Office, 1973.

Wilde, P., T. E. Chase, M. L. Holmes, W. R. Normark, J. A. Thomas, D. S. McCulloch and L. D. Kulm, Oceanographic data off northern California-southern Oregon, 40° to 43° North including the Gorda deep-sea fan, Lawrence Berkeley Laboratories, publication 251, University of California, Berkeley, 1978.

Willmore, P. L. and A. M. Bancroft, The time-term approach to refraction seismology, Geophysics J., 3, 419, 1960.

Wilson, J. T., Transform faults, oceanic ridges and magnetic anomalies southwest of Vancouver Island, Science, 150, 482-489, 1965.

Wilson, W. D., Equation for the speed of sound in sea water, Journal of the Acoustical Society of America, 32, 1357, 1960.

Wrolstad, K. W., Applications of source signature deconvolution to air gun seismic profiling and the measurement of attenuation from reflection seismograms, Ph.D. thesis, Oregon State University, Corvallis, 1978.

Wrolstad, K. W. and S. H. Johnson, Sonobuoy velocity profile from the continental shelf to the Gorda Ridge, Abstract in: EOS Trans. AGU, 58, 161, 1976.

APPENDICES

APPENDIX I

Generalized Flow Chart for Data Reduction and Delay-Time-Function Procedure

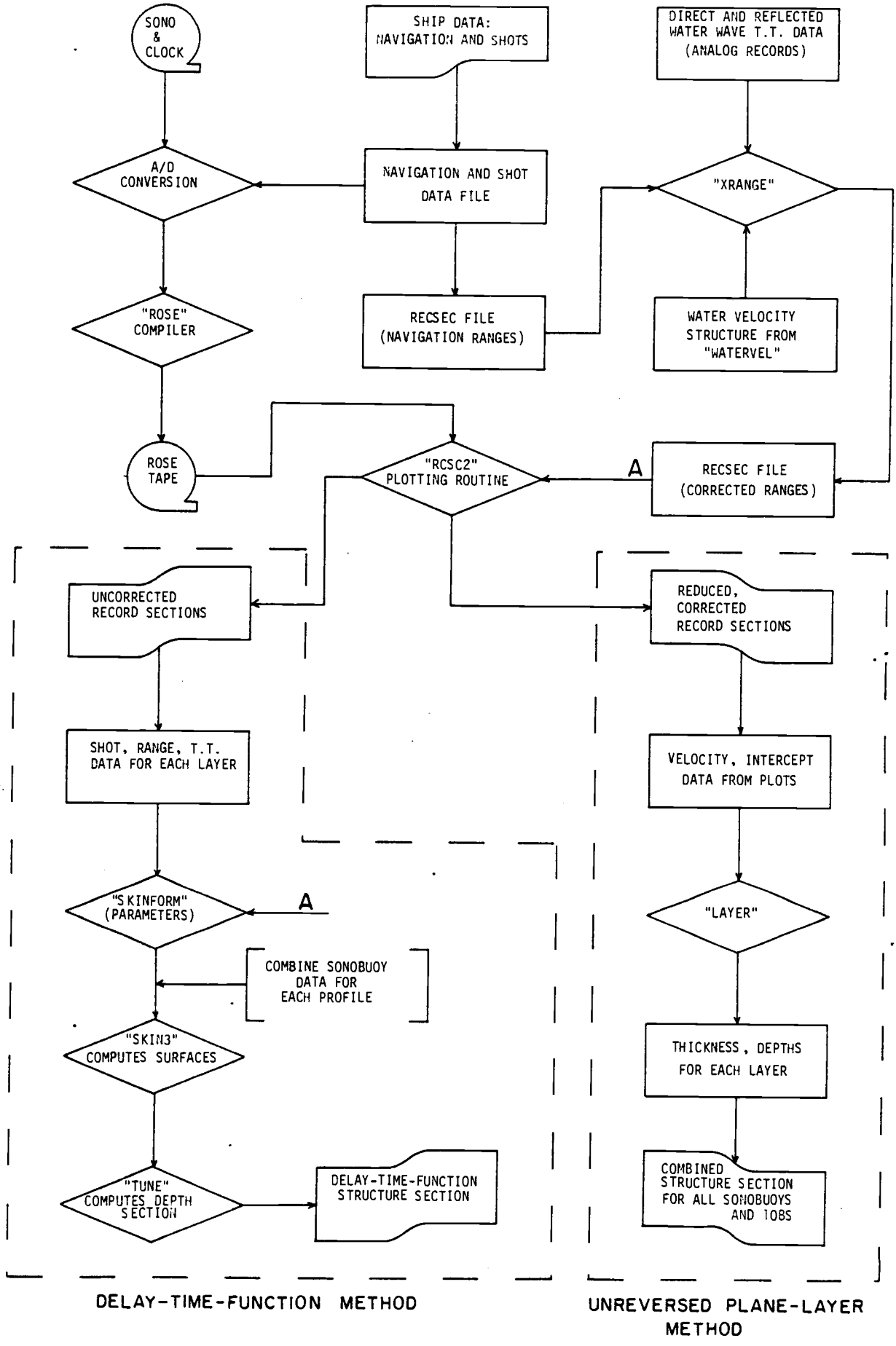
SONO & CLOCK
SHIP DATA: NAVIGATION AND SHOTS
DIRECT AND REFLECTED WATER WAVE T.T. DATA (ANALOG RECORDS)
A/D CONVERSION
NAVIGATION AND SHOT DATA FILE
"XRANGE"
"ROSE" COMPILER
RECSEC FILE (NAVIGATION RANGES)
WATER VELOCITY STRUCTURE FROM "WATERVEL"
ROSE TAPE
"RCSC2" PLOTTING ROUTINE
A
RECSEC FILE (CORRECTED RANGES)
UNCORRECTED RECORD SECTIONS
REDUCED, CORRECTED RECORD SECTIONS
SHOT, RANGE, T.T. DATA FOR EACH LAYER
VELOCITY, INTERCEPT DATA FROM PLOTS
"SKINFORM" (PARAMETERS)
A
"LAYER"
COMBINE SONOBUOY DATA FOR EACH PROFILE
"SKIN3" COMPUTES SURFACES
THICKNESS, DEPTHS FOR EACH LAYER
"TUNE" COMPUTES DEPTH SECTION
DELAY-TIME-FUNCTION STRUCTURE SECTION
COMBINED STRUCTURE SECTION FOR ALL SONOBUOYS AND IOBS
DELAY-TIME-FUNCTION METHOD
UNREVERSED PLANE-LAYER METHOD

APPENDIX II

Sonobuoy Record Sections

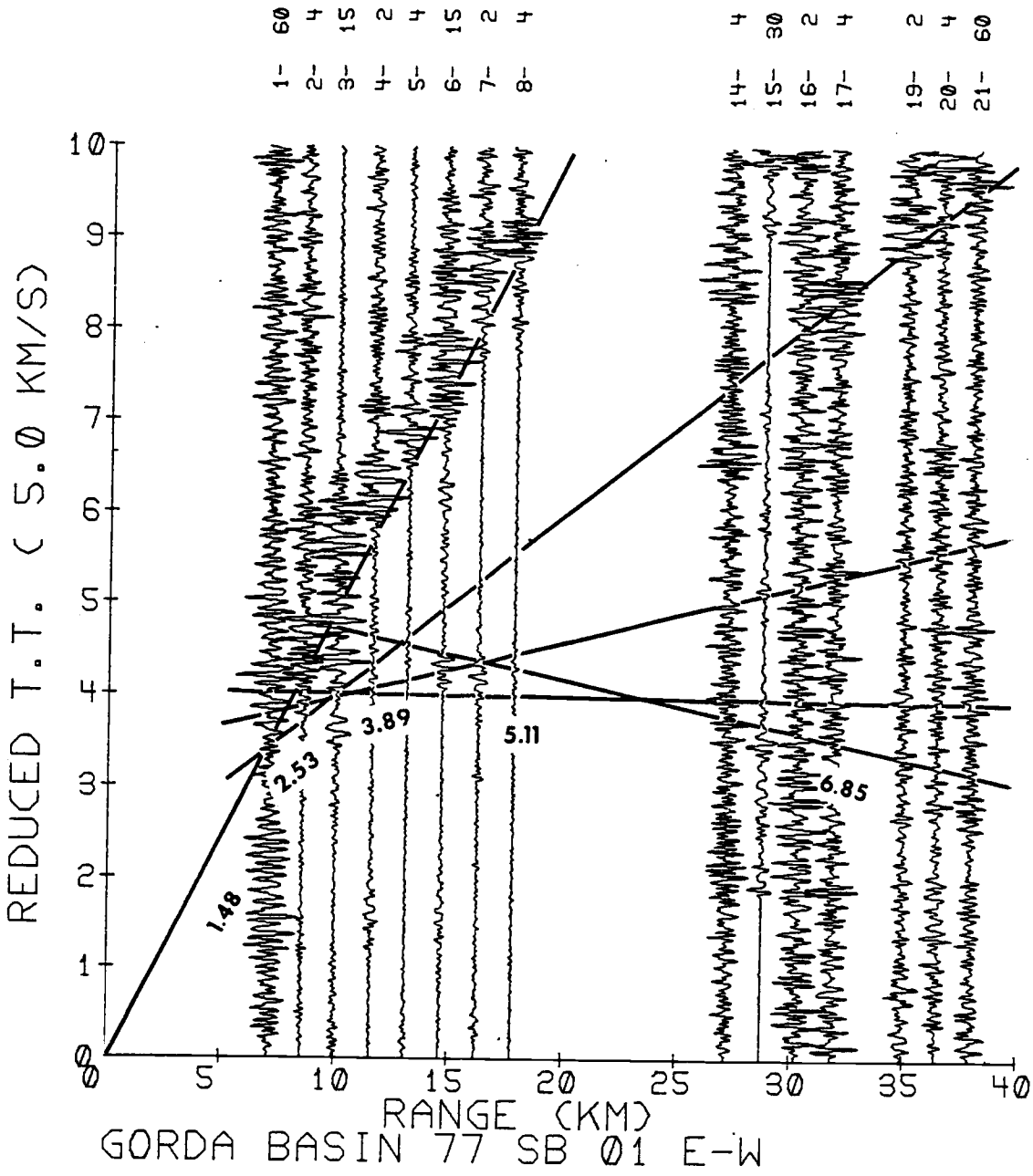

Figure 31. Reduced record section for sonobuoy SB1. Apparent seismic velocities in km/sec.

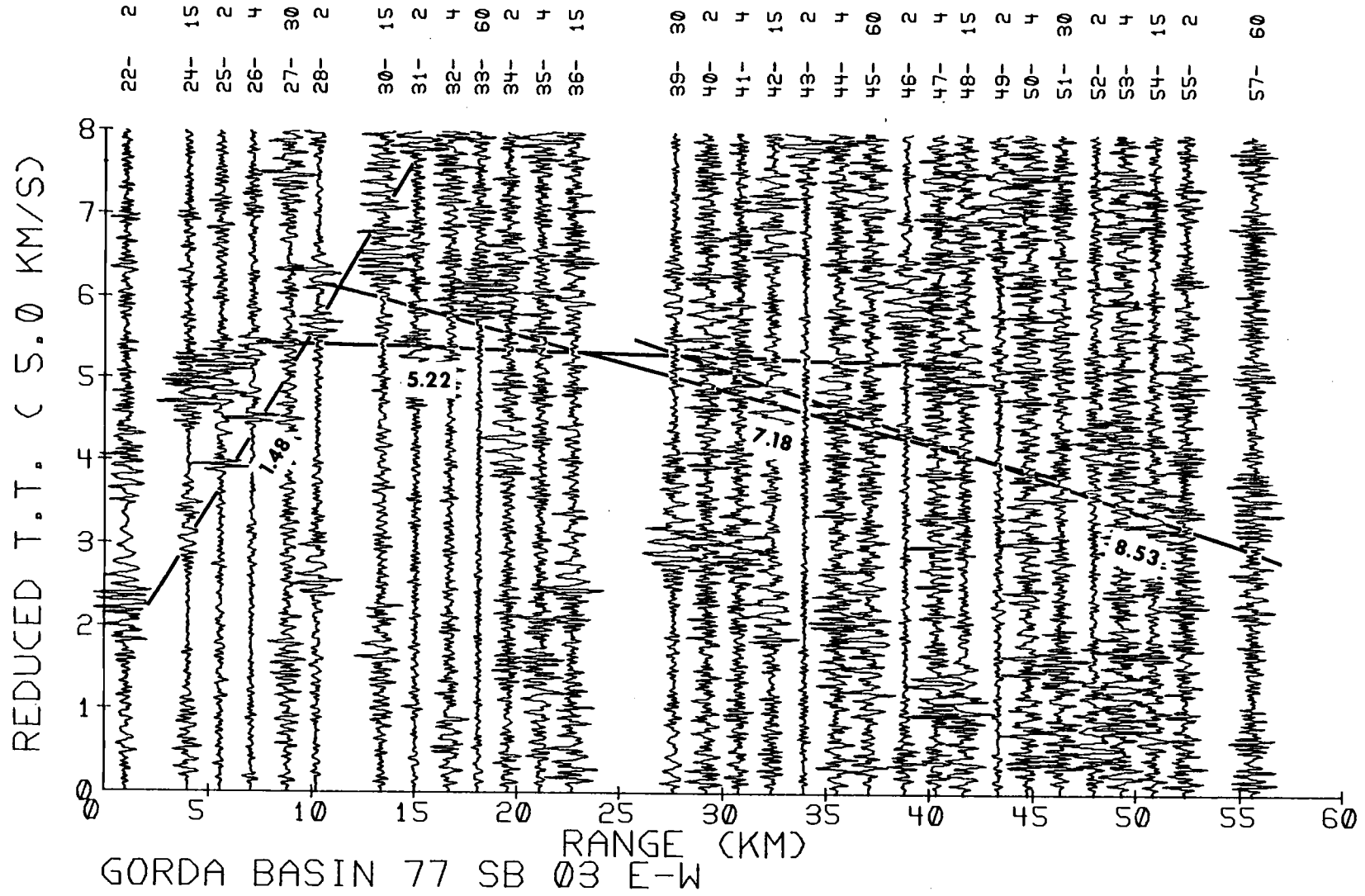

Figure 32. Reduced record section for sonobuoy SB3. Apparent seismic velocities in km/sec.

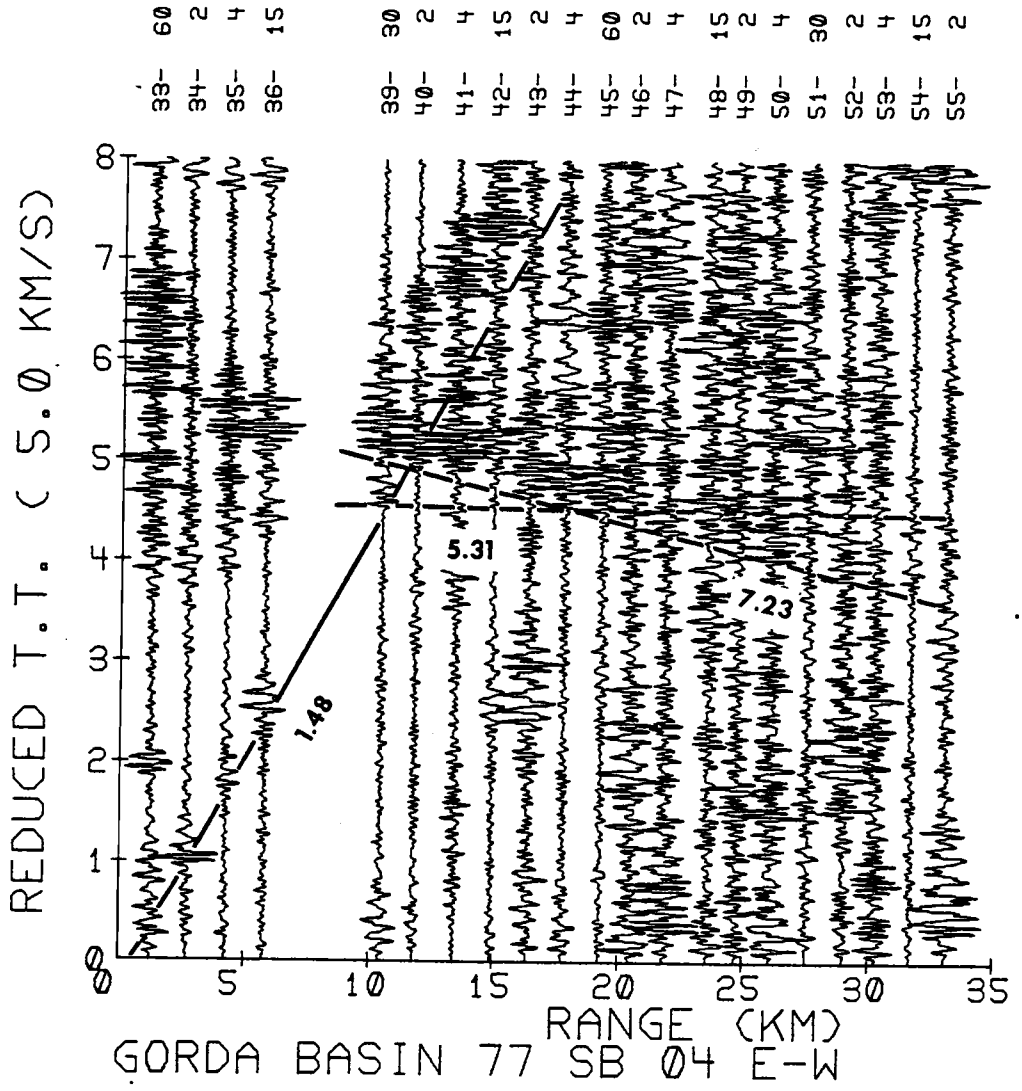

Figure 33. Reduced record section for sonobuoy SB4. Apparent seismic velocities in km/sec.

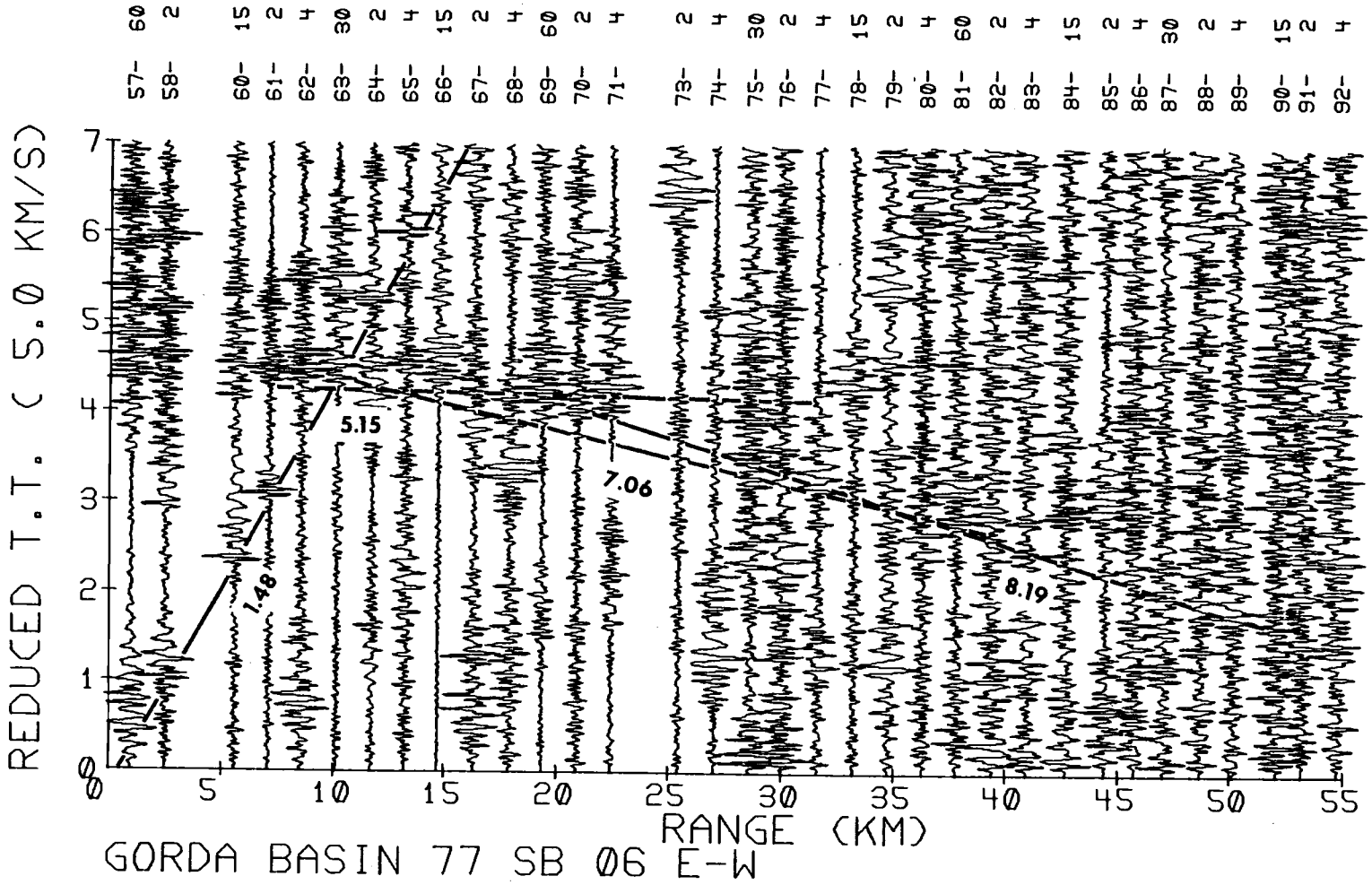

Figure 34. Reduced record section for sonobuoy SB6. APparent seismic velocities in km/sec.

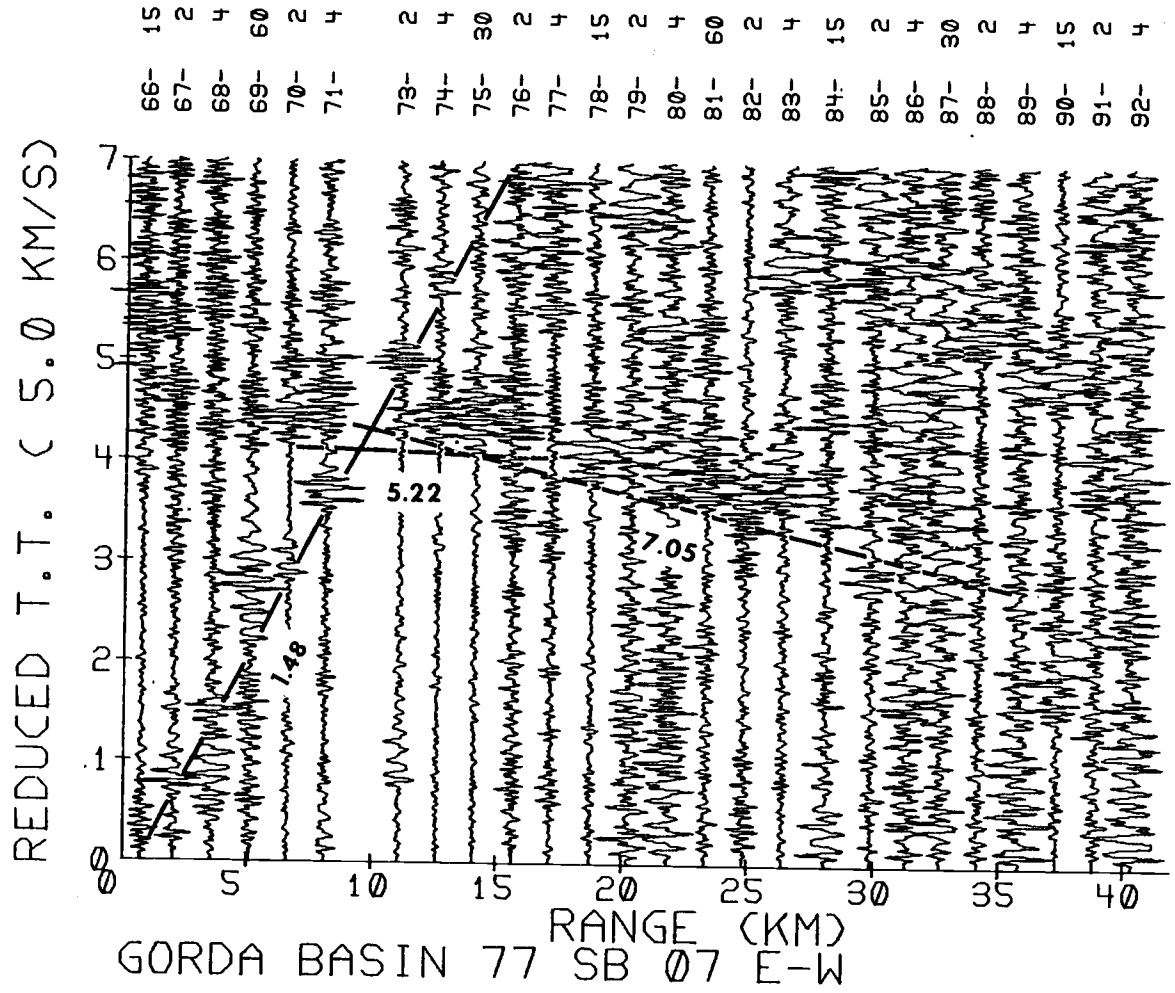

Figure 35. Reduced record section for sonobuoy SB7. Apparent seismic velocities in km/sec.

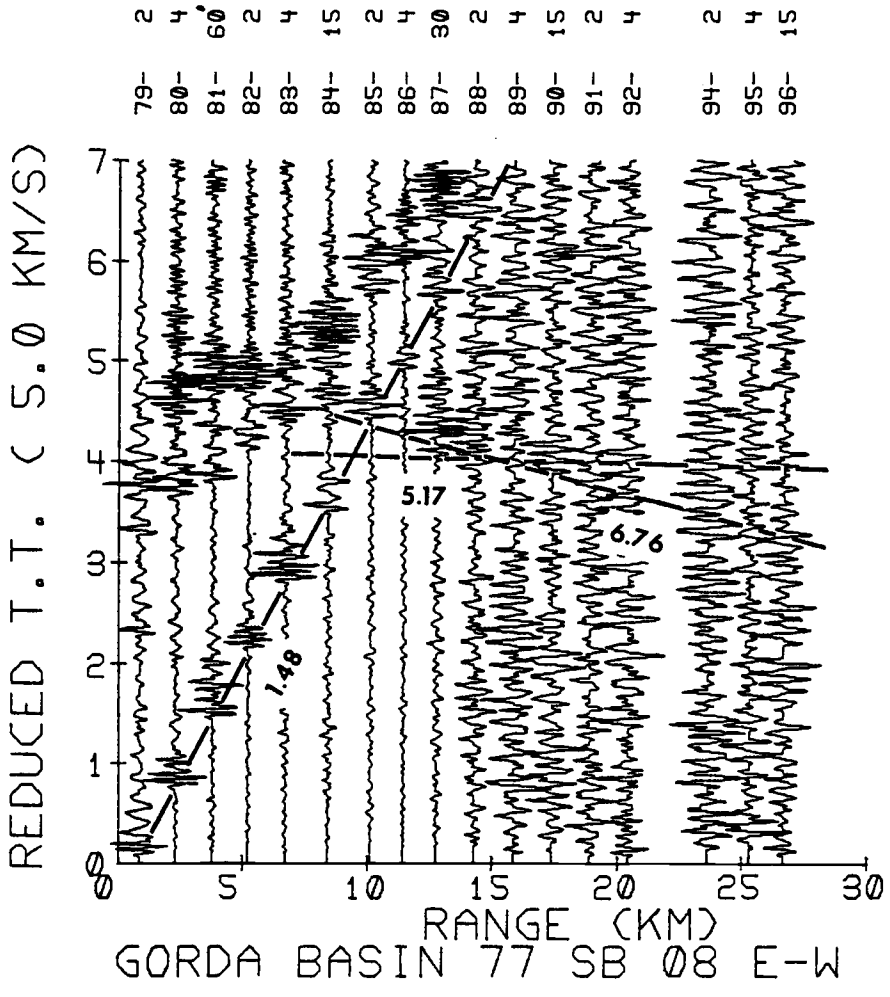

Figure 36. Reduced record section for sonobuoy SB8. Apparent seismic velocities in km/sec.

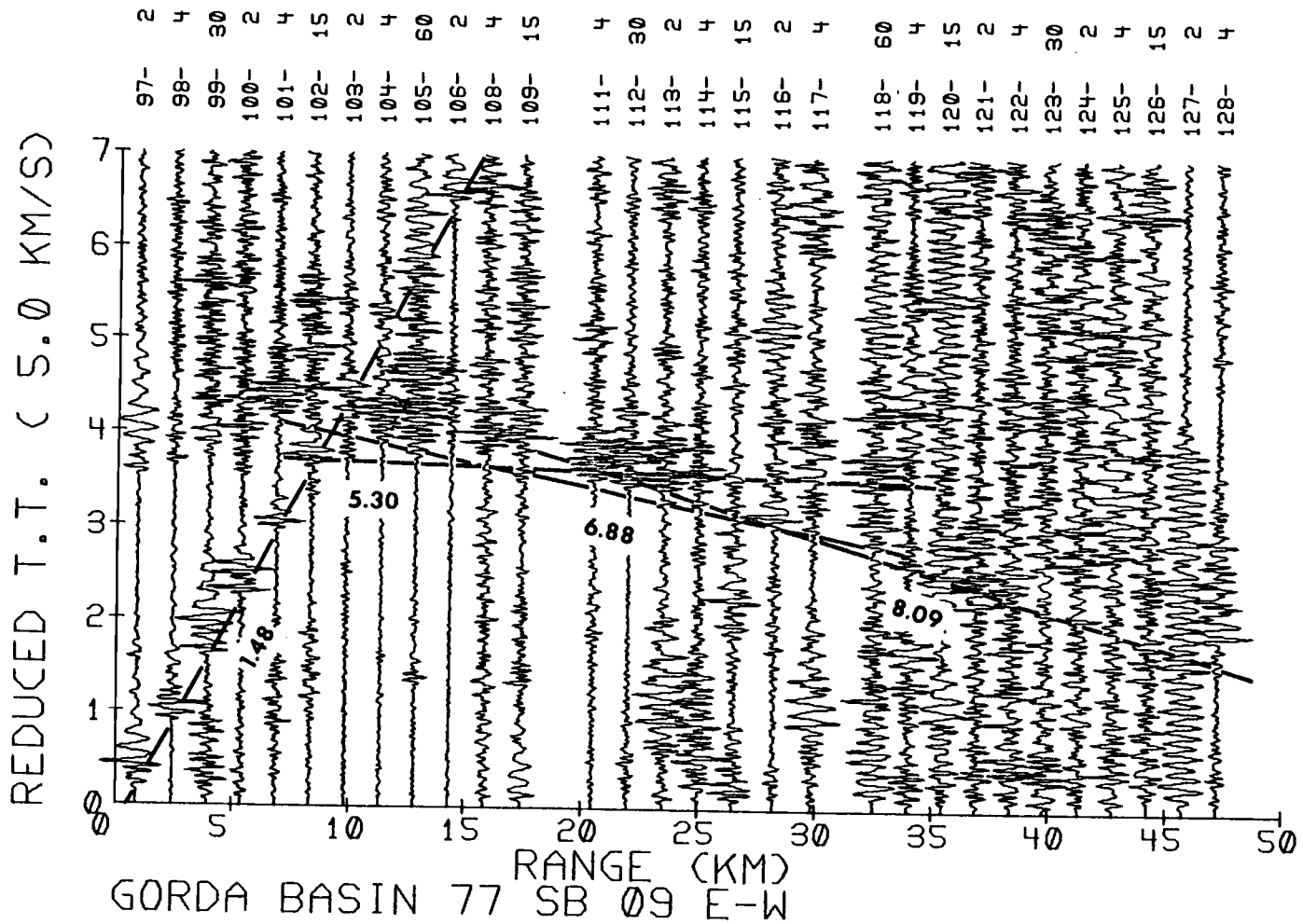

Figure 37. Reduced record section for sonobuoy SB9. Apparent seismic velocities in km/sec.

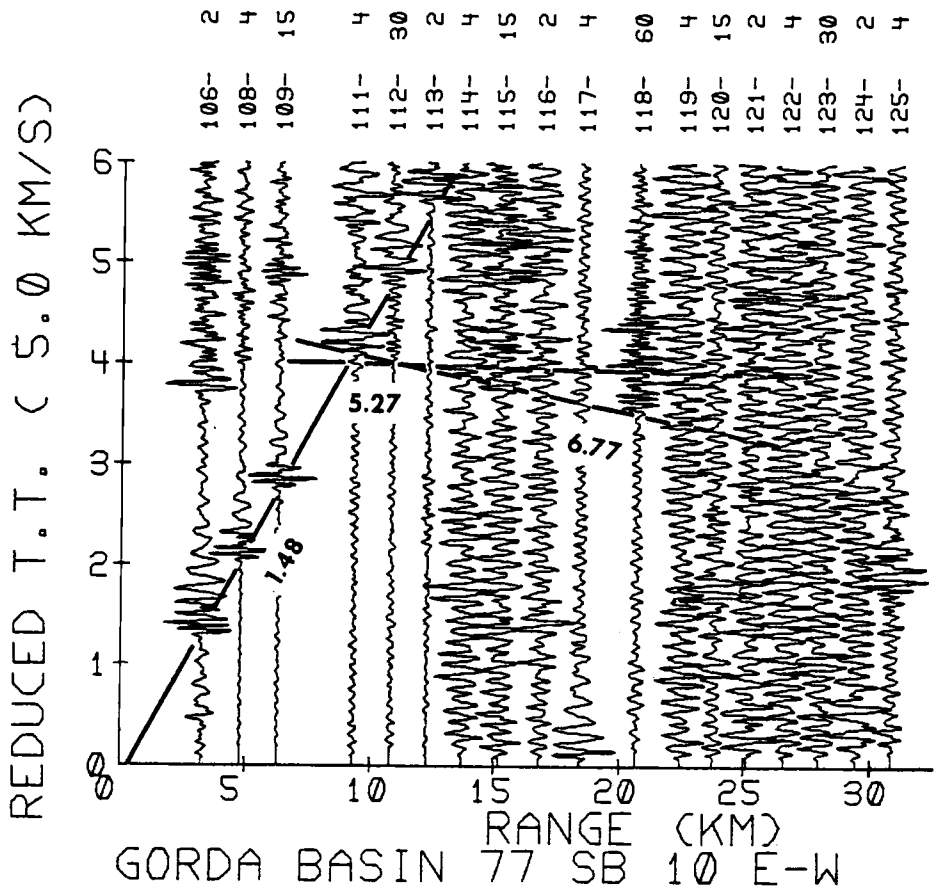

Figure 38. Reduced record section for sonobuoy SB10. Apparent seismic velocities in km/sec.

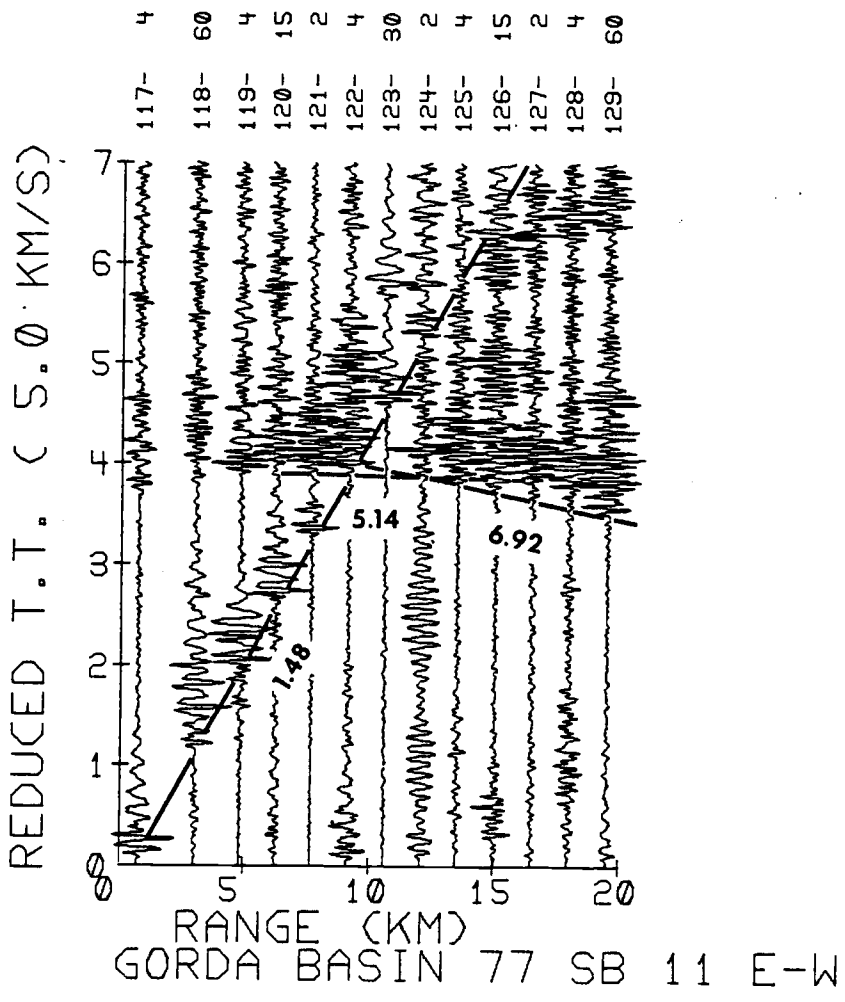

Figure 39. Reduced record section for sonobuoy SB11. Apparent seismic velocities in km/sec.

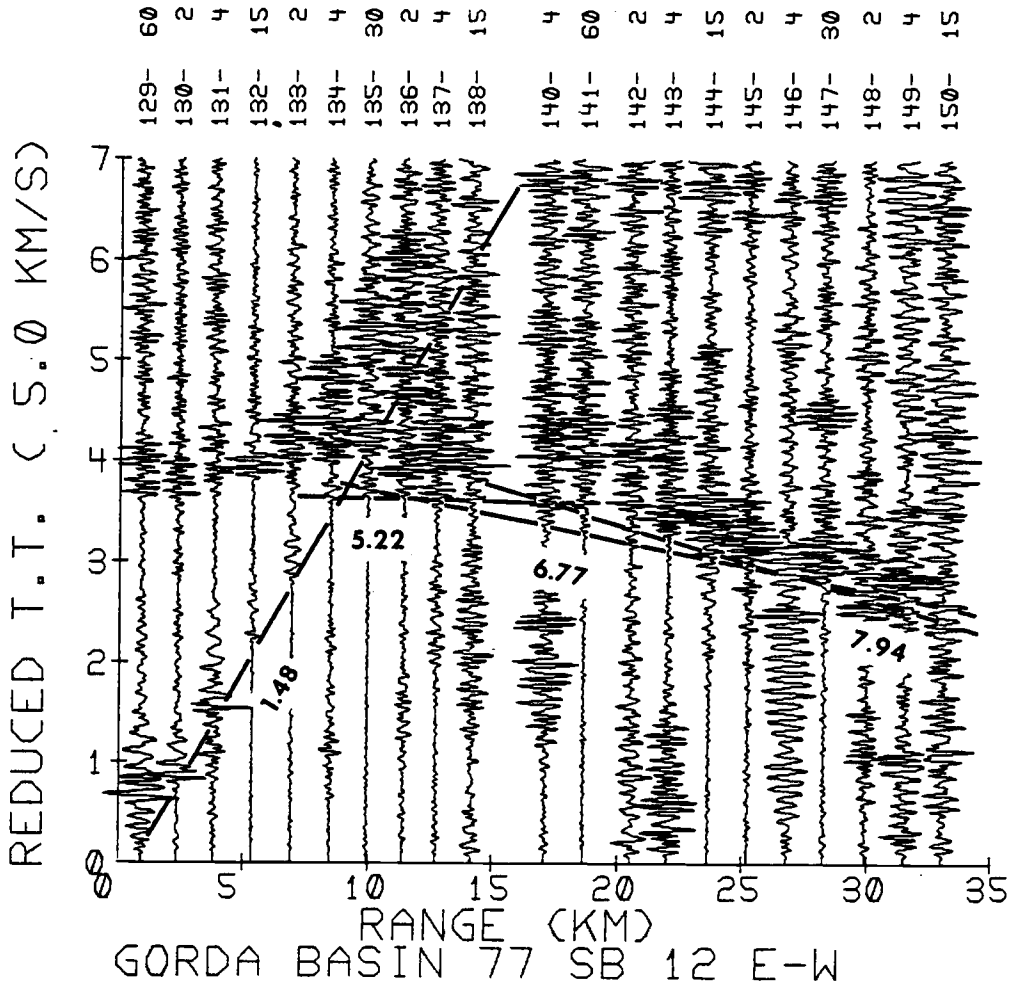

Figure 40. Reduced record section for sonobuoy SB12. Apparent seismic velocities in km/sec.

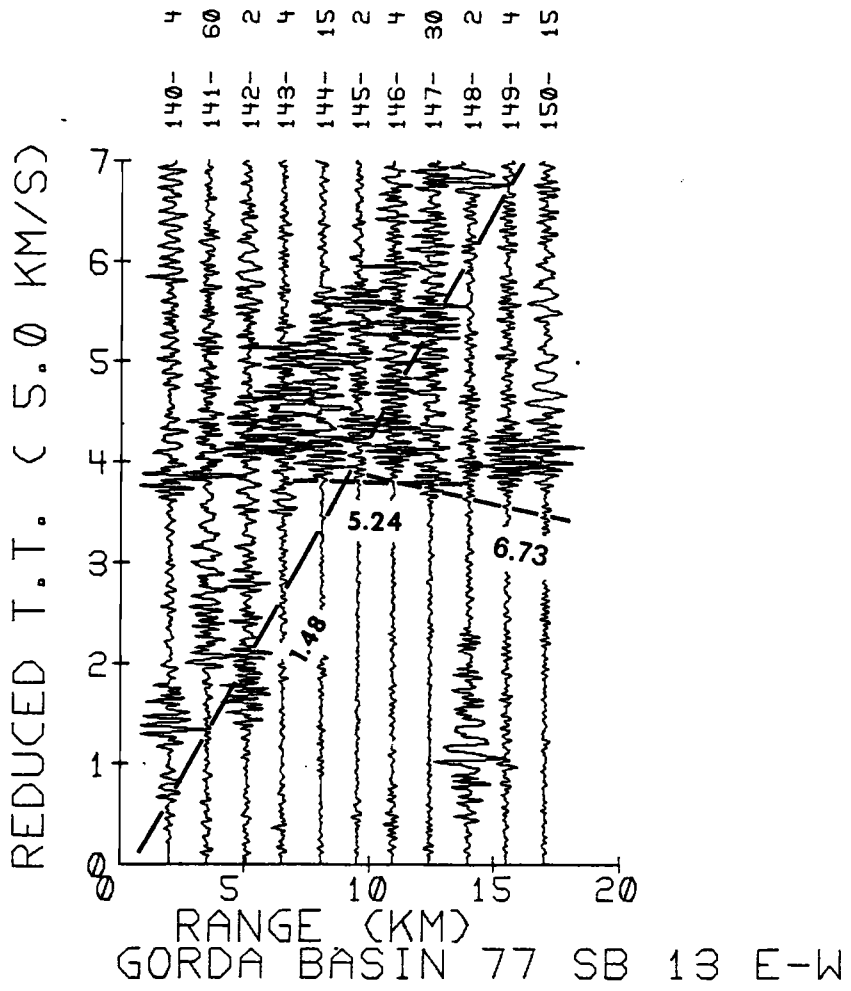

Figure 41. Reduced record section for sonobuoy SB13. Apparent seismic velocities in km/sec.

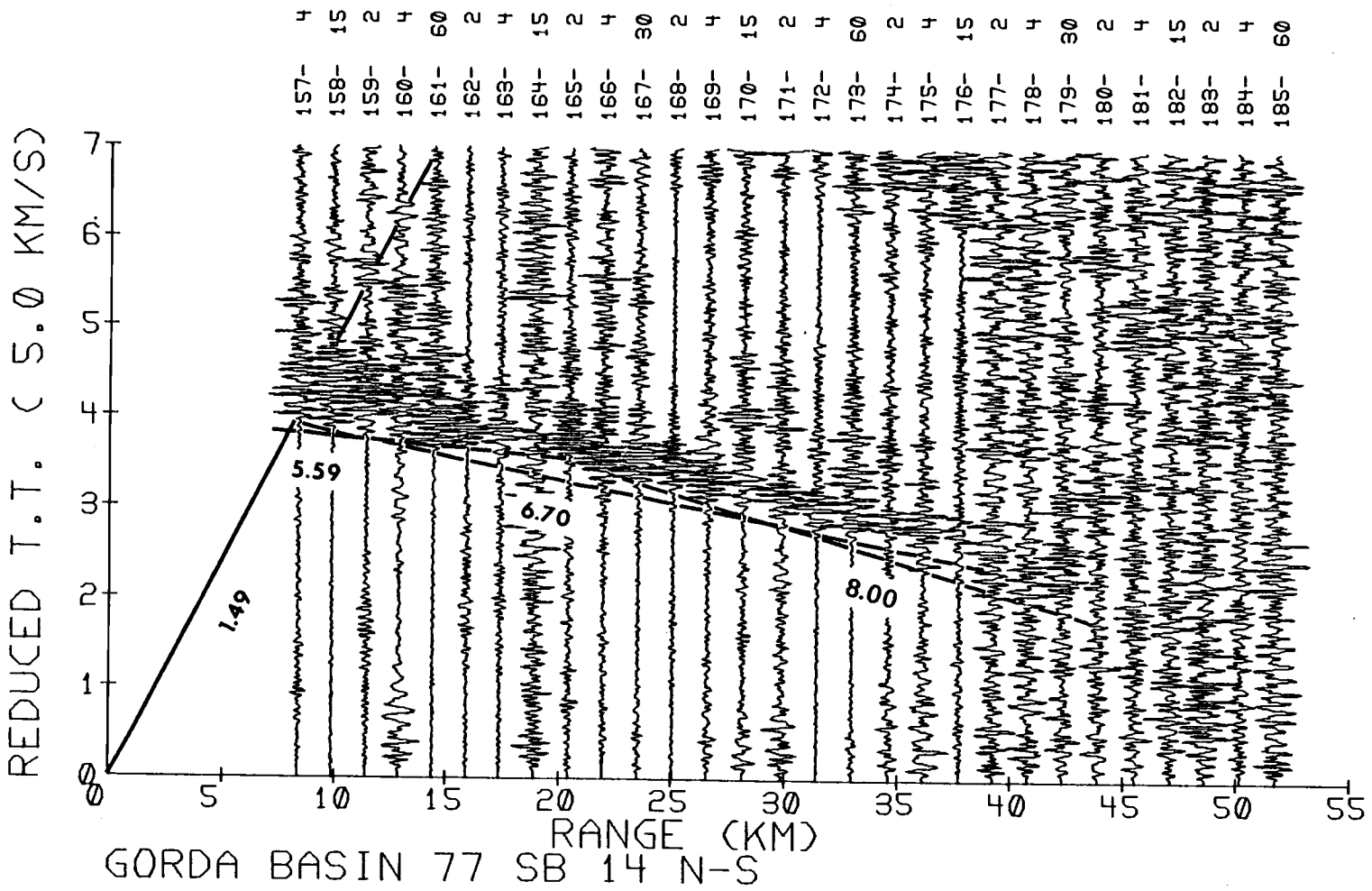

Figure 42. Reduced record section for sonobuoy SB14. Apparent seismic velocities in km/sec.

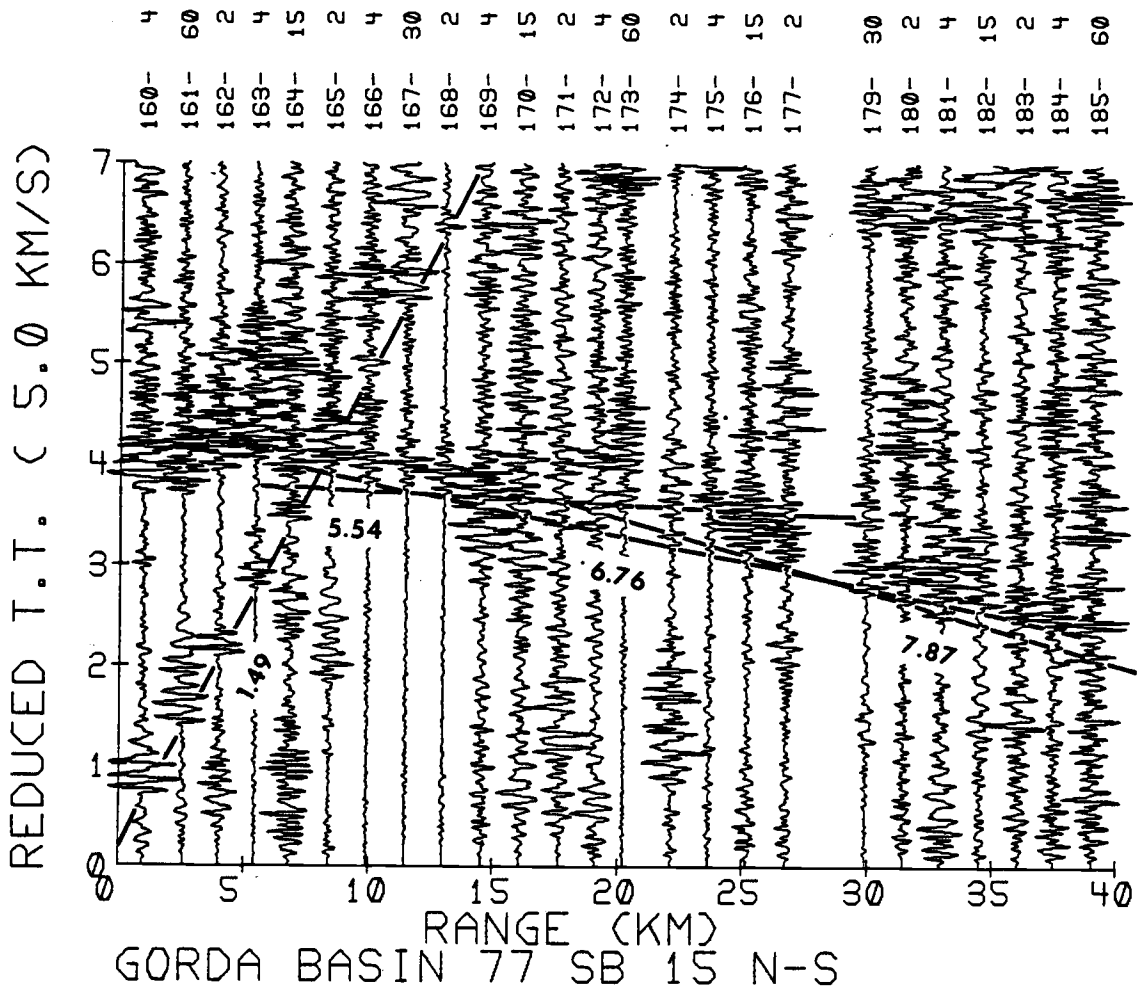

Figure 43. Reduced record section for sonobuoy SB15. Apparent seismic velocities in km/sec.

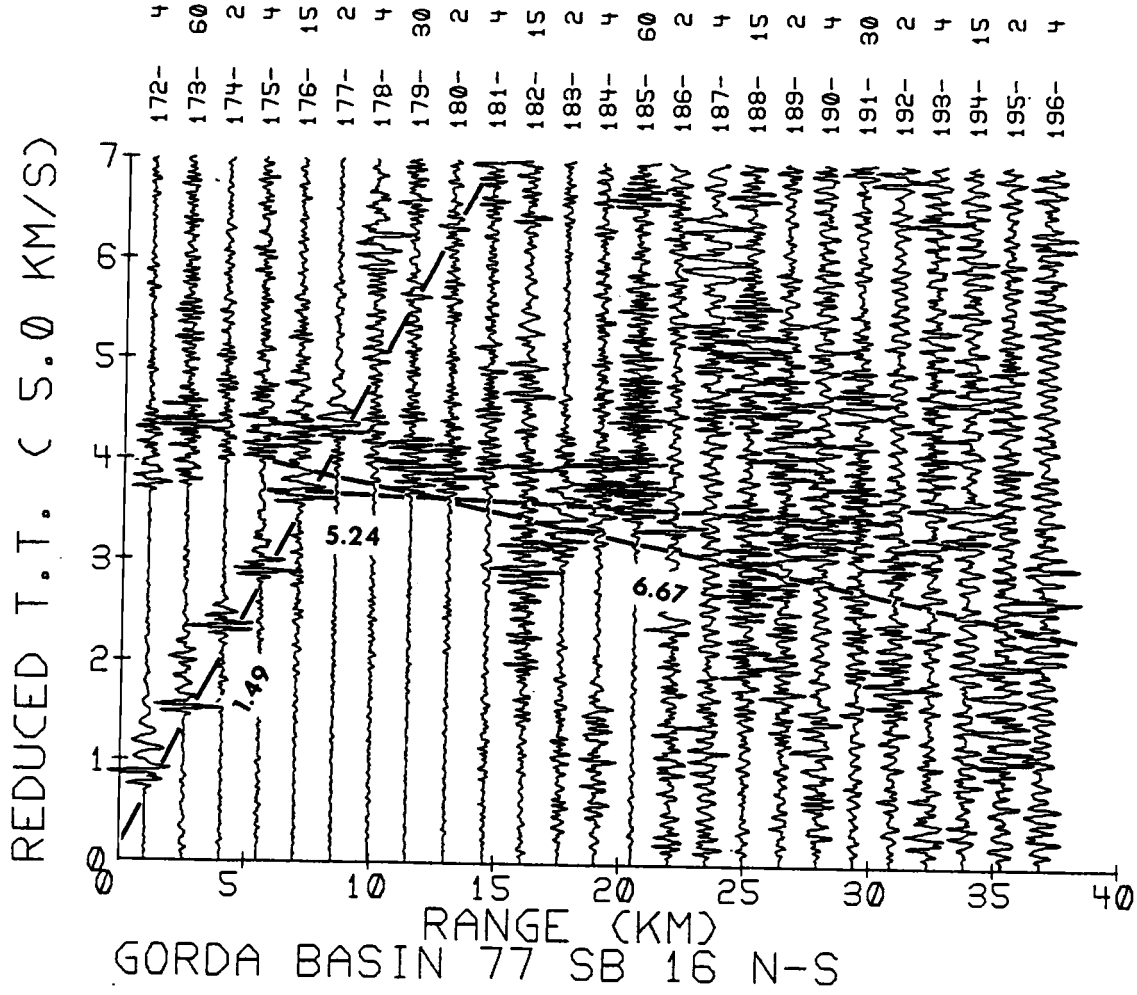

Figure 44. Reduced record section for sonobuoy SB16. Apparent seismic velocities in km/sec.

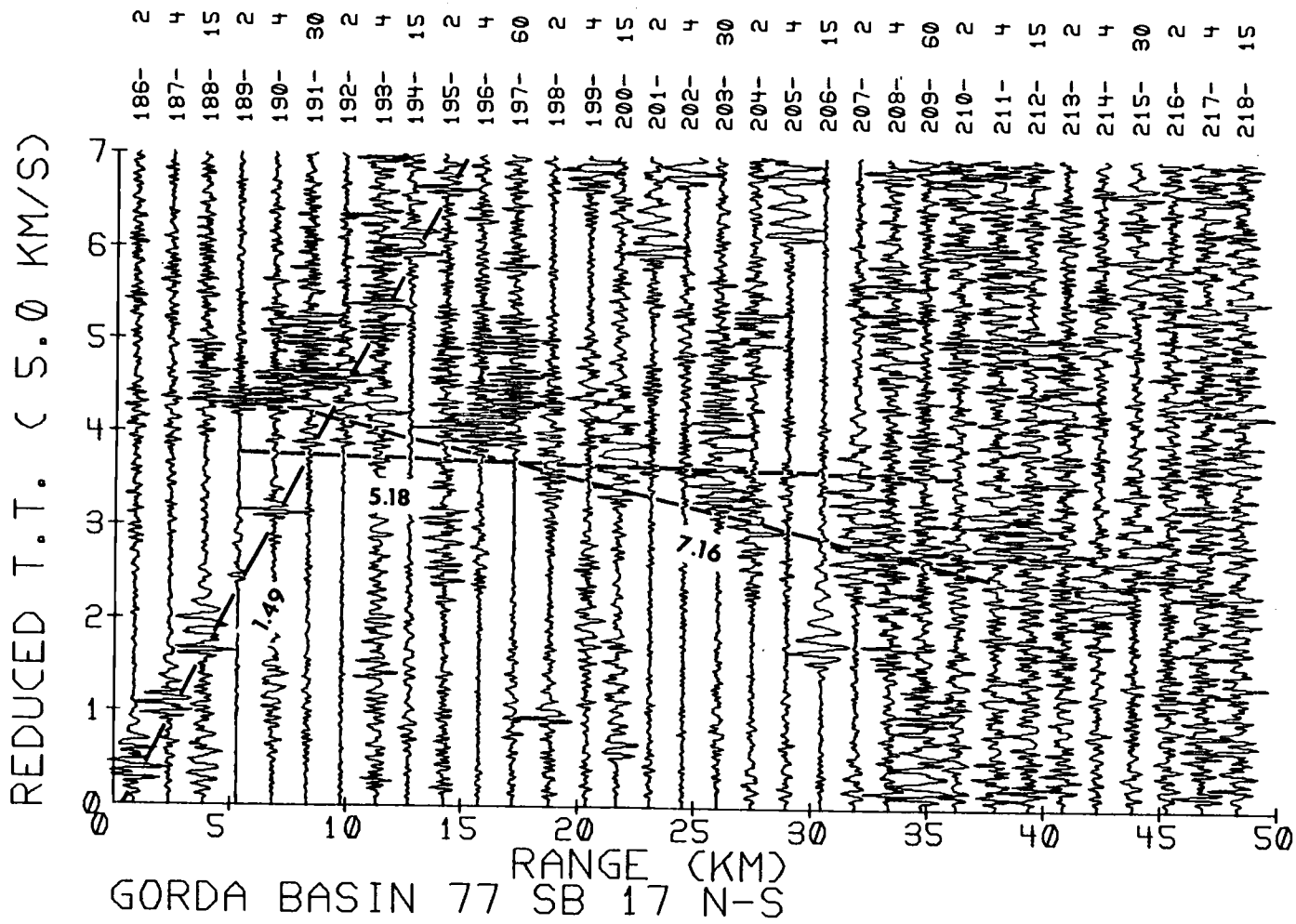

Figure 45. Reduced record section for sonobuoy SB17. Apparent seismic velocities in km/sec.

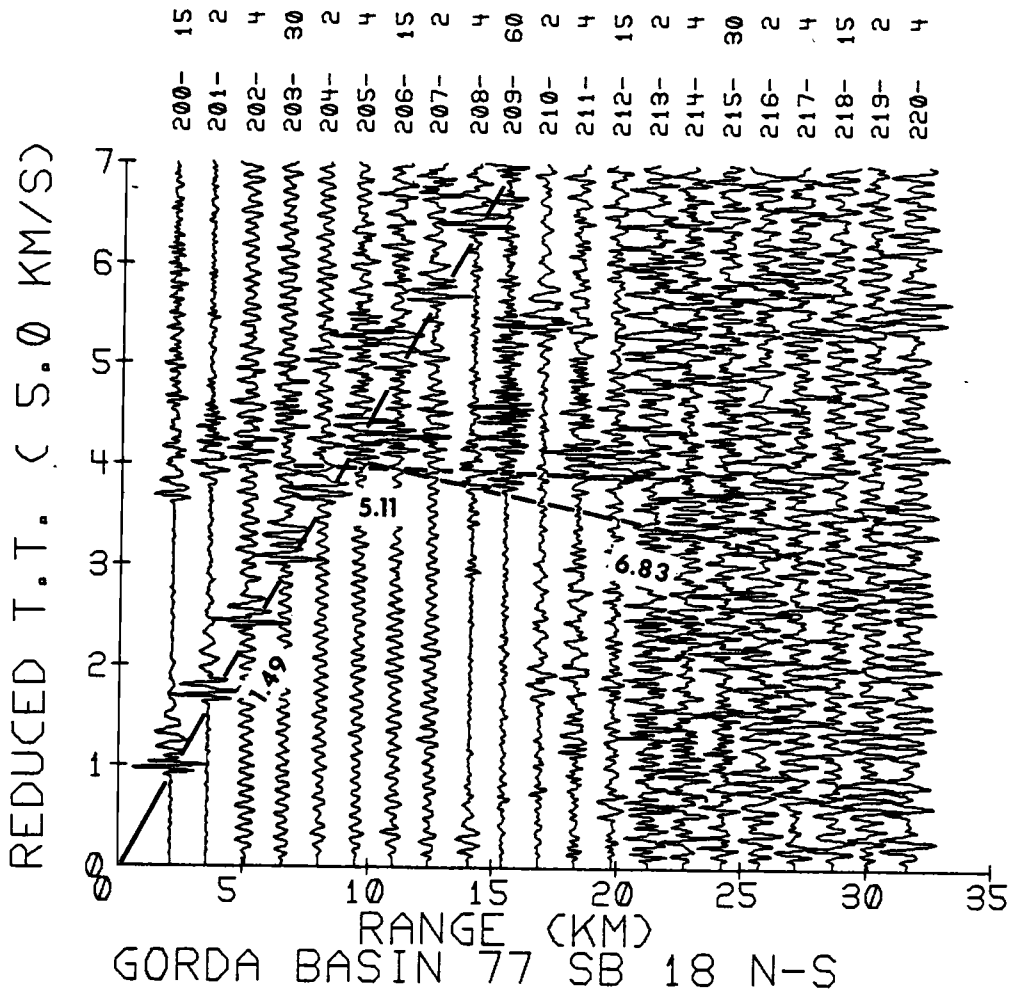

Figure 46. Reduced record section for sonobuoy SB18. Apparent seismic velocities in km/sec.

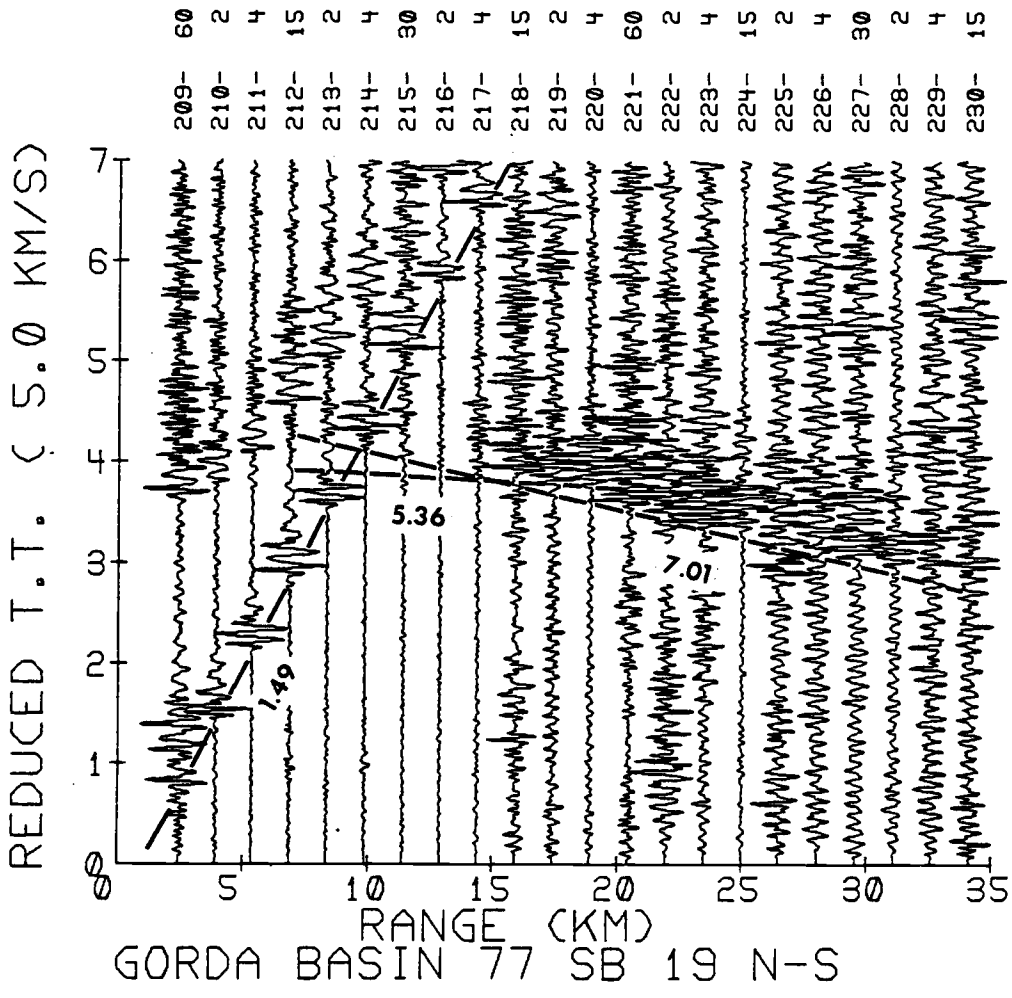

Figure 47. Reduced record section for sonobuoy SB19. Apparent seismic velocities in km/sec.

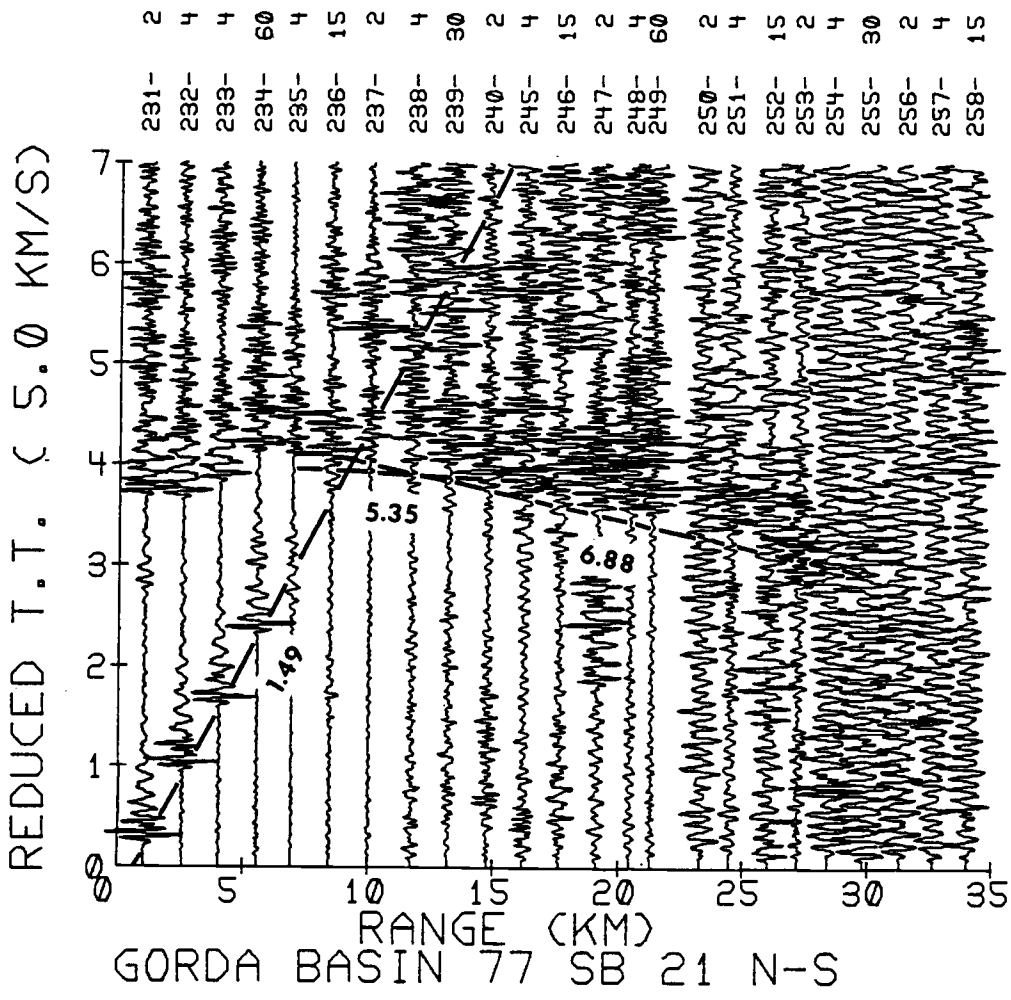

Figure 48. Reduced record section for sonobuoy SB21. Apparent seismic velocities in km/sec.

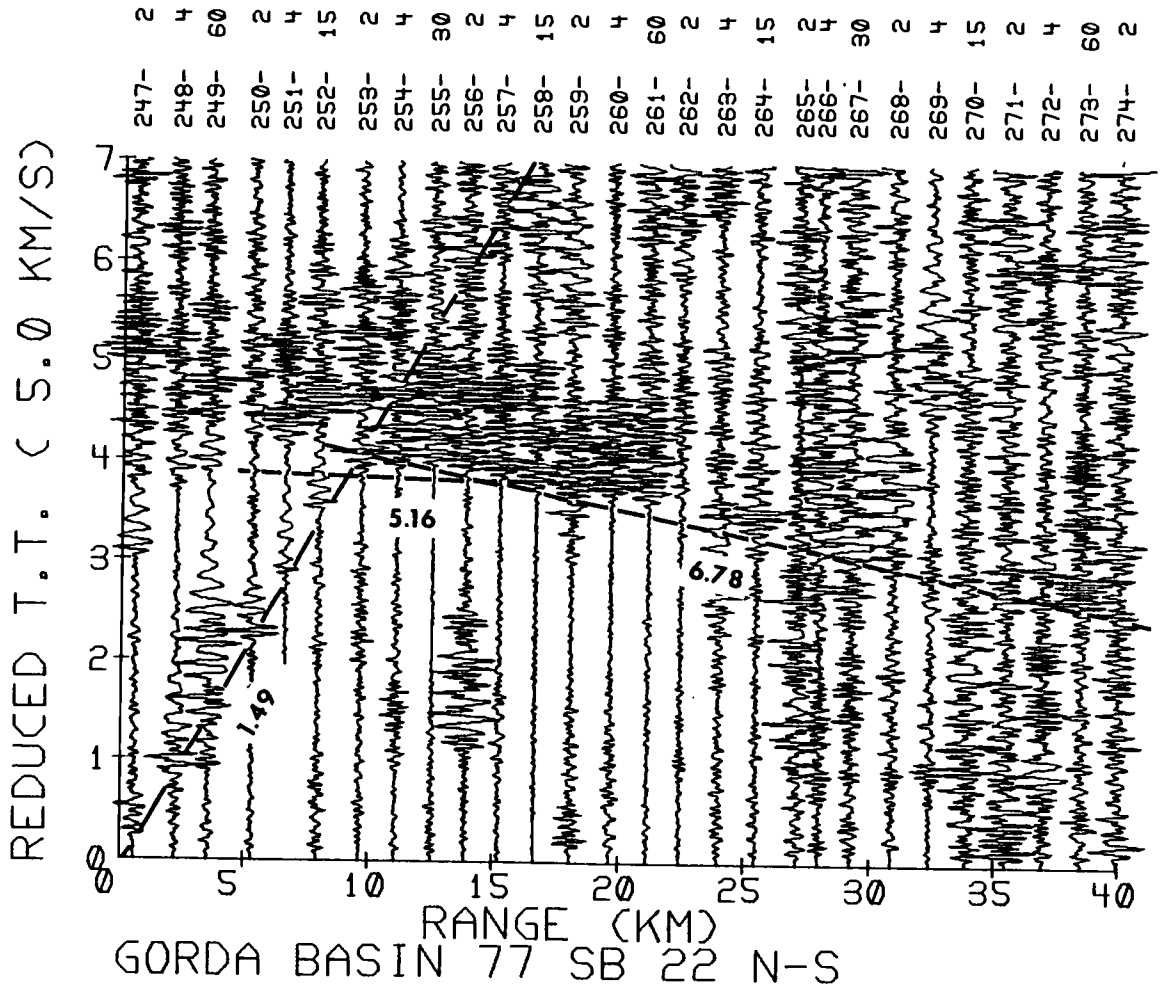

Figure 49. Reduced record section for sonobuoy SB22. Apparent seismic velocities in km/sec.

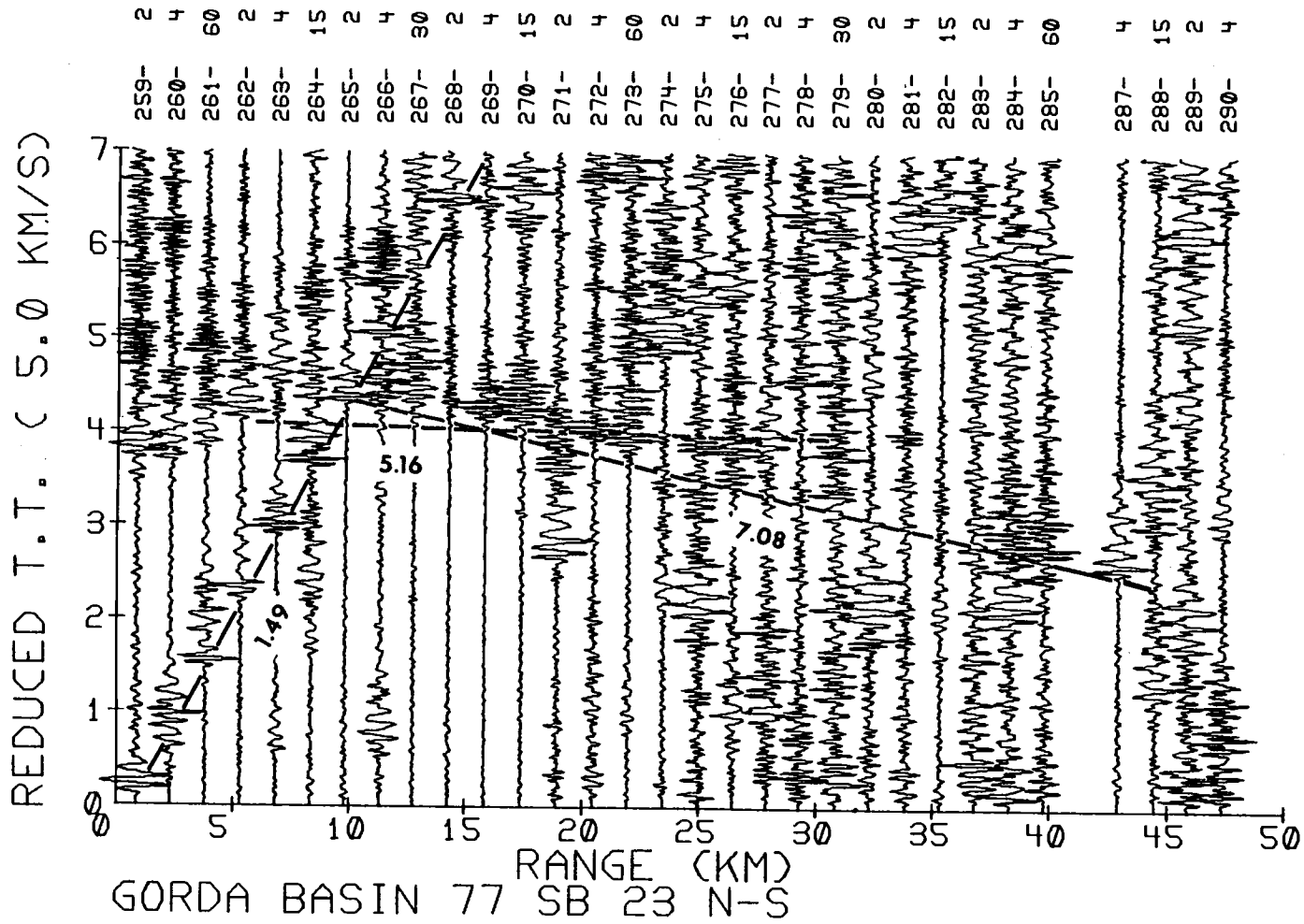

Figure 50. Reduced record section for sonobuoy SB23. Apparent seismic velocities in km/sec.

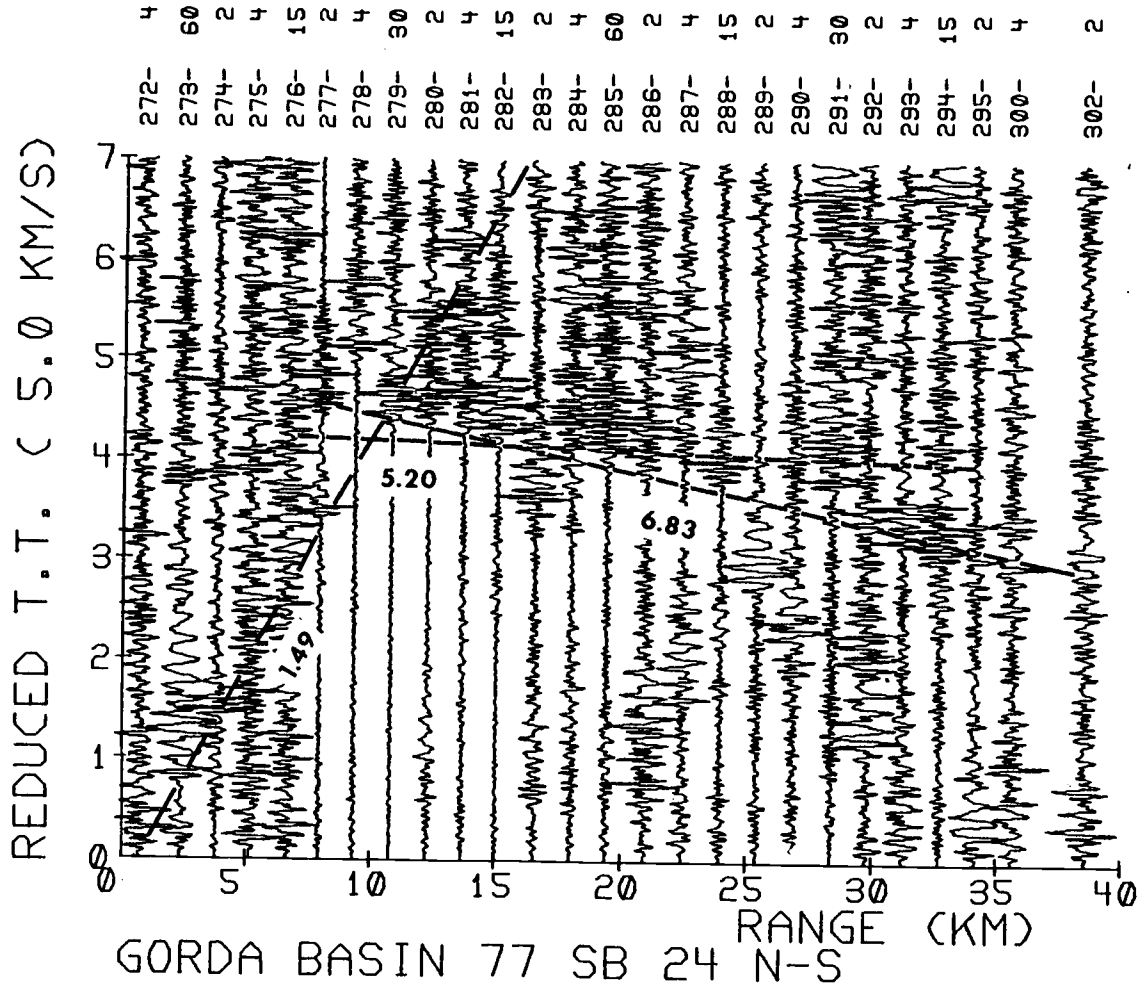

Figure 51. Reduced record section for sonobuoy SB24. Apparent seismic velocities in km/sec.

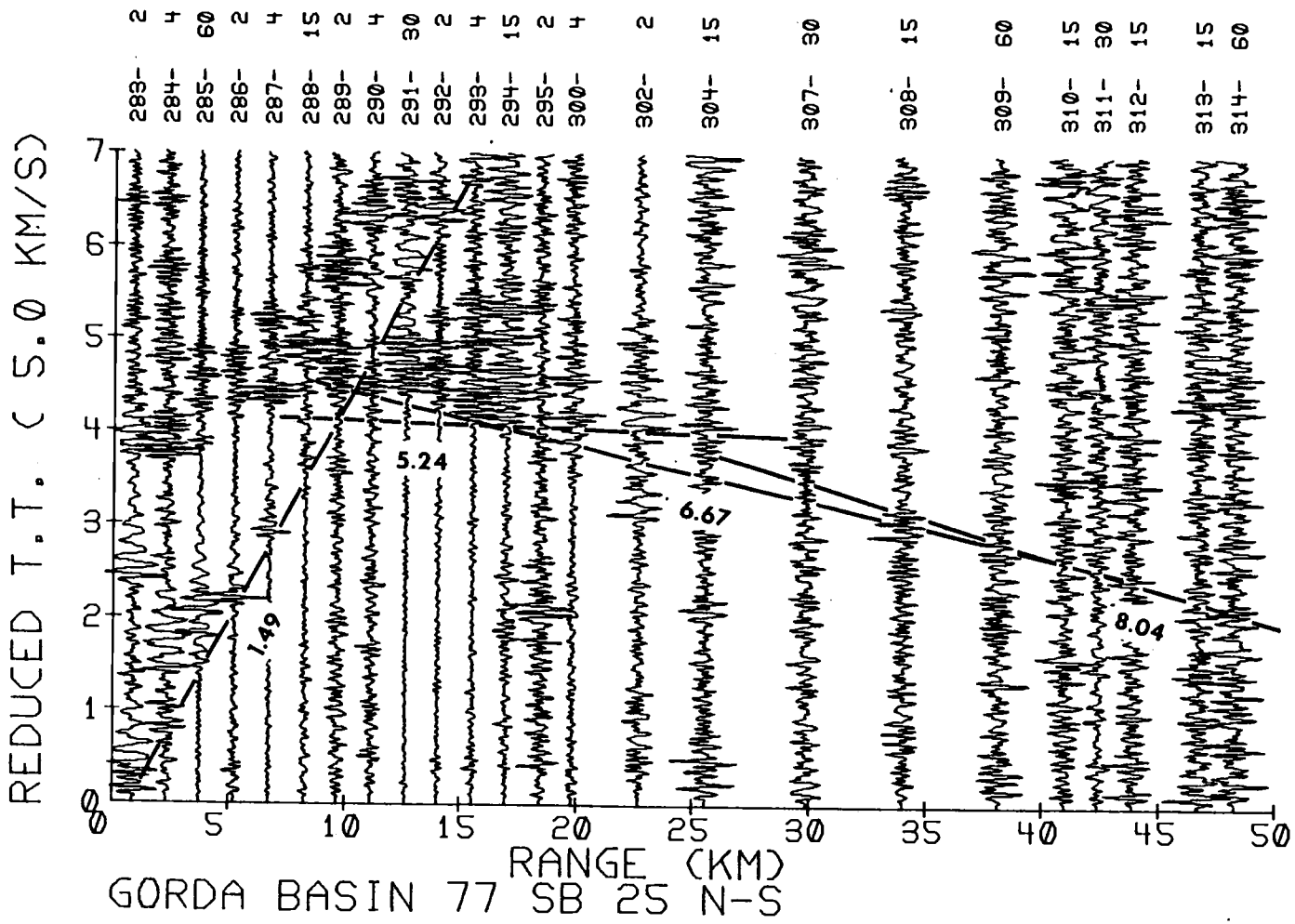

Figure 52. Reduced record section for sonobuoy SB25. Apparent seismic velocities in km/sec.

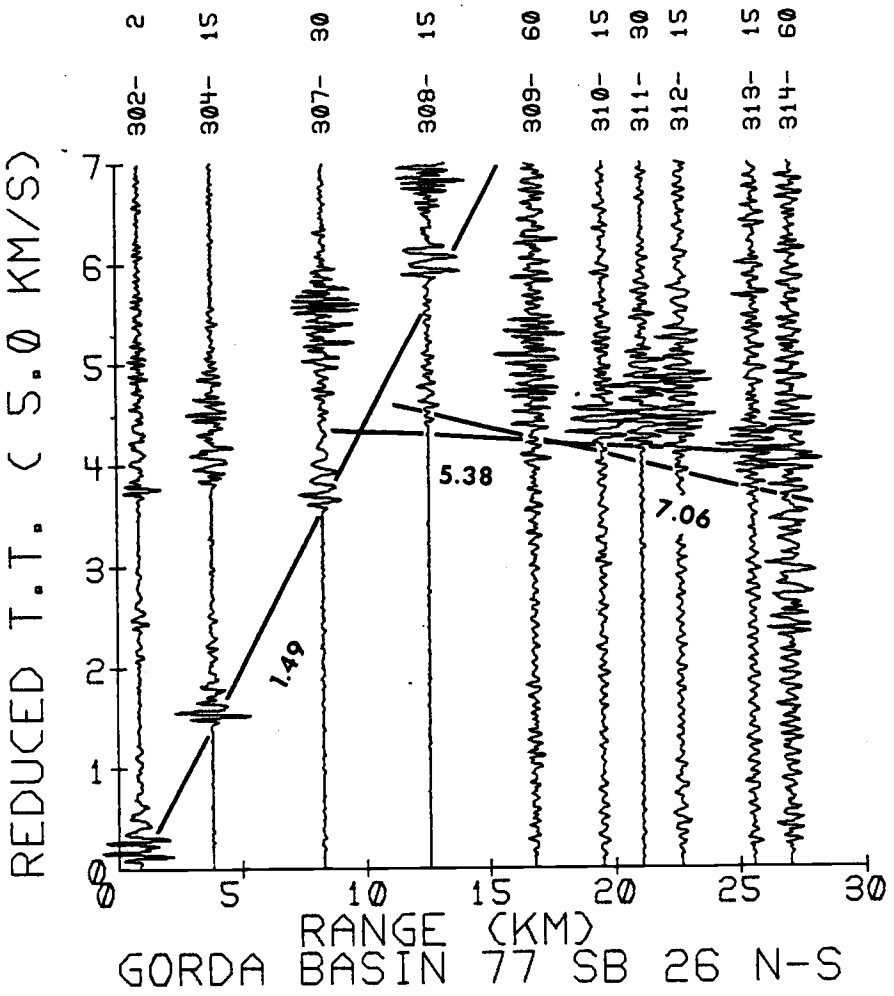

Figure 53. Reduced record section for sonobuoy SB26. Apparent seismic velocities in km/sec.